NAGOYA UNIVERSITY

Fundamental Friction and Wear Properties of Structure-Controlled ta-C

by

Mohd Muhyiddin Bin Mustafa

A thesis submitted in partial fulfillment for the degree of

Doctor of Engineering

in the

DEPARTMENT OF MICRO NANO MECHANICAL
SCIENCE AND ENGINEERING
GRADUATE SCHOOL OF ENGINEERING

2020

“knowledge is not measured by what is memorized, but rather how much it is benefited”

This thesis is dedicated to…

the memory of my father MUSTAFA Bin Ibrahim, who always encouraged me to pursue my study,

Specially dedicated to my beloved mom, wife, son and daughter, brother, sister, and friends for their love, support and prayers.

and to all my family for their endless love, support, and encouragement.

Declaration of Authorship

I, Mohd Muhyiddin Bin Mustafa, declare that this thesis titled, “Fundamental Friction and Wear Properties of Structure-Controlled ta-C” and the work presented in it are my own. I confirm that:

- This work was done wholly or mainly while in candidature for a Ph.D. degree at Nagoya University.
- Where any part of this thesis has previously been submitted for a degree or any other qualification at this University or any other institution, this has been clearly stated.
- Where I have consulted the published work of others, this is always clearly attributed.
- Where I have quoted from the work of others, the source is always given. With the exception of such quotations, this thesis is entirely my own work.
- I have acknowledged all of the main sources of help.
- Where the thesis is based on work done by myself jointly with others, I have made clear exactly what was done by others and what I have contributed myself.

_____

Signed: Mohd Muhyiddin Bin Mustafa

January 15th, 2020, Nagoya, JAPAN

Dissertation Committee

The thesis of Mohd Muhyiddin Bin Mustafa was reviewed and approved by the following:

Chair of Committee, Thesis Advisor:
Professor Dr. Noritsugu UMEHARA
Advanced Materials and Manufacturing Laboratory
Department of Micro-Nano Mechanical Science and Engineering
Graduate School of Engineering
Nagoya University

Committee Member:
Professor Dr. Takashi NAKAMURA
Manufacturing Engineering Laboratory
Department of Aerospace Engineering
Graduate School of Engineering
Nagoya University

Committee Member:
Professor Dr. Yang JU
Material Characterization and Mechanics Laboratory
Department of Micro-Nano Mechanical Science and Engineering
Graduate School of Engineering
Nagoya University

Committee Member:
Assoc. Professor Dr. Takayuki TOKOROYAMA
Advanced Materials and Manufacturing Laboratory
Department of Micro-Nano Mechanical Science and Engineering
Graduate School of Engineering
Nagoya University

Abstract

DEPARTMENT OF MICRO NANO MECHANICAL SCIENCE AND ENGINEERING, GRADUATE SCHOOL OF ENGINEERING

Doctor of Engineering

by Mohd Muhyiddin Bin Mustafa

Environmental concern regarding climate change and pollution due to human and industrial activity have alarming the researchers around the world to focus on sustainable development ranging from daily life product to the industrial heavy machinery. One of the biggest sources of environmental pollution and global energy source depletion is the automotive industry. From well to wheel of a passenger car, fuel did not efficiently consume due to friction and wear which cause both the waste of burning of limited fossil fuel and releasing of harmful gasses. Thus, diamond-like carbon (DLC) coating with excellent mechanical and tribological properties has been introduced to control and reduce the friction and wear in mechanical parts. In general, the tribological performance of the DLC is depending on several factors which are the properties of the coating itself and the environment such as working temperature, load, mating material, and the presence of chemical reaction. As such, mechanical components are often operated under severe high load conditions that cause DLC coating to react differently depending on the types of DLCs. Tetrahedral amorphous carbon (ta-C) is one of the hydrogen-free DLC coating types with

excellent properties and the hardness of ta-C coating is varied upon its sp^3 content. Under low load conditions, ta-C coating could provide excellent friction and wear resistance. Nonetheless, high hardness ta-C coating could not sustain high wear resistance properties under severe high load conditions. Recently, the advancement in coating deposition technology has led to the introduction of structure to the as-deposited DLC. At such, two novel ta-C coatings were develops which are Pillar ta-C and Mesh ta-C. Both of these coatings present the new characteristic of ta-C which are hardness controlled along with the coating depth. Since both coatings were newly developed, thus clarification on the mechanical and tribological properties of the Pillar ta-C and Mesh ta-C needs to be done before the application. The aim of this study is to clarify the friction and wear mechanism of Pillar ta-C and Mesh ta-C under boundary lubricated conditions.

The first part of this study examined the tribological properties of novel Pillar and Mesh tetrahedral amorphous carbon (Pillar ta-C and Mesh ta-C). Subsequently, the comparison was made with conventional ta-C coating under base-oil lubrication via cylindrical-pin-on-disk tribo-tester. Analysis of wear track was conducted using field-emission-scanning-electron-microscope (FE-SEM), atomic-force-microscopy (AFM), and Raman-spectroscopy. The friction coefficient for Mesh ta-C and conventional ta-C revealed a similar pattern with regard to loads. The Mesh ta-C had excellent wear resistance, where the wear rates at loads of 20 N was 10 and 20 times lower than Pillar ta-C and conventional ta-C, respectively. High wear resistance of Mesh ta-C characterized by inhibition of brittle micro-fracture propagation, less in abrasive particle created during friction test, and suppressing the effect of graphitization-induced wear on the contact surface.

Wear by fracture is among the factors associated with the DLC coating failures in the tribological application. The study continues with the investigation on the link between the

wear and the fracture-toughness on the novel Pillar and Mesh structure ta-C coatings, in addition to conventional ta-C coatings. The tribological properties of these coatings were examined under base-oil lubrication via ball-on-disk tribo-tester and the micro indentation technique was used to characterize the fracture toughness. The wear track and the indentation mark were analyzed using the optical microscope, 3D laser microscope and FE-SEM. The friction coefficient for ta-C, Pillar ta-C and Mesh ta-C is within the range of 0.071 to 0.106. Mesh ta-C indicated the highest wear resistance, followed by the Pillar ta-C and conventional ta-C. Also, Mesh ta-C demonstrated the highest fracture-toughness value with 16.6 $MPa \cdot m^{1/2}$, followed by Pillar ta-C with 13.4 $MPa \cdot m^{1/2}$ in contrast to ta-C. Greater resistance to wear for ta-C with Pillar and Mesh structure was detected with an increased fracture-toughness and improvement in crack propagation inhibition. Moreover, the Pillar and Mesh ta-C provides a superior rate of crack-energy dissipation as compared to the ta-C.

The effect of lubricant additives to the novel Pillar ta-C and Mesh ta-C coating, as well as conventional ta-C for comparison has been investigated. Three type of lubricants used in this study are, Mineral oil with MoDTC + ZnDTP + 5 CA, PAO4 + MoDTC, and PAO4 + ZnDTP. Subsequently, a comparison was made with the lubrication under base oil PAO4 via cylindrical-pin on disk tribo-tester. The result shows that the friction coefficient is lower under single additive PAO4 + MoDTC and PAO4 + ZnDTP lubricants due to the formation of Mo-derived and Zn-derived tribo-film. Furthermore, ta-C, Pillar and Mesh ta-C shows excellent wear resistance under Mineral oil with MoDTC + ZnDTP + 5 CA lubrication condition, followed by the lubrication under PAO4 + MoDTC and PAO4 + ZnDTP. Higher wear resistance of ta-C, Pillar ta-C and Mesh ta-C under additive oil lubrication is characterized by the formation of Mo and Zn derived tribo-film which protect against high wear, as well as improved the coating resistance to microfracture. In addition, the friction coefficient reduction only can be observed under the used of single additive lubrication.

Acknowledgments

First of all, I would like to thank God for giving me the strength and health to complete this thesis. This thesis would not have been possible without the guidance and help of several individuals who directly or indirectly extend their valuable assistance in the preparation and completion of this study.

I would like to express my sincerest gratitude and respect to my supervisor, Professor Dr. Noritsugu Umehara, who has supported me throughout my research with his patience and knowledge whilst allowing me the room to work in my own way. For all I have learned from him and for his excellent guidance, continuous help, patience, motivation, and support in all stages of this thesis. I would also like to thank him for being an open person to ideas, and for encouraging and helping me to shape my interest and ideas. Without his guidance and persistent help this dissertation would not have been possible.

The success of this thesis is attributed to the extensive support and assistance from all members of Advanced Material and Manufacturing Laboratory. Especially, I would like to express my grateful gratitude and sincere appreciation to Associate Professor Dr. Takayuki Tokoroyama, Assistant Professor Dr. Motoyuki Murashima and Mr. Shinkoh Senda for their kindness in examining the research work and providing technical suggestions for improvement and encouragement during my time here. I am indebted to Mr. Akinori Shibata, Mr. Yoshiharu Utsumi and Dr. Hideki Moriguchi from Nippon ITF Inc., Japan for their kind continuous support and help in my work.

My special thanks are given to my labmates for their cheerful cooperation, encouragement, help, support, and enjoyment during the course of my study. I hope our friendship will remain the same in the coming years.

My heartfelt thanks go to my parents, wife, sons, and daughter for their inseparable support and prayers. My late father, Mustafa Bin Ibrahim, my beloved mother, Siti Fatimah Binti Salleh, and my wife, Noor Masnira Binti Muhammed Salleh in the first place is the person who put the fundamental to my learning character and sincerely raised me with their love and caring. My special thanks are extended to my dearest child, Adam Haikal Bin Mohd Muhyiddin, Aisyah Humaira Binti Mohd Muhyidddin and Aidan Yusuf Bin Mohd Muhyiddin, my sister and brother, and their family for their understanding and continuous prayers and supports.

List of Figures

List of Tables

Contents

Chapter 1
Introduction

1.1 Background and social needs of DLC coating

Environmental issues concerning pollution, energy waste, and resource depletion have triggered an alarm to the modern advancement in technology. Friction and wear of material have become one of the important issues relating to energy conservation and efficiency. The interaction between the two materials has led to the loss of both material and energy. Aristotle raised concerned on the concept of friction and wear from 384-322 BC, which then continue by the introduction of two empirical laws of friction by Leonardo Da Vinci which stated that friction force is proportional to the applied load and independent of contact area [1]. Friction can be described as the force that resists the sliding motion of a body in the opposite direction. Likewise, wear is defined as the loss of material at the contact surface which led to the mechanical failure of components [2]. Furthermore, lubrication is introduced and widely being used with the aim to reduce both friction and wear loss.

The energy dissipated to overcome the friction force has taken one-third of the total world energy resource in mechanical applications [3], [4]. It is further reported in details that tribological contacts have consumed a total of 23% (119 EJ) of the world's total energy, in which 20% to overcome the friction and 3% was used for reproducing and replacement of the part due to wear and wear-related failures [5]. Thus, the tribology field is emerging as a result of the need to achieve the reliable, sustainable and efficient operation of the mechanical component and devices.

Dictionaries defined tribology as the science, technology, and engineering of interacting surfaces in relative motion, which includes the study and application of friction principles, wear and lubrication. The need to understand and applied these principles has led to the revolution of the used of material and lubrication so as to achieve the goal of energy consumption saving and cost reduction. Tribological studies have been applied and benefited to the development of sustainable components and parts in various fields of industries. The tribological study field has gained attention and attracts many researchers in physics, chemistry, material science, and engineering. From individual components such as gears, pistons, camshaft, and bearings to the assembly or product such as engines and manufacturing processes, a wide range of tribology applications can be found. Nowadays, tribological applications are not only applicable to the automotive industry but also has been applied in medical and consumer product due to its economic and social impacts.

In the field of mechanical engineering, the aspect of tribology is very important specifically in the automotive industry where most of the parts were rubs against each other. Under the direct contact, the movements of the parts generate friction force that leads to the heat generation and wears that causing parts failure. A passenger car consumes 340 L of fuels on average to overcome the friction, in which by taking the advantage of tribological technologies could reduce the friction losses and CO_2 emission by 18 % and 290 million tonnes between 5 to 10 years, respectively [4]. Thus, the ultimate goal in the view of the automotive industry is to reduce the friction to the desired level that results in a sustainable part design which includes improving energy consumption as well as prolongs the parts lifetimes. Lubrication is one of the important ways used to achieve the goals by altering the properties of the lubricant such as adding the additives. In general, lubrications are classified into two types which are fluid lubrication and solid lubrication. The fluid lubrication system used the liquid lubricants to create lubrication films in between the contact surfaces.

Likewise, solid lubrications employs self-lubricated surface which slides against each other to achieve low friction and high wear resistance such as graphite and molybdenum disulfide [6].

Diamond-like carbon (DLC) coatings are one of the solid lubricants that offer excellent mechanical and tribological properties. Since the beginning of the 1990s, researches on DLC have rapidly grown and attracted many industries and academic institutions around the world. Research has been progressively made on the deposition method, structural and morphology of the coating, lubrication and additive effect, an intrinsic and extrinsic factor which leads to ultra-low friction and improved wear resistance. However, several aspects of the DLC coating itself remain unclear such as very hard DLC coating tends to produce excessive wear under boundary lubrication conditions. Also, the effect of the introduction of structure to the DLC coating during the deposition process on the tribological properties has not been clarified. This thesis aims to clarify those remained questions under the fundamental of structure controlled DLC.

1.2 Diamond-like carbon

Carbon is one of the elements that exist with outstanding properties that can bond with various elements to form organic and inorganic material. The carbon sp^3 bond hybridization leads to the perfect symmetry of the diamond structure, which provides properties like extremely high hardness, excellent thermal conductivity, high electrical resistivity, chemical inertness, optical transparency, wide bandgap, and low wear rate. Graphite has strong anisotropic properties in one direction, in which there is sp^2 hybridization of the carbon atoms, whereas in the perpendicular direction there is only weak van der Waals force acting. The sp^2 hybridization results in low hardness, low electrical resistivity and high wear rate, combined with low friction. Amorphous carbon consists of a disordered network of carbon

atoms with a mixture of both sp^3 and sp^2 coordinated bonds. The family of amorphous carbon films is called diamond-like carbon, or DLC [7]. These combinations of excellent properties offered an excellent approach to increase the lifespan of a component subjected to friction and wear.

With the aim to fulfill legal regulations concerning energy efficiency and greenhouse gas emissions, diamond-like carbon (DLC) coatings are increasingly used on highly stressed components of internal combustion engines to reduce friction and prolong component lifetime [8]. DLC coatings display a low friction coefficient under non-lubricated conditions, similar to molybdenum disulfide (MoS_2) and graphite, and also have outstanding wear resistance, which is an issue with solid lubricants. Additionally, they also exhibit excellent anti-seizure properties owing to their surface hardness, which greatly surpasses that obtained in the heat treatment and plating treatment processes traditionally applied to steel [9]. DLC can be categorized in main groups, the hydrogenated amorphous carbon (a-C:H, ta-C:H) and the hydrogen-free amorphous carbon (a-C, ta-C). Superhard hydrogen-free ta-C films are characterized by a high fraction of tetrahedrally bonded, sp^3 carbon atoms. By adding other elements like metals (a-C:H:Me) or non-metal elements like silicon, oxygen, fluorine or others (a-C:H:X), several modifications of the properties can be made according to application requirements [10]. The deposition method of DLC can be classified into two groups which are through chemical vapor deposition (CVD) and physical vapor deposition (PVD).

1.2.1 Tetrahedral amorphous carbon (ta-C) coating

Among DLC coating available is free hydrogen ta-C coating which can be prepared using PVD arc method. The important properties of ta-C coating are the hardness which is

relatively higher as compared to the other types of coating due to the high sp^3 content. Due to its high hardness and durability, ta-C coating has been applied to the high-pressure contact engine parts [11]. Furthermore, friction reduction between piston rings and bore is also achieved by applying ta-C coating on the contact area [12].

Despite the excellence ta-C coating performance, several reports indicate that the used of high hardness coating only results in friction coefficient improvement but with high wear rates that limit the coating lifetimes under boundary lubrication condition. Wear rate ta-C coating under the lubricated condition is inversely proportional to the hardness of the coating [9]. The further report also stated that the ta-C coating incapable to sustain in a high-temperature condition which results in high wear due to cracking and peeling off [13]. In a different study, ta-C coating shows the lowest friction coefficient as compared to the a-C:H coating but result in the highest wear rates [14]. As reported by Ronkainen et al., the wear resistance of ta-C coating was higher compared to the a-C:H and the ta-C coating produce higher wear on the counterpart material [15].

With regard to the previous study, excellent tribological properties of ta-C coating can be achieved by a lower surface hardness coating. In other words, lower friction coefficient, as well as high wear resistance of the ta-C coating, could be achieved by controlling the contact surface hardness. Recent advances in PVD technology and in particular sputter coating deposition, have led to the development of nanolayered and 'superlattice' films which, especially in the case of ceramic–ceramic or ceramic–amorphous multilayers, can typically possess super hardness or ultra hardness properties, if the individual layer thickness can be accurately controlled [16]. A work performed by Gilewicz et al. has proved that CrCN/CrN+ta-C multilayer with ta-C hardness of 45 GPa formed using pulse cathodic arc evaporation method results in excellent friction and wear properties [17].

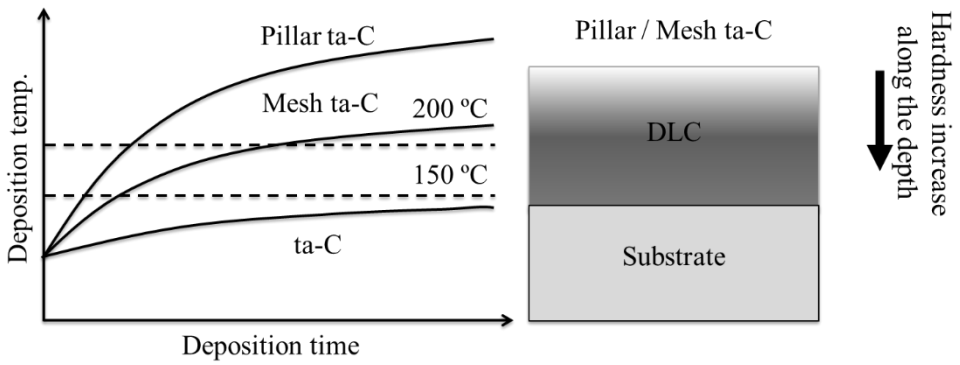

Figure 1 Conceptual deposition method for conventional ta-C coating, Pillar and Mesh ta-C DLC coating

1.3 Structure controlled ta-C coating (Pillar ta-C and Mesh ta-C)

Recent technology in the deposition method has broadened the development of intelligent coating. This allows the hardness of the coating to be controlled along with the coating depth as well as to introduce the specific structure within the coating growth. A novel ta-C coating with Pillar and Mesh structure has been developed by using the M720 PVD apparatus through modification of the conventional method to deposit ta-C.

In the deposition process of the conventional ta-C, the substrate temperature must be controlled to keep below 150 °C by means of a cooling system as illustrated in Figure 1. Likewise, the manufacturing of Pillar and Mesh ta-C were conducted at a higher temperature throughout the deposition procedure by applying continuous heat to rise and keep the temperature of the substrate at above 200 °C [18]. As a result, the graphitic structure was developed during coating growth and the coating hardness decreased as the thickness of the coating increased. These phenomena were confirmed by the crystallinity evaluation as further discussed.

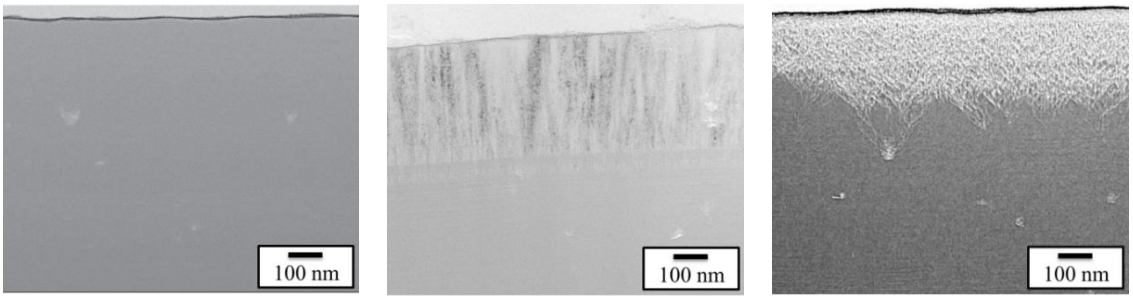

(a) (b) (c)

Figure 2 Cross sectional images of (a) conventional ta-C, (b) Pillar ta-C, and Mesh ta-C

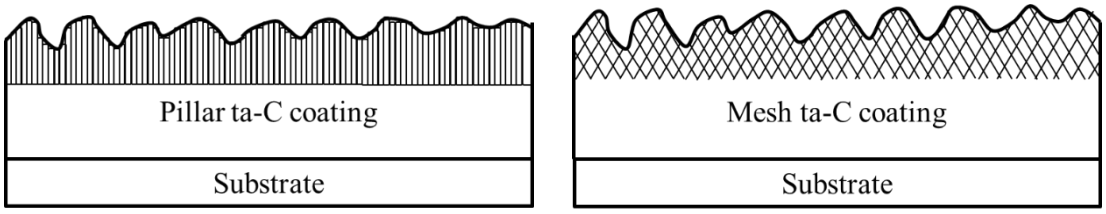

(a) (b)

Figure 3 Schematic cross sectional images of (a) Pillar ta-C, and (b) Mesh ta-C coatings

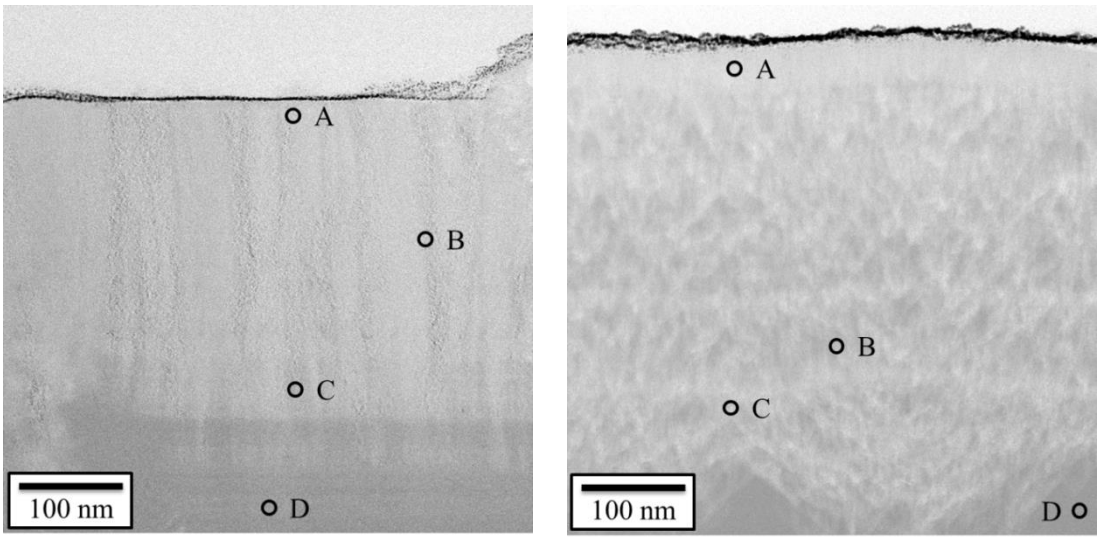

(a) (b)

Figure 4 Micro-electron diffraction acquisition position for (a) Pillar ta-C, and (b) Mesh ta-C

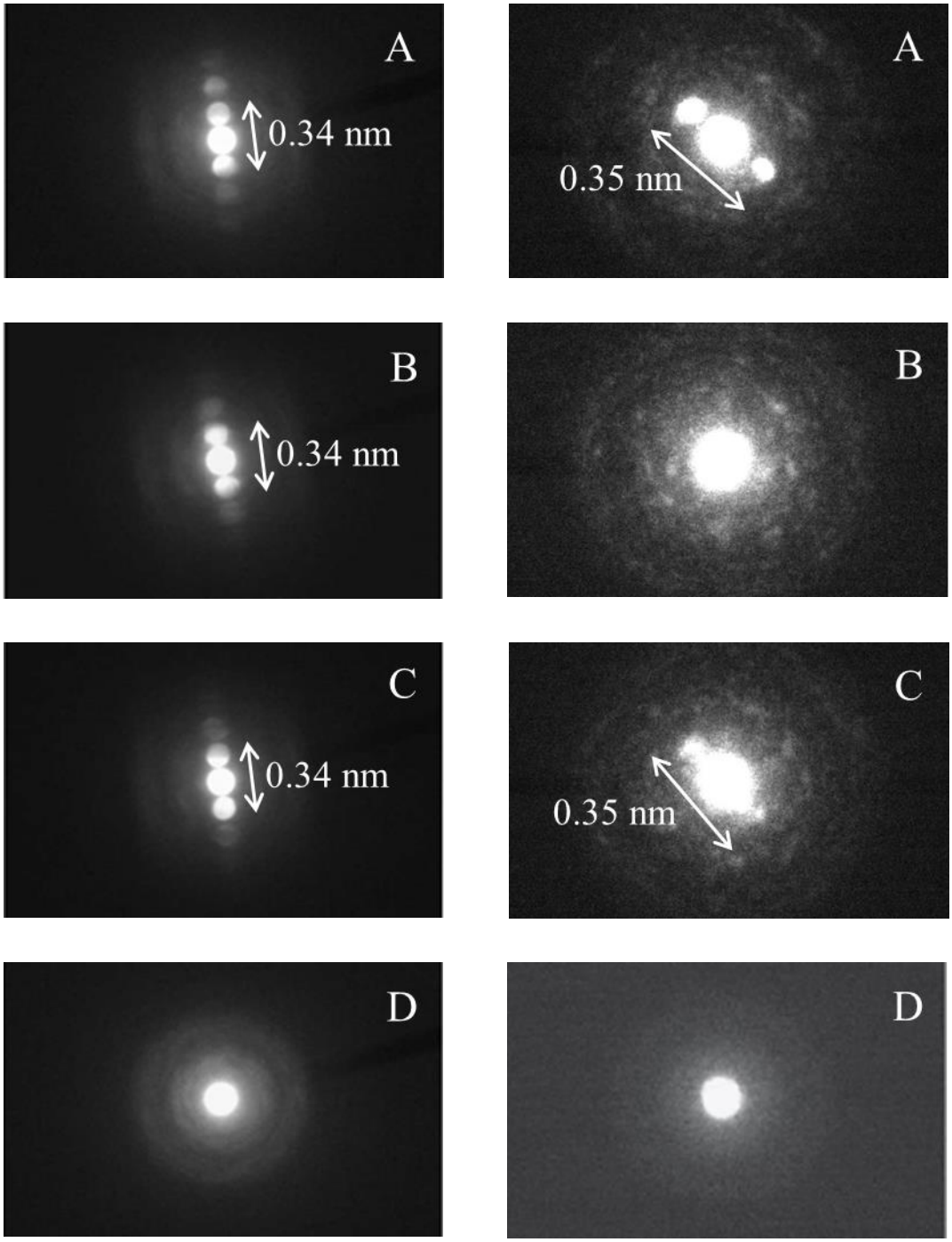

(a) (b)

Figure 5 Crystallinity evaluation result at different position for (a) Pillar ta-C, and (b) Mesh ta-C

The cross-sectional of the conventional ta-C, Pillar ta-C and Mesh ta-C coating were prepared using the focused ion beam (FIB), which being observed under the transmission

electron microscope (TEM H9000 UHR), Figure 2. The conventional ta-C cross-sectional images, Figure 2(a) demonstrates a homogenous structure characteristic. Furthermore, the Pillar and Mesh ta-C reveal a reticulated structure originated from the microparticle, produces by the arc deposition technique as presented in Figure 2(b) and Figure 2(c), respectively. Moreover, Figure 3(a) and Figure 3(b) shows the schematic cross-sectional images of the Pillar ta-C and Mesh ta-C coating, respectively.

Micro-electron diffraction analysis was conducted at different locations on the cross-sectional cut of the Pillar ta-C and Mesh ta-C as shown in Figure 4(a) and Figure 4(b), respectively. The crystallinity analysis by the electron diffraction technique via FE-SEM JEM2100F result are as shown in Figure 5(a) and Figure 5(b). An approximately 0.34 nm and 0.35 nm diffraction images was observed for the Pillar ta-C and Mesh ta-C, respectively. According to the International Center for Diffraction Data (ICDD) database, the crystalline graphite lattice spacing constant is 0.33756 nm. The obtained crystallinity result is almost similar to the ICDD data which indicates the presence of crystalline graphite microstructure at the quarter of the coating thickness of Pillar ta-C and Mesh ta-C.

1.4 Fracture toughness

Fracture toughness refers to the capability of the material to resist the pre-existing crack growth. Toughness is the measure of energy utilized to produce crack and facilitating crack to propagate causing the fracture. Meanwhile, fracture toughness is known as the energy that is needed for crack propagation to failure [19]. Frequently, toughness is known as the energy absorption capacity of film material for the duration of the transition from deformation to fracture. Toughness is an essential mechanical property with regard to the

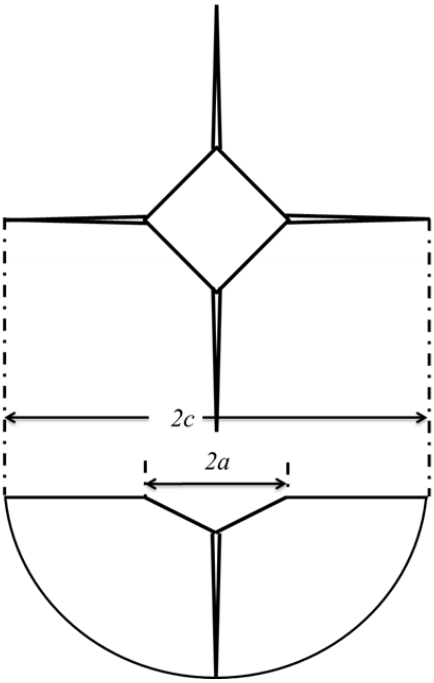

Figure 6 Top and cross-sectional views of median (half-penny) cracks

cohesive force of DLC film in which it indicates the film capacity to resist the formation of cracks near the defects in the film caused by the stress accumulation [20]. The mechanical properties are well-known to limit the performance and reliability of a thin coating like DLC.

Application of DLC coating such in the automotive components by means of rubbing of two components leads to enhancing the features including the friction and wear characteristics. Therefore, there have been increased studies on enhancing the tribological characteristics of the coatings by modifying the deposition methods and doping elements. Nevertheless, there are several limitations in evaluating the DLC coating wear performance via the fracture toughness. Evidence has shown that harder coatings like ta-C are highly brittle and can be easily fractured by high-pressure contact throughout the application. Hence, in order to examine the brittleness of the thin coating, it is crucial to quantify the fracture toughness.

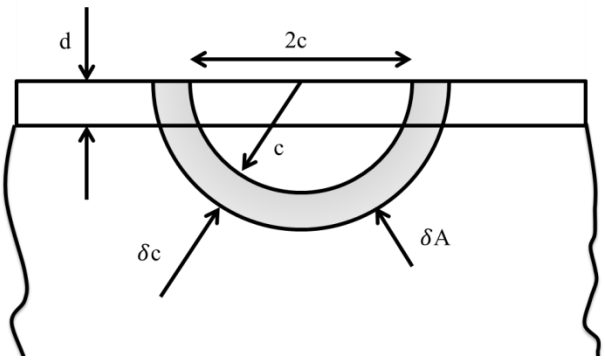

Figure 7 Schematic side view of a radial crack in a substrate coated with a film of thickness d. The schematic shows a crack extension of δc occurring in a semicircular radial crack of initial radius c [21]

Hardness is among the key factors in regulating the wear performance of the DLC coating. As such, high hardness with low crack resistance is associated with severe wear due to through-thickness crack [22]. Similarly, high sp^2 carbon atoms DLC coating that is low in hardness could lead to high wear as the results of structural alteration including graphitization of the contact surface under severe condition [23], [24]. DLC is frequently deposited with a layer of homogeneous structure excluding multilayer coating patterns. Therefore, tailoring the properties, particularly the hardness by employing the DLC structure could promote superior wear performance.

1.4.1 Fracture toughness for thin film

The DLC coating is associated with the deposition of the coating onto a substrate. Therefore, the technique that was employed to examine the fracture toughness for the bulk material is not feasible for evaluating the fracture toughness for the coating [25]. It should be noted that the quantification of the fracture toughness of the coating is still challenging owing to the thickness limitation of the DLC coating [26]. The measurement of the crack length

during indentation could be utilised to evaluate the fracture toughness. On that account, the current study applied Vickers indenter as it has been demonstrated to form bigger radial cracks that provide better accuracy of cracks length measurement. Thus, the radial crack formed follows the axis of diagonal of the indent and restraint the coating from secondary crack growth and chipping [27], [28].

As shown in Figure 6, the criterion of a well-defined crack was taken as c > 2a, where c is half the crack length and 2a is the diagonal length of the indentation mark [29]. The plastic zone that is prolonged under the loading condition deploys the tensile stress into the coating. Moreover, additional stress is generated throughout the unloading condition when the elastically strained coating started to resume to its actual shape. Nonetheless, the aforementioned process is limited by the permanent deformation linked to the plastic zone [30]. Radial crack on the coating is generated during the unloading process, which forms the residual tensile stresses [31].

Frequently, the indentation on specimens leads to both elastic and plastic deformations. In brittle materials, plastic deformation generally exists with pointed indenter including Vickers. The amount of work for elastic/brittle fracture is the amount of work to form two novel surfaces. The system fracture-toughness is measured by the combination of the total work of fracture of the system and the composite modulus of the system, which include a substrate and the coating. The fracture-toughness is denoted as;

$$K_f = \sqrt{GE} \qquad \textbf{Eqn. 1}$$

Where K_f is the fracture-toughness, E is the modulus of elasticity of the coating, and G denotes the total work of fracture. The total work of fracture for elastic/brittle fracture is the amount of work required to produce two new surfaces.

The total system fracture toughness is obtained by combining the total work of fracture of the system and the composite modulus of the system which encompassing substrate and the coating. Applying boundary condition at d=0; effective fracture toughness, $K_r = \sqrt{G_s/E_s}$ and $c = c_0$ yield;

$$\left[\left(\frac{c_0}{c}\right)^3 - 1\right] = \frac{2d}{\pi c}\left(\frac{G_f}{G_s} - \frac{E_f}{E_s} - 2\right) \quad \textbf{Eqn. 2}$$

Where c is the half radial crack length in the coated substrate, c_0 is the half radial crack length in the uncoated substrate, E_s is the modulus of the substrate, and E_f is the modulus of the film, G_S and G_f are the work of fracture in the substrate, and the work of fracture in the film, respectively.

1.5 Boundary lubrication condition

The friction and wear sensitively depended on a system comprising of coating, lubricant (oil + additive) and counterpart. Modifications of pure carbon coatings can lead to superior tribological properties. This kind of modification has been observed for chromium-containing a-C:H coating beside other variables such as their structure, test environment and temperature [15], [32], [33]. Mabuchi et al. report that a higher sp^3 bond in sp^2/sp^3 ratio of DLC could result in a higher frictional coefficient under lubricated condition [34]. While high hardness DLC could provide lower frictional coefficient and high wear-resistant as a result of structural change at the contact area [35]. Furthermore, under relatively severe contact conditions in boundary lubrication regime, oil additives and DLC doping elements show the significant and beneficial influence on the wear behavior [36], [37].

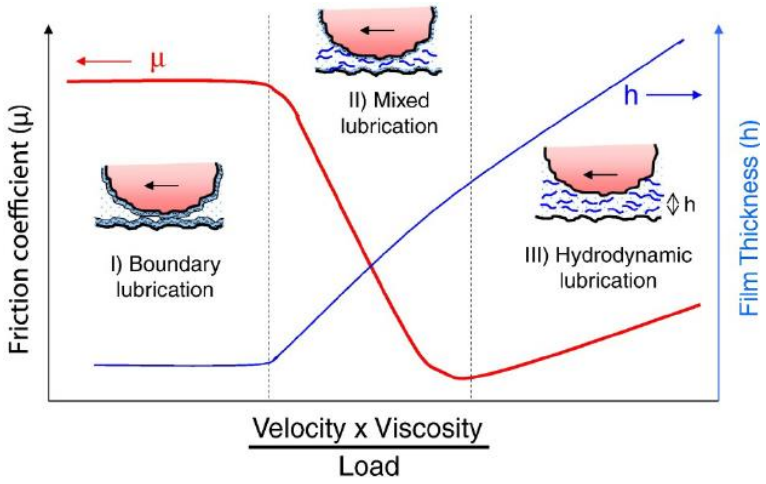

Figure 8 Stribeck curve and lubrication regimes [38]

Lubrication conditions can be classified into three regions which are boundary lubrication (BL), mixed lubrication (ML) and hydrodynamic lubrication (HL). The friction and wear performance depends on the lubrication regimes in which the tribo system is operated as illustrated by the Stribeck curve shown in Figure 8.

The friction coefficient and the fluid film thickness are plotted as a function of velocity, fluid viscosity, and load. The thickness of the fluid film between two solid surfaces determines the lubrication condition. In the view of automotive engines, the components experience a various combination of hydrodynamic, elastohydrodynamic, boundary and even the mixed lubrication during engine operation as the engine speed and load constantly change [39]. Boundary lubrication mark as the severe lubrication condition where direct contact of the surface and asperities. The friction and wear properties in this region were predominantly determined by the interaction between the solid asperities and the lubricants. The loads were primarily supported by the contacting surface or asperities which cause high wear. Furthermore, plastic shearing between the asperities within contact interface leads to high friction. In the extreme condition such as high load and low speed, high wear and friction is not avoidable which also may cause seizure and failure of the contact surfaces. Therefore, to

improve and realizing the excellence tribological performance under boundary lubrication conditions, surface modification such by advance coating application could be the solution.

1.6 Purpose and research method of this work

The excellent tribological properties of DLC coating application can offer a sustainable technological development. This could be a viable solution the modern development mainly in the automotive components industry which involving the direct contacts between parts. However, further research is needed to answer the remained question regarding tribological behavior in boundary lubrication conditions. This research framework was developed base on the hypothesis that the hard ta-C coating was experiencing mechanical wear which proceeds with microfracture that leads to excessive wear of the coating. The mechanical wear by means of microfracture is associated with the contact surface hardness and brittle characteristics of the coating. Thus, two novel ta-C coatings which is Pillar ta-C and Mesh ta-C were introduced that have hardness controlled along with the coating depth.

Thus, this study aims to clarify the effect of fracture toughness on the friction and wear properties of ta-C coating with the different structures under boundary lubrication conditions. Three types of ta-C coating which are conventional ta-C, Pillar ta-C and Mesh ta-C were investigated in this study. Since both Pillar ta-C and Mesh ta-C coating newly developed, thus focus of this study also were given to characterizes the tribological properties under base-oil and base-oil with additive lubrication condition.

To achieve the objectives of this study, tribological testing and investigations were scant to characterize the friction and wear phenomena under poly-alpha-olefin 4, PAO4 and PAO4/ Mineral oil with MoDTC and ZnDTP additive boundary lubrication condition, as well as micro-indentation testing, to determine the fracture toughness and fracture mechanism.

The mechanical properties and structure of the coating were first investigated by using the Nano-indenter, atomic force microscopy (AFM), Raman spectroscopy, field emission scanning electron microscope (FE-SEM), and transmission electron microscope (TEM). Experimental conditions, results and interpretations are further discussed in the following chapters.

1.7 Organization of this dissertation

This thesis presents the latest research in the field of tribological behaviors of DLC hard coatings in boundary lubrication. The first chapter presents an overview of DLC coatings and their tribological behaviors/mechanisms in boundary lubrication conditions, as well as the focus and purpose of this study. Chapter 2 presents the result of the investigations on the tribological properties of conventional ta-C, Pillar ta-C and Mesh ta-C coating/SUJ2 steel tribopair under PAO4 boundary lubrication conditions. Furthermore, Chapter 3 presents the result of the investigations on the effect of fracture toughness on the tribological behaviors of DLC coatings. Moreover, Chapter 4 presents the outcomes of the investigation of the effect of MoDTC and ZnDTP additives oil on the tribological properties of conventional ta-C, Pillar and Mesh ta-C. Lastly, Chapter 5 summarized all the findings of this dissertation. Figure 9 graphically presents the organization of the dissertation.

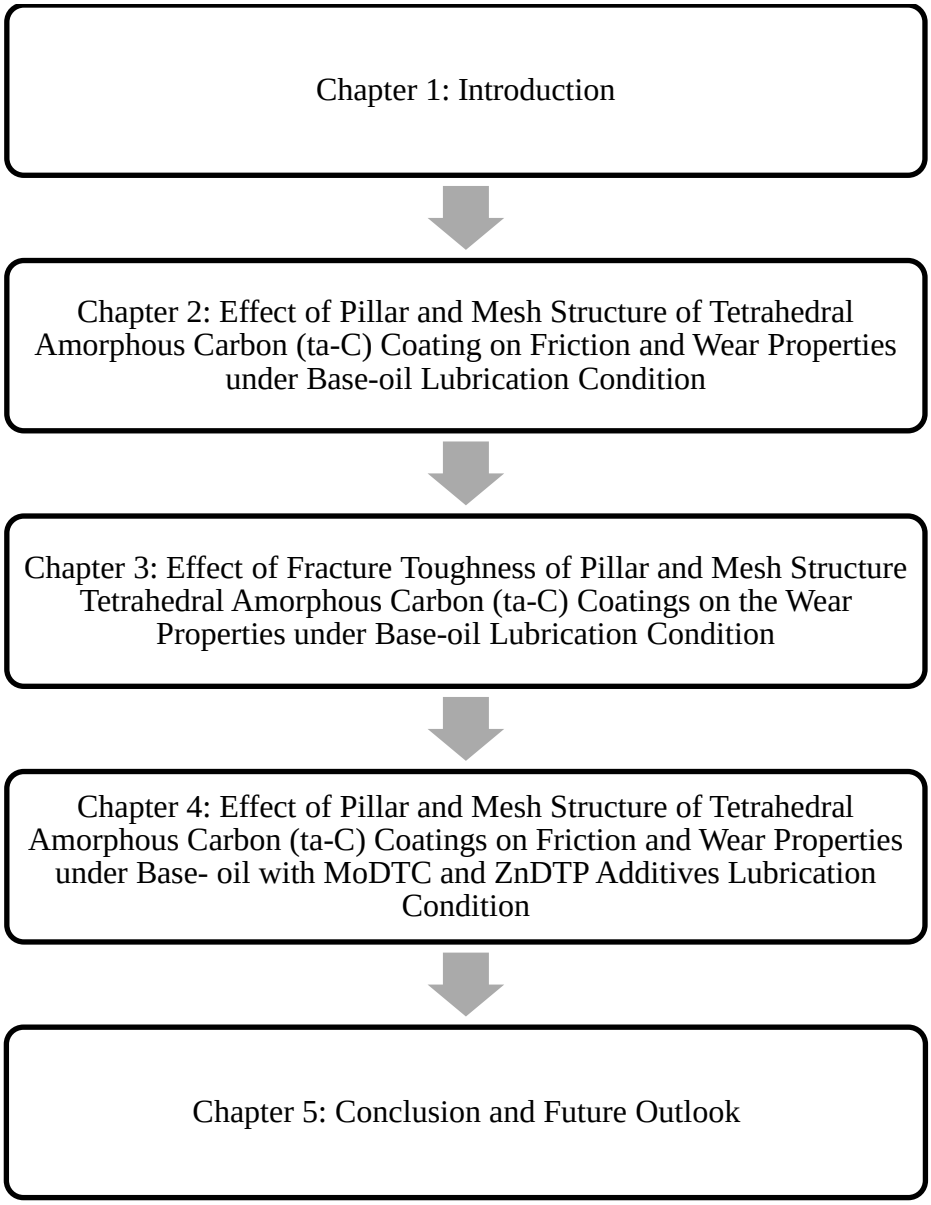

Figure 9 Organization of the dissertation

Chapter 2

Effect of Pillar and Mesh Structure of Tetrahedral Amorphous Carbon (ta-C) Coating on Friction and Wear Properties under Base-oil Lubrication Condition

2.1 Introduction

Diamond-like carbon (DLC) coatings are known as remarkable features applied as the solid lubricants because of low friction, high hardness as well as wear resistance and chemical inertness. Presently, the DLC coating has been widely utilized in various industrial applications to reduce friction and wear, particularly in the automotive industry. As such, this industry continuously is pursuing lower energy loss and low gas emissions. In order to achieve legal regulations in relation to energy efficiency and greenhouse gas emissions, DLC coatings could be a promising surface material applied on extremely stressed components of internal combustion engines to reduce friction and to extend component lifetime [8].

DLC is divided into two major categories, namely the hydrogenated amorphous carbon (a-C:H, ta-C:H) and the hydrogen-free amorphous carbon (a-C, ta-C). Both hydrogenated amorphous carbon (a-C:H) and hydrogen-free tetrahedral amorphous carbon (ta-C) coatings offer low friction performance and excellent wear resistance with diverse characteristics of friction and wear properties owing to their particular hydrogen contents and microstructure

[15]. Friction and wear sensitively rely upon system encompassing surface material, lubricants (oil and additive), environment (temperature, humidity) and lubrication condition [8], [15], [32], [33], [40]–[45]. It should be noted that most engine components are operated in the boundary lubrication regime. Under moderately severe contact conditions in the boundary lubrication regime, direct contact occurs between the sliding surfaces.

Numerous studies have conducted the friction test under the boundary lubricated regime for DLC coating [36], [46]–[48]. Nevertheless, many researchers studied the effect of different lubricating oil and additive to the tribological performance of the DLC coatings. Under appropriate base oil and lubricant additives, the tribological performance of various types of DLC coating provides ultra-low friction and high wear resistance [49]. Oil additives and DLC doping elements demonstrated substantial and valuable impact on the wear behavior [36], [37]. Nonetheless, evidence has shown that the use of oil additives containing phosphorus and sulfur results in substantial harmful effects to the environment upon the refinement process [50].

High hardness material commonly provides a higher wear resistance compared to the low hardness material under a moderate experimental setup. Nevertheless, with a severe condition, hard and brittle material with lesser crack resistance results in coating damage due to microfracture. Wear by means of fracture-induced, which has been regarded as a significant wear mechanism of brittle material can increase approximately ten times compared to abrasive wear [51]. In the case of DLC coatings, wear is accelerated by a through-thickness crack that causes spalling of the coating [22]. Furthermore, low hardness coating that forms of high fraction sp^2 carbon atoms also results in high material removal rates under severe conditions due to the structural modification such as graphitization of the

contact surface [23], [24]. The hardness of the DLC coating depends on the fraction of the sp^3 and sp^2 carbon structure [52].

Many studies have focused on the ta-C and a-C:H coatings, which demonstrated high wear or damage to the coating as the sliding distance, speed, temperature, and load are increased. According to a study by Ronkainen et al. [15], ta-C coating shows high wear resistance in contrast to the a-C:H, however, the ta-C coating created larger wear on the counterpart material. Superhard hydrogen-free ta-C coatings are denoted by a high fraction of tetrahedral bonded (sp^3) carbon atoms [10]. A study by Al Mahmud et al. [32] revealed that the coefficient of friction (CoF) for both ta-C and a-C:H coatings decreased and largely affected by the coating graphitization that consequently increased the wear rates. This finding is in agreement with a previous study by Tasdemir et al. [45], where the ta-C coating had limited durability causing high wear rates at high temperatures. In addition, the ta-C performance also degraded due to an increase in the sliding distance and load when ta-C slides against steel in pure base oil lubrication due to fracture-induced wear. These led to coatings worn out due to polishing wear combined with tribo-chemical wear [33]. Notably, several studies have shown that a-C:H coating had larger wear rates under a similar experimental condition with ta-C coating [23], [53].

Commonly, DLC is deposited with a layer of the homogeneous structure except for multilayer coating design. The current research introduced and investigated a novel Pillar and Mesh ta-C with as-deposited pillar and mesh structure. At present, investigation on the as-deposited coating structure and its influence on the tribological performance have been scant. Therefore, the current study is aimed to investigate the tribological features of the as-deposited pillar and mesh-type structure of tetrahedral amorphous carbon coating under base-oil lubrication conditions. Unlike the aforementioned DLC, Pillar and Mesh ta-C coating

properties are unique for its' pillar-like and mesh-like structure, which is characterized by the hardness controlled DLC in the direction of the coating thickness. This novel DLCs consists of a softer topmost surface layer (sp^2–rich mesh structure) and hard substrate-side layer (sp^3–rich conventional ta-C), proposed to improve both frictions and wear resistance of the coating.

2.2 Experimental details

2.2.1 Materials and lubricants

Cylindrical pin and disk were made of high carbon chrome steel (SUJ-2). Three forms of tetrahedral amorphous carbon (ta-C) supplied by the Nippon ITF Incorporated. These three forms of ta-C were described by the structure, which is conventional tetrahedral amorphous carbon (ta-C), pillar tetrahedral amorphous carbon (Pillar ta-C) deposited with pillar structure, and mesh tetrahedral amorphous carbon (Mesh ta-C) deposited with mesh structure. All three forms of ta-C coating were produced through physical vapor deposition (PVD). Additionally, fluid polishing was applied to remove the droplets on the coating surface that originate from the deposition process, which could affect the tribological performance of the coating. The base-oil applied in this research was poly-alpha-olefin 4 (PAO4) with a viscosity of 6.11 mm^2/s and a pressure-viscosity coefficient of 12.85 GPa^{-1} at 80 °C. The application of additive-free oil in this research permits the evaluation of the performance on the friction and wear of the DLC coating itself devoid of any impact from the additive in the lubricant.

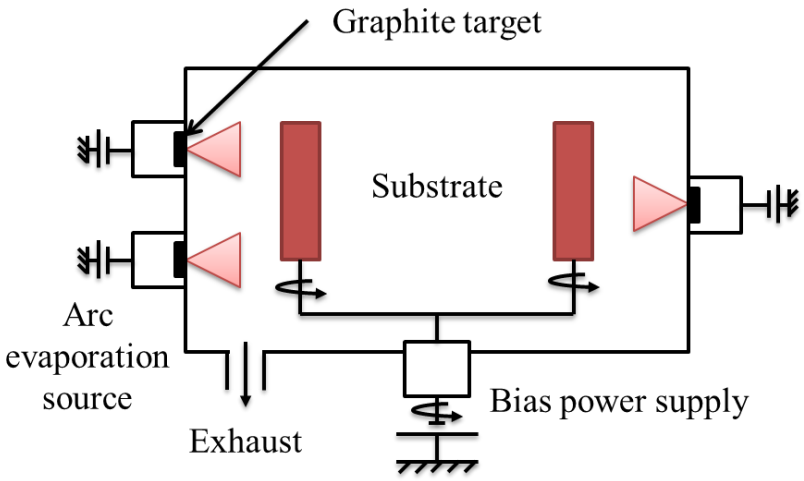

Figure 10 Schematic diagram of arc PVD equipment [18]

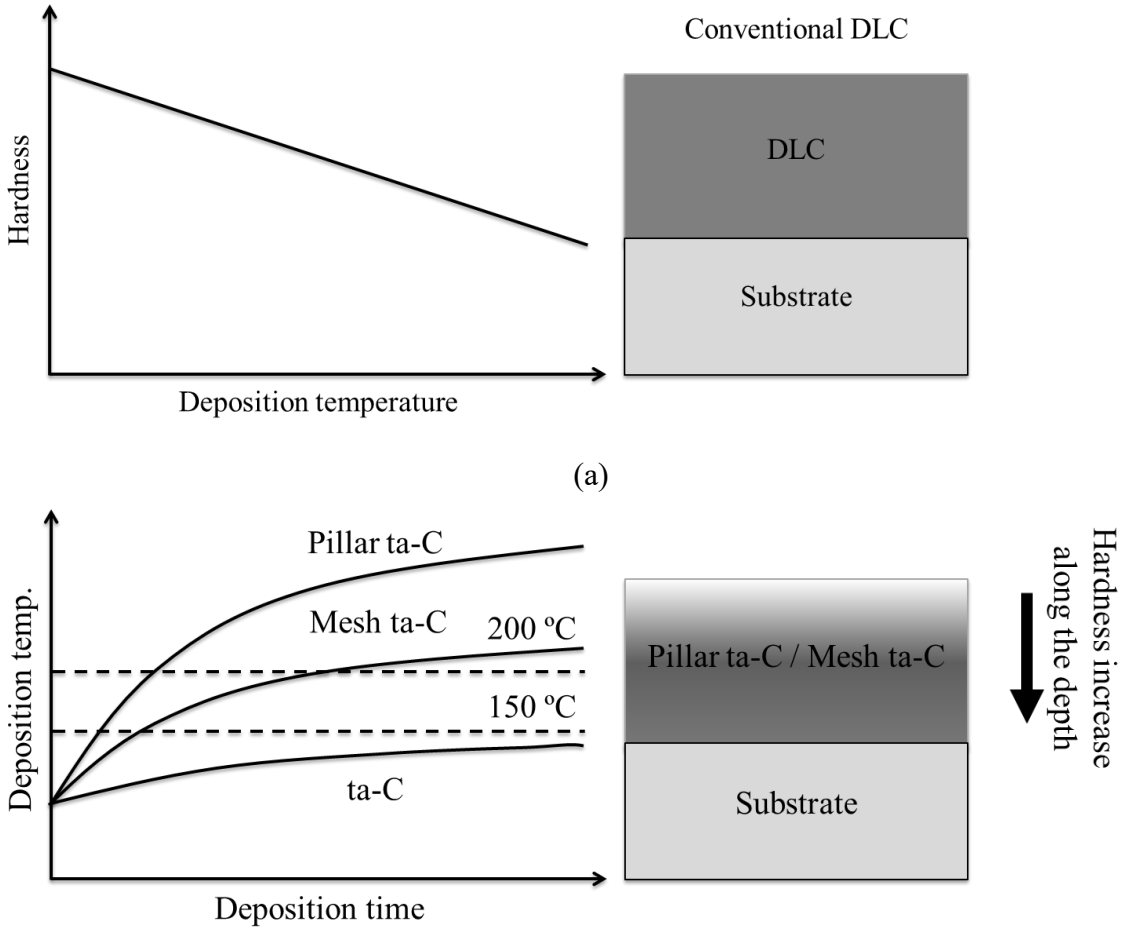

Figure 11 Deposition method and material concept of (a) conventional ta-C , and (b) novel Pillar and Mesh ta-C coating [18]

2.2.2 Details characteristic of Pillar ta-C and Mesh ta-C coating development

2.2.2.1 Deposition method and concept

Figure 10 illustrates the arc PVD equipment used to deposit hydrogen-free (H-free) DLC. Conventional ta-C and newly developed Pillar and Mesh ta-C DLC were deposited using the arc PVD equipment (M720) that could produce an arc discharge on a solid graphite target.

Typically, ta-C coating was deposited using the PVD method by controlling the deposition temperature below 150 °C by means of the cooling system during the coating growth as in Figure 11(a). Nevertheless, for the Pillar ta-C and Mesh ta-C deposition process, the substrate was heated up from room temperature to 200 °C continuously during the deposition process as illustrated in Figure 11(b). The hardness of the DLC coating decreased due to heating during the deposition process. By controlling the temperature distribution, the substrate-side coating is harder compared to the topmost surface coating. This feature is expected to reduce the effect of fracture-induced wear which is one of the reasons for ta-C coating short lifespan.

2.2.2.2 Coating structure

Transmission electron microscope (TEM) was used to observe the deposited ta-C, Pillar and Mesh ta-C structure. All samples were cut using a focused ion beam (FIB). Subsequently, the cross-sectional surface was observed using TEM H9000 UHR at an acceleration voltage of 300kV. The TEM images of the conventional ta-C, Pillar ta-C and Mesh ta-C are shown in Figure 12.

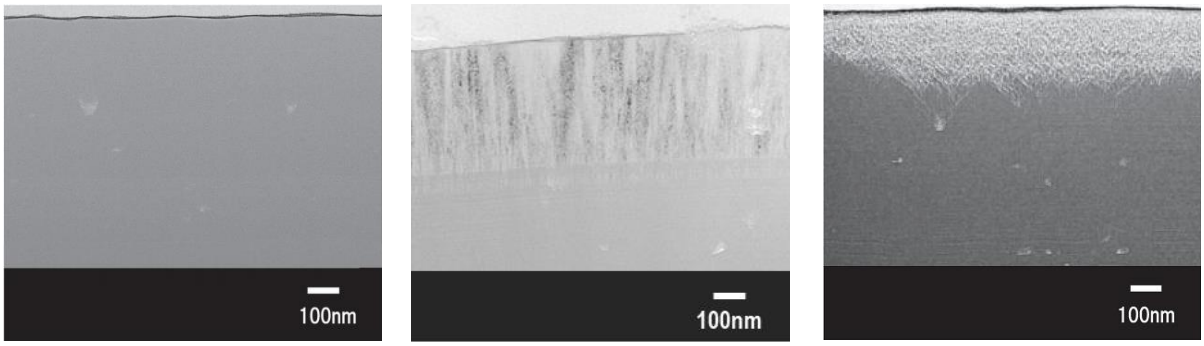

(a) (b) (c)

Figure 12 Cross-sectional TEM images of (a) conventional ta-C, (b) Pillar ta-C, and (c) Mesh ta-C [18]

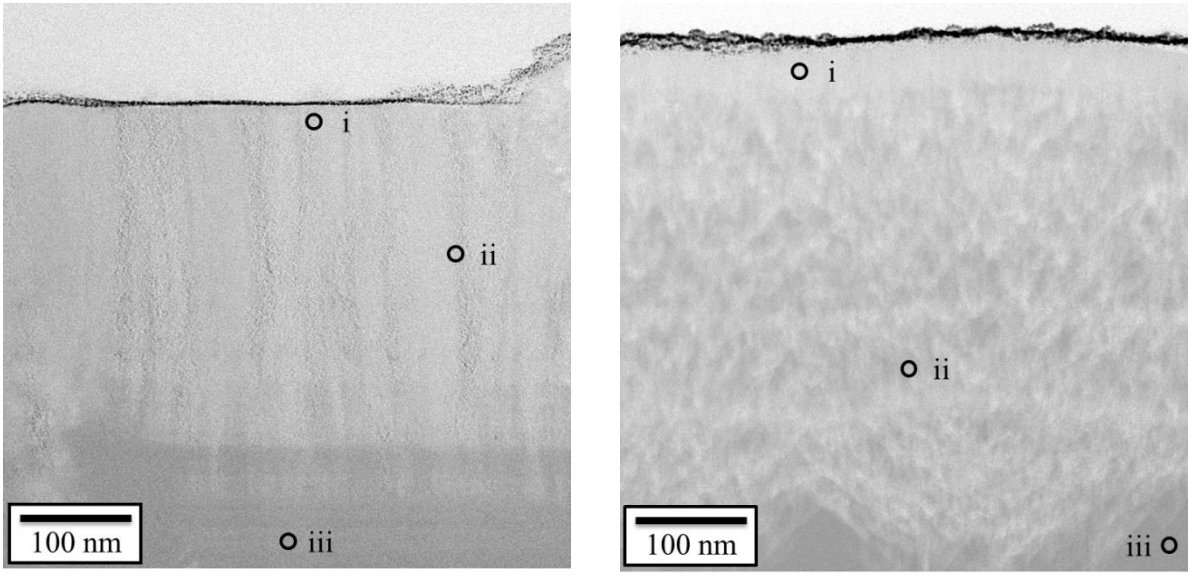

(a) (b)

Figure 13 Bright-field scanning transmission electron microscopy (BF-STEM) reticulated structure images of (a) Pillar ta-C and (b) Mesh ta-C

Figure 12(a) demonstrates that the structure of conventional ta-C did not undergo changes from the substrate to the surface of the coating. The structure can be classified as homogenous despite the presence of some micro-particles. On the other hand, Pillar ta-C and Mesh ta-C demonstrates a white layer that is located at a quarter of the coating thickness as

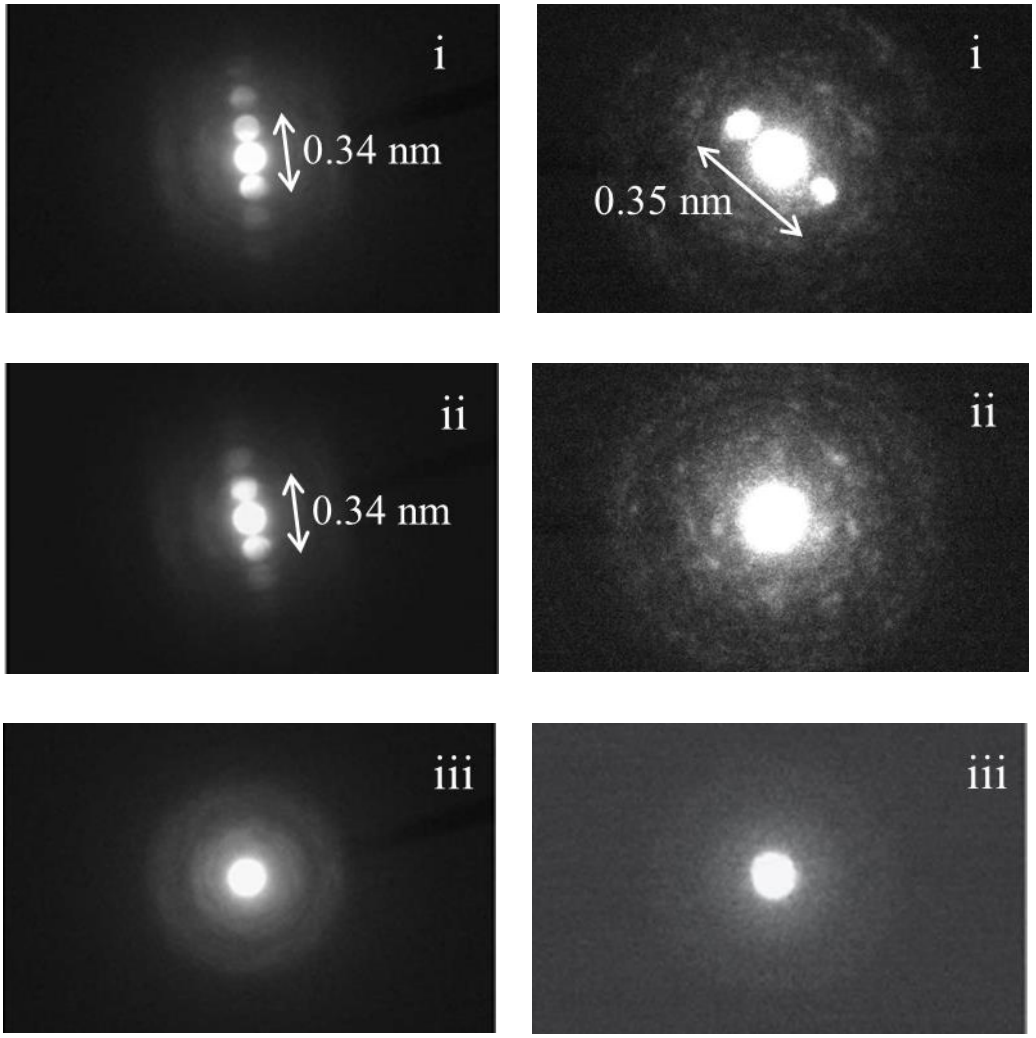

(a) (b)

Figure 14 Crystallinity evaluation at the specific area result for (a) Pillar ta-C and (b) Mesh ta-C

observed in Figure 12(b) and Figure 12(c), respectively. Moreover, the magnified image of the white layer as shown in Figure 13(a) and Figure 13(b) illustrates the reticulated structure growth from a microparticle, which is a feature of the arc technique applied for deposition.

The crystallinity analysis was conducted by electron diffraction method using Field Emission Electron Microscope JEM2100F, with 200 kV and 10^{-9} A acceleration voltage and absorbed current, respectively. Crystallinity assessment was performed at a specific area as

demonstrated in Figure 13(a) and Figure 13(b), where there were the distinct structures observed. The results of electron diffraction of both coatings are shown in Figure 14. At the diffraction spot indicated by number (i) for Pillar ta-C and Mesh ta-C coating, 0.34 nm and 0.35 nm diffraction image were observed, as shown in Figure 14a(i) and Figure 14b(i). This indicates the existence of a crystalline graphite microstructure in the Pillar and Mesh ta-C coating. Likewise, the crystallinity investigation at the spot indicates by number (iii) reveals the evidence of amorphous with the disordered pattern. On the other hand, no characteristic structure was observed for conventional ta-C coating, where only diffused disordered patterns observed, which indicates that it only consists of an amorphous structure.

2.2.3 Tribological experiments

The friction tests were performed via the cylindrical pin-on-disk tribo-tester, Figure 15(a) under boundary lubrication regime with a constant normal load of 5, 10 and 20 N on the DLC-coated cylindrical pin, corresponds to the maximum Hertzian contact pressures of 156, 220, and 311 MPa, respectively. The cylindrical pin holder, Figure 15(b) designed so it could create a large interference fit where it results in the large area of the cylindrical pin contact, and thus prevent the cylindrical pin from rolling during friction test. The cylindrical pin-on-disk tribo-tester method is mainly used for investigating the link between wear mechanisms, and the parameters including the contact pressure, sliding velocity, and environmental conditions. Cylindrical pin-on-disk can simulate the real line contact condition in the engineering application of sliding components (main bearing, etc.) inside the engine.

The DLC-coated cylindrical pin was rubbed against an uncoated SUJ-2 disk positioned 6.65 mm eccentrically from the center of the disk under a pure sliding condition through

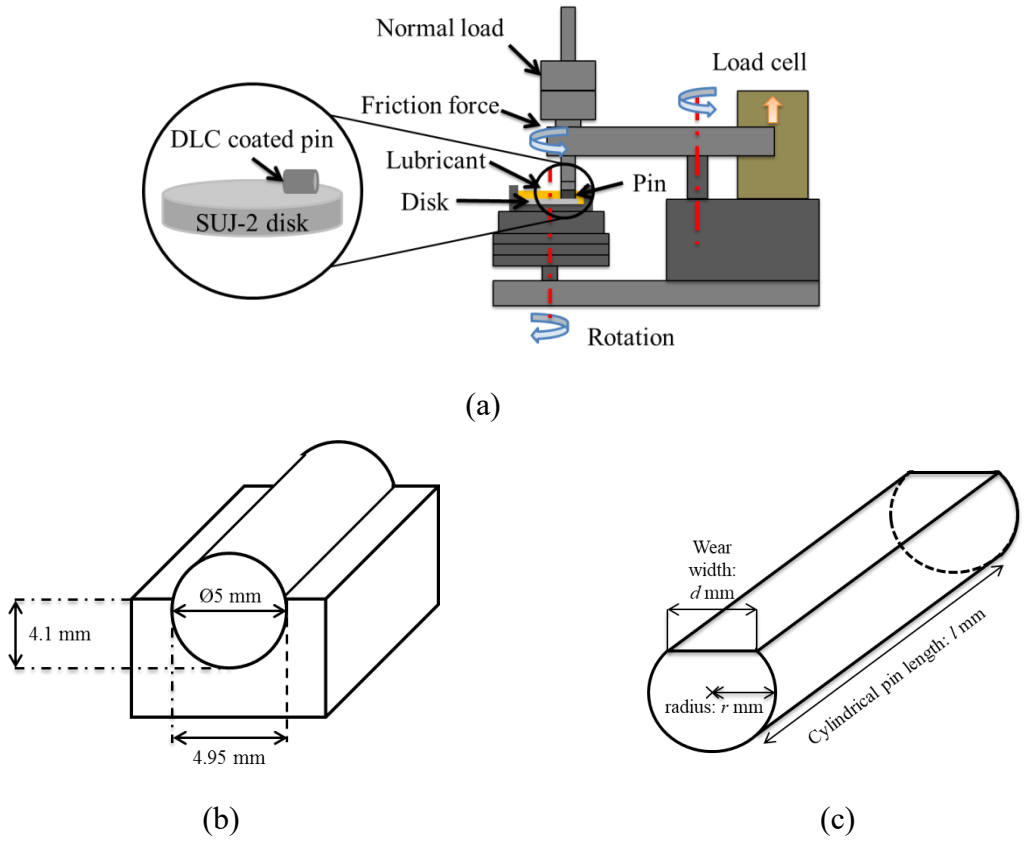

Figure 15 (a) Tribo-tester schematic and cylindrical pin-on-disk configuration, (b) cylindrical pin holder fixture with a pin attached, and (c) schematic diagram of the worn cylindrical pin

fixing the cylindrical pin to the upper jig to prevent it from rotating. Additionally, the disk was fixed on the lower holder, which was positioned on the rotary turntable. The speed and temperature of the tests were fixed at 0.068 m/s (100 rpm) for 60 minutes that corresponds to 250 m of sliding distance and 80 °C, respectively (Table 1). Both cylindrical pin and counterpart disk were making sure submerged under the PAO4 oil level at which heat was applied to uphold 80 °C temperature during the friction test. The dimensions of the cylindrical pin were 5 mm diameter and 5 mm length, whereas disk of 22.5 mm diameter and 4 mm thick were used in all experiments. In order to ensure the verification and reproducibility of the findings, each friction test were replicated three times. Liquid benzene

Table 1 Friction test setup parameters

Experimental setup	
Specimens (Cylindrical pin)	ta-C Pillar ta-C Mesh ta-C
Specimens (Disk)	SUJ-2 Hardness: 9.9 GPa Ra: 0.01μm
Rotation speed (m/s)	0.068
Constant normal load (N)	5, 10, 20
Temperature (°C)	80
Lubricant	PAO4
Duration (minutes)	60

and acetone was used as a cleaning agent in an ultrasonic bath to eliminate any contaminants on the DLC-coated cylindrical pin and disk.

Wear volume loss and specific wear rates of the DLC-coated cylindrical pin were quantified via Archard wear equations by calculating the width of the worn area by assuming that the shape of the wear track is rectangular-shape Figure 15(c) observed under the optical microscope as below:

$$k = \frac{V}{Fs} \qquad \textbf{Eqn. 3}$$

$$V = 2l \int_{\sqrt{r^2-\left(\frac{d}{2}\right)^2}}^{r} \sqrt{r^2 - x^2}\,dx \qquad \textbf{Eqn. 4}$$

Where k denotes the dimensional wear rates, F characterizes the applied normal load, s indicates the sliding distance, V symbolizes wear volume loss, d denotes the wear track width, l and r indicates the cylindrical pin length and radius, respectively. The relation

between the lambda ratio (Λ) and the minimum film thickness (h_{min}) for a rectangular shape are given by Eqn. 5, and h_{min} are quantified using Eqn. 6[54];

$$\Lambda = \frac{h_{min}}{\sqrt{R_{q.a}^2 + R_{q.b}^2}} \quad \textbf{Eqn. 5}$$

$$h_{min} = 1.806(w_z')^{-0.128}(\eta_0 \tilde{u})^{0.694}\zeta^{0.568}{R_x}^{0.434} \quad \textbf{Eqn. 6}$$

Where;

$R_{q.a}$ = roughness of the coated cylindrical pin

$R_{q.b}$ = roughness of the disk

w_z' = load per unit width (N/m)

η_0 = absolute viscosity at 0 Pa pressure and constant temperature (Pa.s)

$\tilde{u}$ = mean surface velocity (m/s)

ζ = pressure-viscosity coefficient (m^2/N)

R_x = effective radius of the cylindrical pin

The calculated film parameter was less than unity which indicates that the friction tests are initially under the boundary lubrication regime.

2.2.4 Surface analysis

NANOPICS 1000 Elionix ENT-1100a Nanoindenter was utilized to quantify hardness and Young's modulus of the DLC coatings. The surface average roughness, Ra was quantified via AFM (SPM-9700HT), and the structure of the DLC was characterized by the Raman spectroscopy (NRS-1000 Laser, Jasco Inc., Japan) through laser excitation wavelength of 532 nm with detection depth of within 300-600 nm [55]. The worn area of the cylindrical pin and disk were examined by optical microscope, FE-SEM (JEOL, JSM-

Table 2 Mechanical properties of the ta-C, Pillar ta-C and Mesh ta-C coatings

Properties	**Disk**	**Cylindrical pin**		
		ta-C	**Pillar ta-C**	**Mesh ta-C**
Dimension (mm)	22.5 x 4	5 x 5	5 x 5	5 x 5
Substrate material	SUJ-2	SUJ-2	SUJ-2	SUJ-2
Coating method	-	PVD	PVD	PVD
Thickness (μm)	-	0.8	1.65	1.17
Elastic modulus, E_f (GPa)	275.5	661	110	232.1
Hardness, *H* (GPa)	9.9	78.3	11.0	27.5
Roughness, *Ra* (μm)	0.010	0.021	0.055	0.026

7000FK), and AFM. Table 2 demonstrates the mechanical properties of the DLC-coated cylindrical pin and disk.

2.3 Result and discussions

2.3.1 Friction properties for DLC films under PAO4 boundary lubrication

The coefficient of friction plotted against the load for all three distinct DLC coatings sliding on-to SUJ-2 disk in PAO4 lubrication are illustrated in Figure 16. The CoF for Mesh ta-C was varied from 0.06 to 0.08. Furthermore, it possesses a similar pattern and range as observed in ta-C results for all loads examined regardless of the high as-deposited average surface roughness of the Mesh ta-C in contrast to ta-C coating. In addition, the Pillar ta-C coating possesses the slightly higher value of CoF at 20 N loads as a result of high average surface roughness of the contact surface on both coating and SUJ-2 disk. Although the CoF

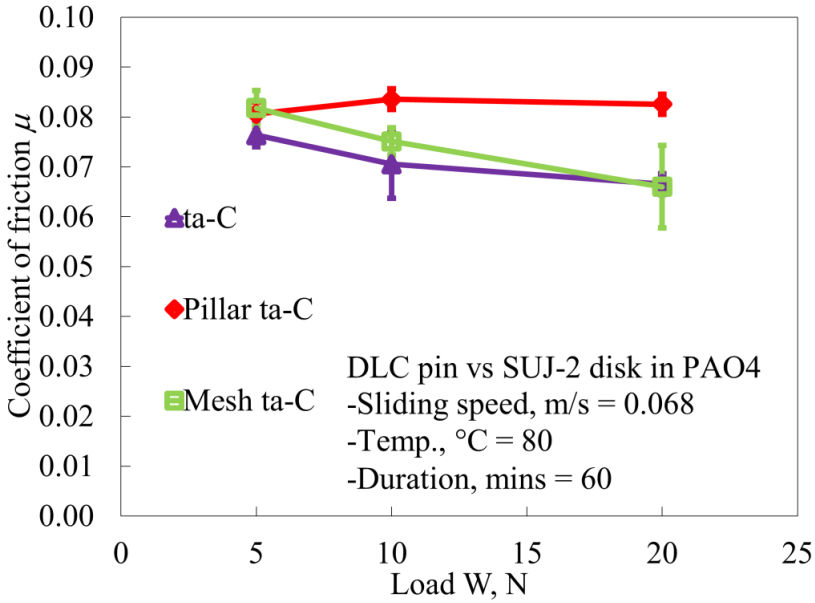

Figure 16 CoF result for ta-C, Pillar ta-C and Mesh ta-C coated specimen as a function of load

Table 3 Calculated lambda ratio Λ for ta-C, Pillar ta-C, and Mesh ta-C coatings

	Before friction test	After friction test
ta-C	0.27	0.46
Pillar ta-C	0.12	0.16
Mesh ta-C	0.24	0.75

for the Mesh ta-C is comparatively high in contrast to the ta-C at lower load, the CoF reduced and had approximately same results with ta-C once the load rise to 20 N. Based on the cross-sectional view of the Pillar and Mesh ta-C coating as illustrated in Figure 12(b) and Figure 12(c), the as-deposited Pillar and Mesh ta-C surface contains micro asperities, which is supported by the high average roughness of the coating. With the rise in load, the micro-asperities removal rates have elevated and reduced the roughness of the contact surface. This leads to a smoother contact surface as discussed in section 2.3.3.2.

There was no transition in the lubrication regime where the calculated lambda ratio Λ after the friction test is less than 1 as shown in Table 3. Since the calculated lambda ratio for every specimen used indicated that the friction test was conducted in the boundary lubrication regime, solid asperities of the coating has become the main mechanism for the improved tribological performance which dominated the contact rather than the oil film. But it is important to note that the lambda ratio measured in the case of Mesh ta-C increased to 0.75 which indicates that the friction test was approaching closer to the mixed lubrication regime. This characteristic could explain the reduction of friction coefficient results by allowing the formation of a thicker oil film.

2.3.2 Wear characteristic of DLC films in PAO4 oil under boundary lubrication

The detailed specific wear rates for every friction test were quantified on the DLC-coated cylindrical pins as to understand the influence of DLC structure on wear behavior and respective wear mechanism of Mesh ta-C coated specimens with regard to the applied loads. Figure 17 and Figure 18 demonstrate the findings of wear volumes and specific wear rates for all three forms of DLC coatings towards applied normal loads. Wear volumes for all examined DLC rise with distinct rates as the normal load increased.

From the optical microscope images shown in Figure 19, and Figure 20, and FE-SEM images shown in Figure 21, there were no tribofilm derived from the oil can be detected. Since the friction test was conducted in the PAO4 base oil which characterizes by its high thermal and oxidative stability, the possibility of tribofilm derived from the oil to form is relatively low.

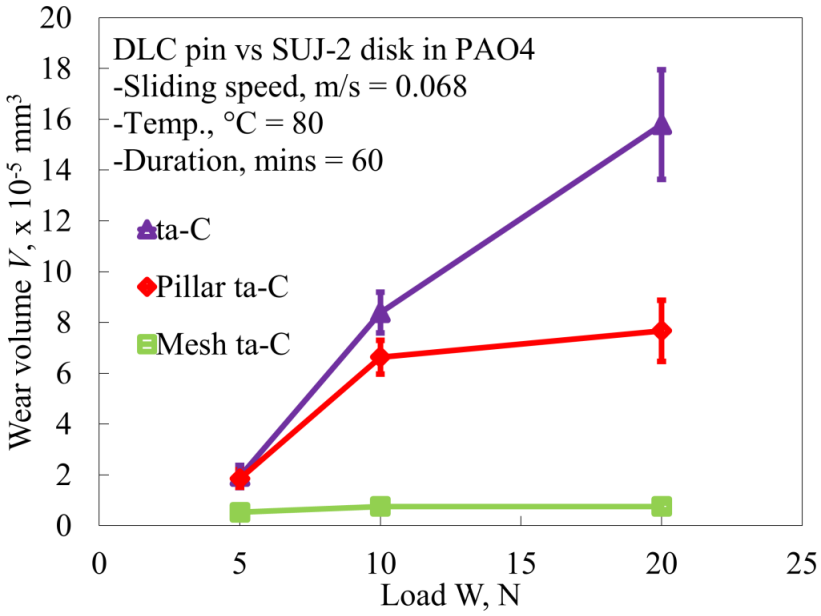

Figure 17 Wear volumes result for ta-C, Pillar ta-C, and Mesh ta-C coated specimen as a function of load

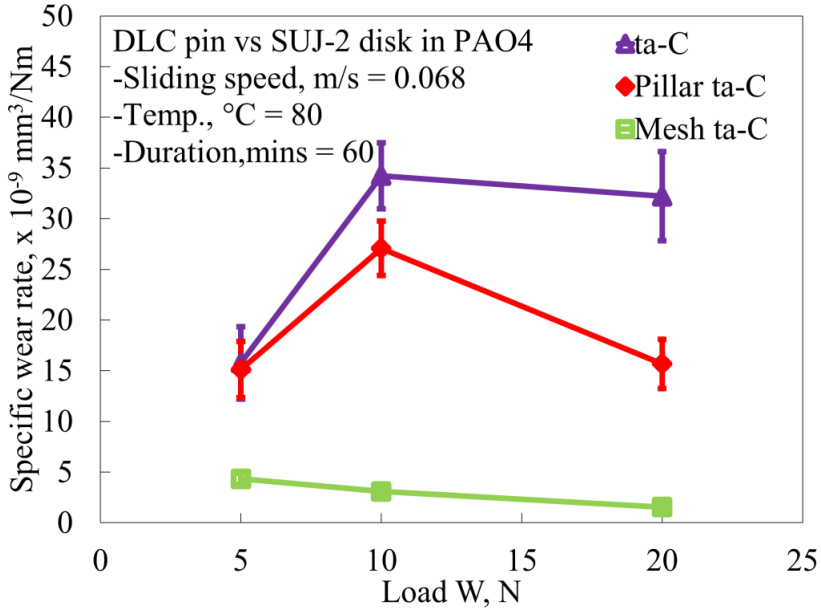

Figure 18 Specific wear rates result for ta-C, Pillar ta-C, and Mesh ta-C coated specimen as a function of load

The ta-C demonstrated severe wear with the increase in applied load, there was a linear increase in the wear volume of ta-C with the applied loads. As illustrated in Figure 19(a), partial spalling and delamination were observed on the contact area for the ta-C coating for entire tested loads. The number of partial spalling elevated with the increase in the load. Furthermore, the color transfer layer was observed at the edge of the wear track, which is discussed in section 2.3.3.1.

As for the Pillar ta-C, the wear scar width produces on the coating is not uniform (evident of ductile wear) as shown in Figure 19(c). Deep grooves and spallation observed in the area where the wear track width is not uniform. The hypothesis of these phenomena to occur is due to the nature of the pillar structure failed to absorb the radial force-induced friction test.

The Mesh ta-C demonstrated excellent wear resistance to entire applied loads. The wear rates of the Mesh ta-C specimens are extremely low ($1.5 – 4.3 \times 10^{-9}$ mm^3/Nm) for the entire applied loads. The wear rate of Mesh ta-C coating is approximately 21 times lesser than specific wear rates of ta-C coating at 20 N loads examined. It should be noted that the wear volume of Mesh ta-C had no impact on the increased applied loads. Figure 19(e) illustrates that there is no formation of micro-crack or partial delamination on the wear track of Mesh ta-C. In some way color transfer layer or wear debris left near the wear track, which is elaborated in section 2.3.3.1.

2.3.3 Worn area analysis

2.3.3.1 Raman spectroscopy and FE-SEM analysis

Raman spectroscopy is a non-destructive instrument for depicting crystalline, nano-crystalline, and amorphous carbons. Raman spectroscopy examination was performed to quantify the alteration in the structure following the friction test. Raman spectra of disordered graphite demonstrate two quite sharp modes, the G peak almost 1580–1600 cm^{-1} and the D peak around 1350 cm^{-1}. Raman spectra are sensitive to carbon alteration, and are linked mainly to the variations of the sp^2 phase and only weakly to the sp^3 phase [56]. Two main indicators demonstrate graphitization is the increase of I_D/I_G ratio, together with the shifting of G-peak to a higher position as depicted by the red dashed line in Figure 19(b), Figure 19(f), and Figure 20(b).

Graphitization of the DLC coating in base oil condition may occur either by the friction-induced heating under contact or high contact/shearing stress condition. However, the temperature-induced graphitization for the DLC requires up to 250 °C of contact temperature to occur, and the actual contact surface temperature also reported to be 100-130 °C higher than the pre-set test temperature as a result of contact area reduction [57]. Furthermore, the transition temperature for graphitization to occur becomes lower with the presence of hydrogen in DLC [58]–[61].

The colored layer observed in the wear track and adjacent to the edge of wear track of ta-C was assessed by the Raman spectroscopy along with samples of Pillar ta-C, Mesh ta-C, and on every counterpart SUJ-2 disk. The quantification performed at four distinct points for DLC coated cylindrical pin, which is inside and outside of the wear track, black/color wear

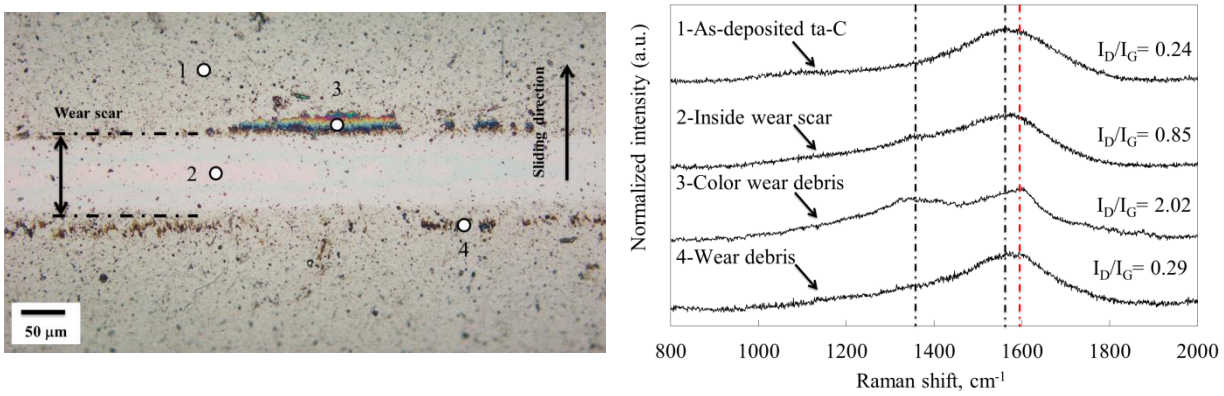

(a) (b)

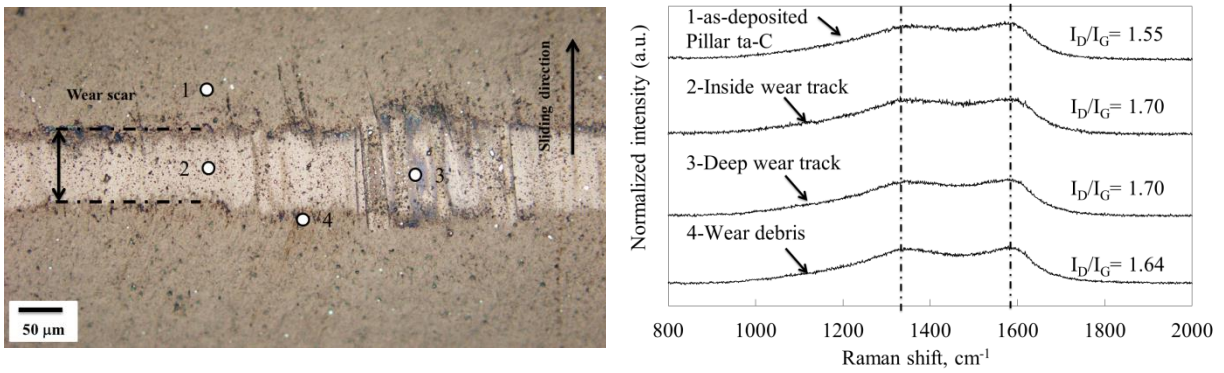

(c) (d)

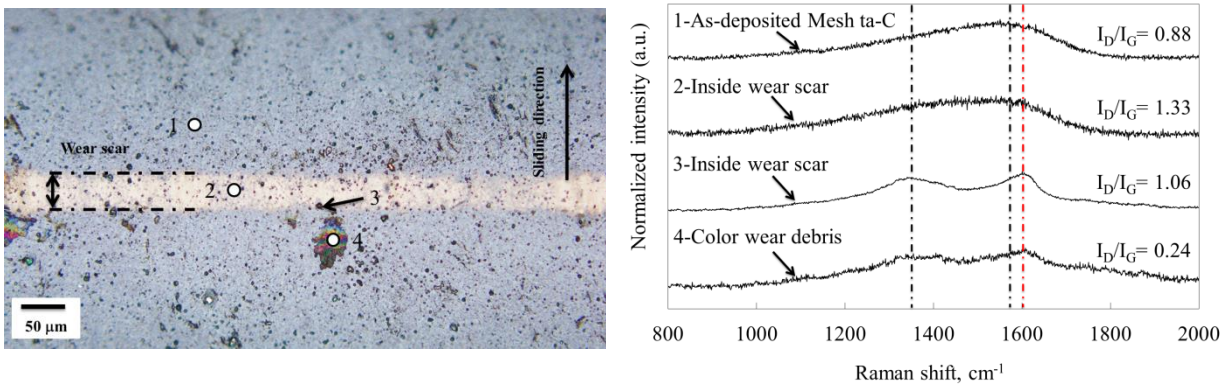

(e) (f)

Figure 19 Optical microscope images of the wear track on DLC coated cylindrical pin for (a) ta-C, (c) Pillar ta-C, and (e) Mesh ta-C; and Raman spectroscopy result of the specific points for (b) ta-C, (d) Pillar ta-C, and (f) Mesh ta-C for normal load of 20 N

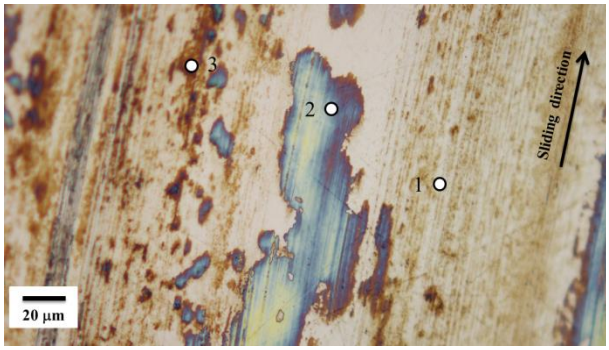

(a)

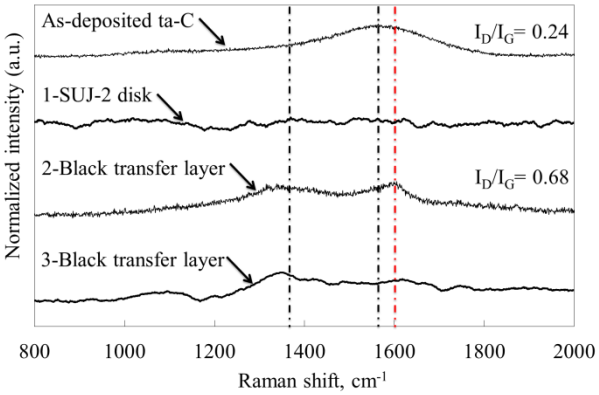

(b)

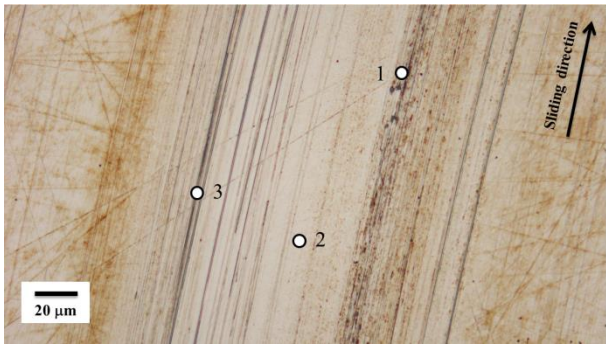

(c)

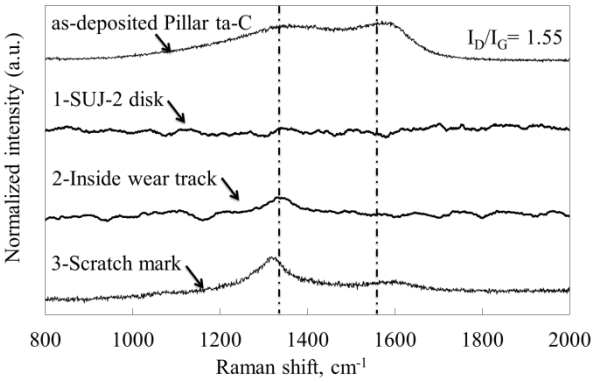

(d)

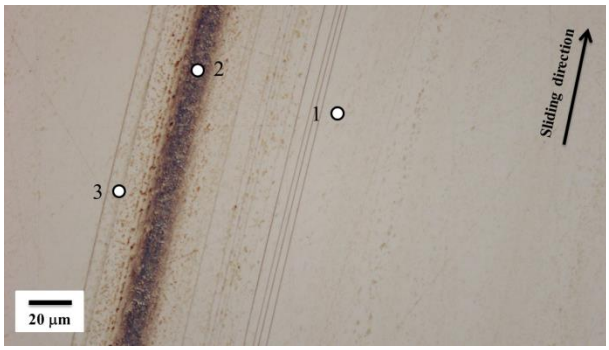

(e)

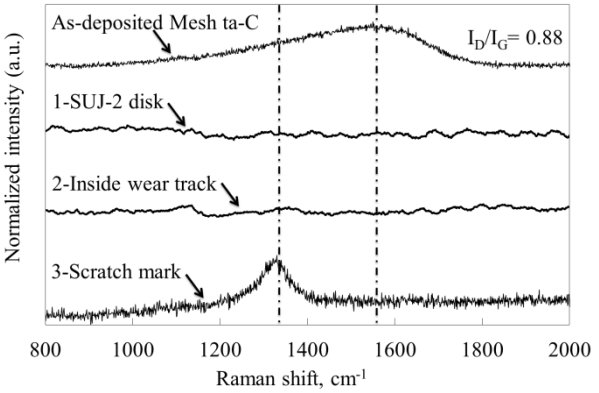

(f)

Figure 20 Optical microscope images of the wear track on SUJ-2 disk counterpart for (a) ta-C, (c) Pillar ta-C, and (e) Mesh ta-C; and Raman spectroscopy result of the specific points measured on the SUJ- 2 disk for (b) ta-C, (d) Pillar ta-C, and (f) Mesh ta-C for normal load of 20 N

debris inside and adjacent to the edge of wear track for ta-C, Pillar ta-C, and Mesh ta-C as illustrated in Figure 19(a), Figure 19(c), and Figure 19(e), respectively. Furthermore, Raman analysis performed at three points on SUJ-2 disk for each counterpart of ta-C, Pillar ta-C, and Mesh ta-C as shown in Figure 20(a), Figure 20(c), and Figure 20(e), respectively. Recent studies have shown that friction-induced graphitization at the sliding interface results in excellent DLC tribological performance through friction reduction and increase wear resistance [62], [63]. The transferred graphite-like layer to the sliding interface can provide excellent tribological performance as a result of the synergetic effect of the lubricant and the DLC.

Raman analysis on the wear track and outside of the wear track for ta-C demonstrates no formation of graphitization as illustrated in Figure 19(b). Nonetheless, the quantification carried out at the color wear debris adjacent to the border of wear track demonstrates the graphitization of the ta-C coating with the rise in intensity ratio from 0.24 to 2.02. The structural alteration in ta-C was demonstrated by X. Deng et al. [64], which indicated that the graphite structure partially formed under high-temperature tribology testing. Regardless of graphitization, the ta-C coating also shows low friction and reduced wear resistance when slides against steel at a temperature of 80 °C and above as a result of thermally activated tribo-chemical interaction between carbon and ferrous atoms [45]. Optical microscope image of the SUJ-2 counterpart material of ta-C show black transferred layer on wear track as shown in Figure 20(a). Raman analysis on this transferred layer reveals high-intensity ratio which confirms as the transferred graphitized layer from the ta-C coating during friction test as shown in Figure 20(b). For the ta-C coating against the steel contact, abrasive wear was observed on the sliding surface when lubricated in PAO4 and the coatings gradually damaged through brittle micro-fracture in the protruding part, which then advances to spalling and delamination of the coatings [9], [32], [35], [44].

Furthermore, Raman analysis results on the wear track of Pillar ta-C and SUJ-2 counterpart disk are shown in Figure 19(d) and Figure 20(d), respectively. The as-deposited Pillar ta-C coating is formed in combination of sp^2 and sp^3 phase, in which it results in a high I_D/I_G ratio of 1.55 as compared to the conventional ta-C which is 0.24. The comparison made between the measured I_D/I_G ratio at every point inside the wear scar and the as-deposited Pillar ta-C show almost similar value which indicates that there was no structural transformation even after the friction test. For the measurement on the wear track of SUJ-2 counterpart disk, it also revealed that there was no indication of transferred film from the Pillar ta-C coating, except the Raman spectra shows a sharp D-peak at measurement point number 2 and 3 which can be explained as the oxidize hematite (α-Fe_2O_3) phases at 290 and 1310cm^{-1} peak position [34], [52], [65]–[67].

Figure 19(f) demonstrates the finding of the Mesh ta-C Raman analysis, where the as-deposited structure also was formed in combination of sp^2 and sp^3 phase. Moreover, the quantification carried out inside the wear track illustrates that the I_D/I_G ratio elevated from 0.88 to 1.33. This characterizes the structural transformation to higher intensity graphitization. Therefore, regardless of the alteration in the average roughness of the as-deposited Mesh ta-C, the graphitization process could also characterize the CoF reduction. Furthermore, the increase in the intensity ratio does not affect the wear performance of Mesh ta-C coating. The Mesh ta-C could prevent the shearing of the graphite-like layer formed on the rubbing surface which results in high wear resistance of the coating. Additionally, the Raman analysis Figure 20(f) conducted on the SUJ-2 disk counterpart material shows no evidence of graphite-like structure being transferred as what can be observed in the case ta-C coating. However, Raman analysis on the scratch mark observed on the SUJ-2 disk Figure 20(f) shows only a D-peak similar to the SUJ-2 disk counterpart for Pillar ta-C, which the existence of oxidize hematite (α-Fe_2O_3) phases.

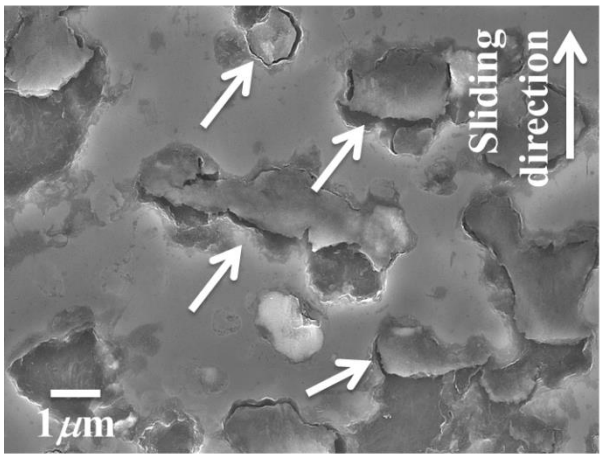

(a)

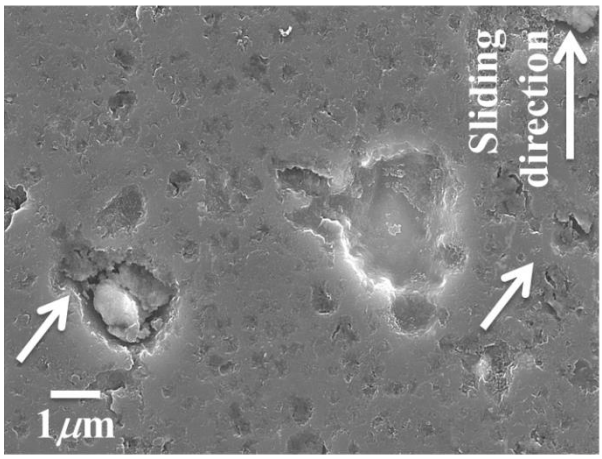

(b)

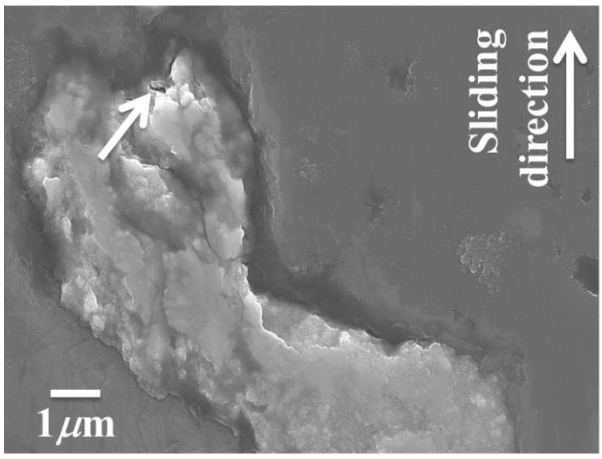

(c)

Figure 21 FE-SEM images of the wear track of DLC coated cylindrical pin for (a) ta-C, (b) Pillar ta-C, and (c) Mesh ta-C for normal load of 20 N

The FE-SEM image for ta-C Figure 21(a) demonstrates brittle micro-crack inside and near to the edge of wear track. This micro-crack turns into severe and propagates to the edge of wear track when the load is elevated. Based on FE-SEM image, it is well-established that the crack is a through-thickness crack, which then results in the spalling out and delamination of the coatings that function as the abrasive wear particles that quicken the wear. The findings of the wear track for the friction test of 10 N loads as illustrated in Figure 25(a) also indicates numerous micro-cracks that propagate and impair the coating.

Moreover, Figure 21(b) shows the FE-SEM image of the wear track on the Pillar ta-C coated pin. The wear track of the Pillar ta-C demonstrates the micro-crack formation which results in the spallation of the coating. Nonetheless, the number of the crack formed and spallation on the Pillar ta-C is less the crack formed on the conventional ta-C. In addition, the surface of the wear track contains numerous asperities which are supported by the high surface roughness of the coating that results in a high friction coefficient.

With regard to Mesh ta-C, the presence of several areas along the wear track demonstrates the non-uniform wear track width. This could be the consequence of the plastic deformation for the wear of ductile material [68]. In addition, there were no formations of micro-crack or delamination observed inside the wear track of Mesh ta-C. Nonetheless, micro-cracks were observed adjacent to the spot where spalling occurs, Figure 21(c) observed by FE-SEM. The crack has been shown to lead to the partial spallation of the coatings. Nevertheless, this micro-crack is not a category of through-thickness crack as it leads to partial spalling without any indication of coating delamination.

2.3.3.2 AFM analysis of worn surface

In order to elucidate the wear mechanism and behavior of ta-C, Pillar ta-C, and Mesh ta-C, the surface examination was performed on the wear track of both DLC coated cylindrical pin and SUJ-2 disk by AFM. The measurement areas were fixed at 50 x 50 μm to capture the surface of inside and outside of the wear track. Figure 22, Figure 23, and Figure 24 demonstrate the findings of AFM quantification on both coated cylindrical pin and SUJ-2 disk surface for ta-C, Pillar ta-C, and Mesh ta-C respectively after 1-hour friction test at 20 N loads.

Examination of the ta-C coated cylindrical pin indicates numerous spots with spallation of the coating and also several deep grooves were observed on the wear track as demonstrated in Figure 22(a). The surface profile of ta-C coated cylindrical pin wear track as illustrated in Figure 22(c) with an average roughness of 8.39 nm. Whereas the SUJ-2 disk also demonstrates clear deep grooves marks with an average roughness of 12.14 nm as in Fig. Figure 22(d). This verifies the spalling fragments of ta-C accumulated at the mating surface and functions as abrasive particles causing a severe scratch on the SUJ-2 mating surface. A combination of the micro-crack of the ta-C coating as described in section 2.3.3.1, spalling and abrasion by the mounted up ta-C fragments cause severe wear of the coating. Since ta-C is harder in contrast to SUJ-2 steel disk, it produces rough abrasive wear scratch lines corresponding to the sliding direction by means of the fragments of abrasive particles. Tasdemir et al. [53] demonstrated that wear behavior of the ta-C cylindrical pin lubricated with PAO4 indicated that wear occurs as polishing for DLC/steel contact.

For the Pillar ta-C as illustrated in Figure 23(a), a deep scratch mark on the surface of wear track is evident in contrast to as deposited. Besides that, the surface profile is illustrated

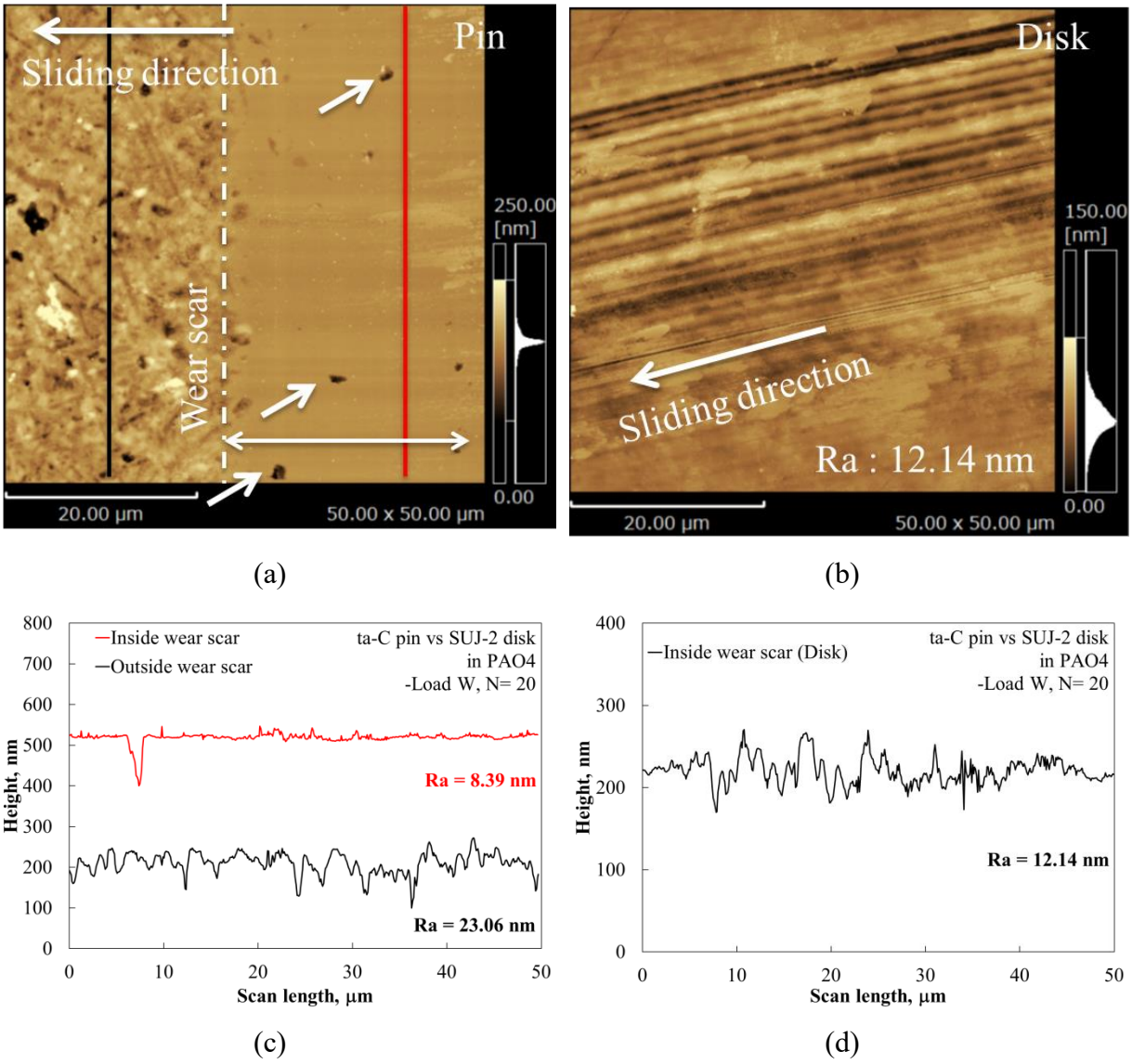

Figure 22 AFM images of the wear track for (a) ta-C coated cylindrical pin (b) SUJ-2 disk; and surface profile measured on the wear track for (c) ta-C coated cylindrical pin, and (d) SUJ-2 disk for normal load of 20 N

in Figure 23(c) where the average roughness of Pillar ta-C wear track decreased from 54.41 nm to 38.34 nm. But, the surface roughness not significant as it still shows the most roughers surface as compared to the ta-C and Mesh ta-C coatings. On the other hand, the counterpart material SUJ-2 disk as shown in Figure 23(b) indicates the scratch mark at numerous contact

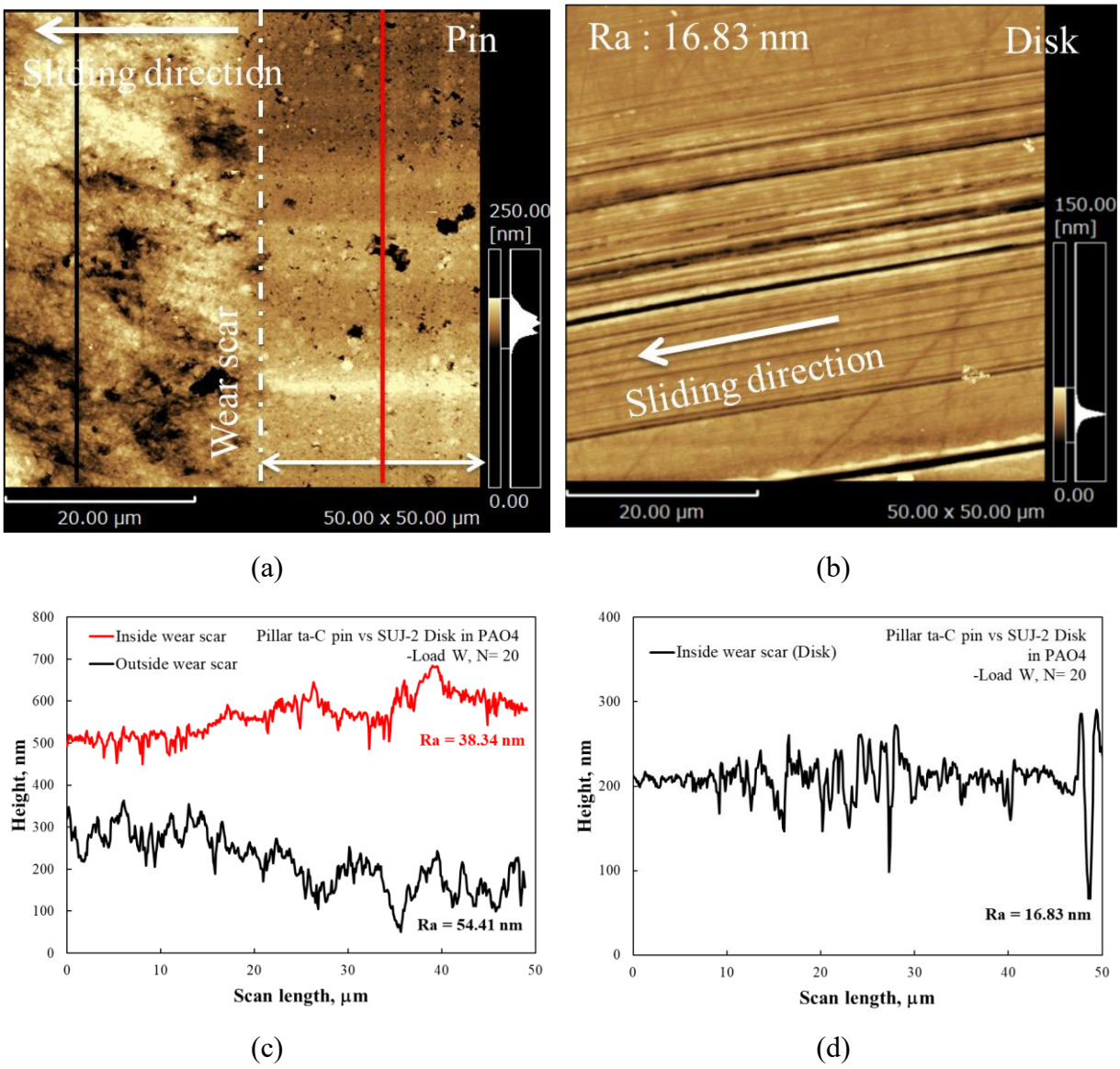

Figure 23 AFM images of the wear track for (a) Pillar ta-C coated cylindrical pin (b) SUJ-2 disk; and surface profile measured on the wear track for (c) Pillar ta-C coated cylindrical pin, and (d) SUJ-2 disk for normal load of 20 N

points with the quantified average surface roughness of 16.83 nm, which is also become the roughest surface of counterpart SUJ-2 disk. This phenomenon explained the result of the high friction coefficient recorded for Pillar ta-C as compared to the other coating.

For the Mesh ta-C, the wear track average roughness reduced nearly 3.5 times to 7.42

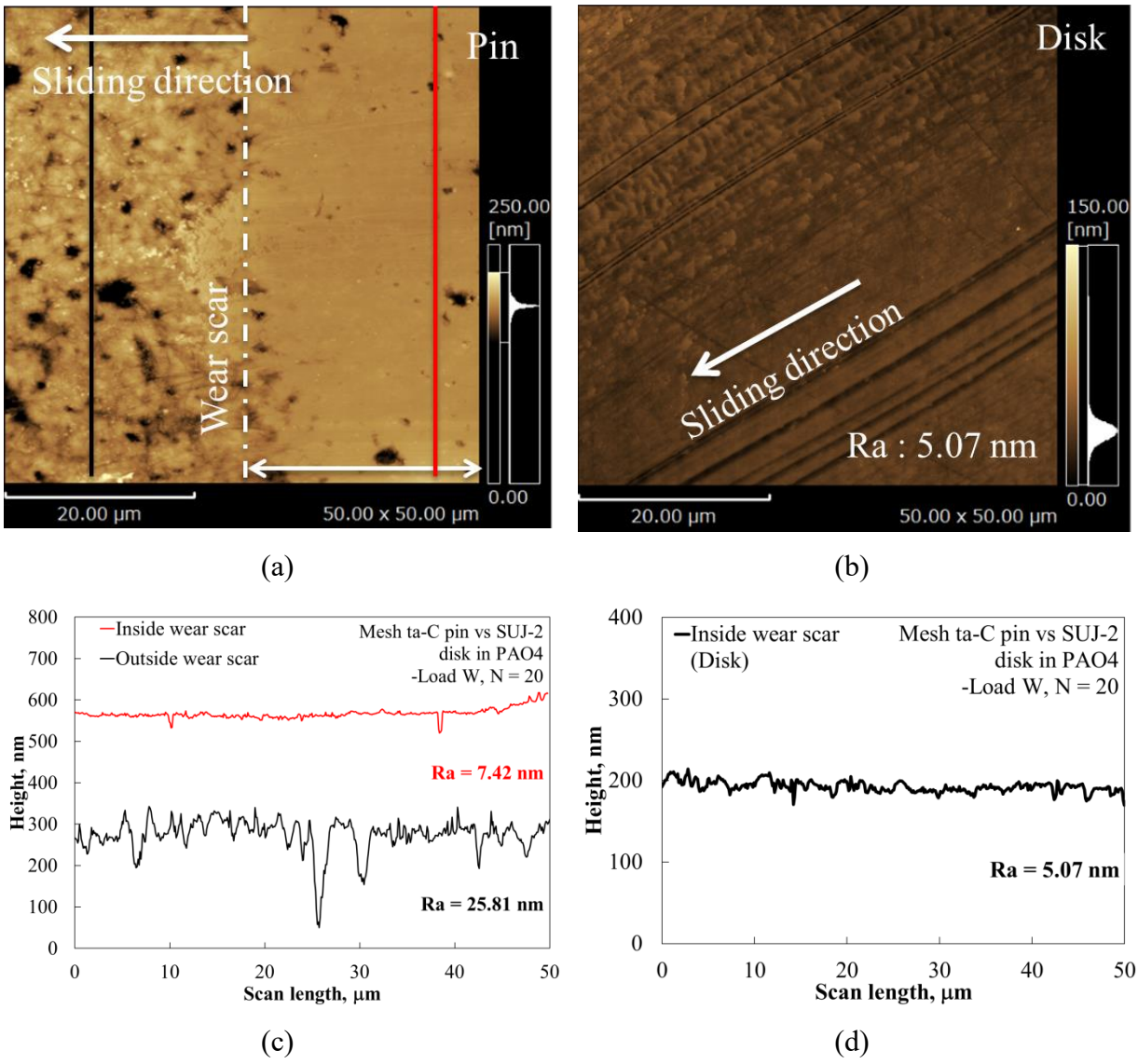

Figure 24 AFM images of the wear track for (a) Mesh ta-C coated cylindrical pin (b) SUJ-2 disk; and surface profile measured on the wear track for (c) Mesh ta-C coated cylindrical pin, and (d) SUJ-2 disk for normal load of 20 N

nm. The surface profiles of the wear track quantified on the Mesh ta-C coated cylindrical pin also indicates smoothers surface in contrast to as-deposited Mesh ta-C as illustrated in Figure 24(a) and Figure 24(c). Further examination on the mating material SUJ-2 disk exposes polishing effects that decrease the disk roughness by 2 times from 10 nm to 5.07 nm as

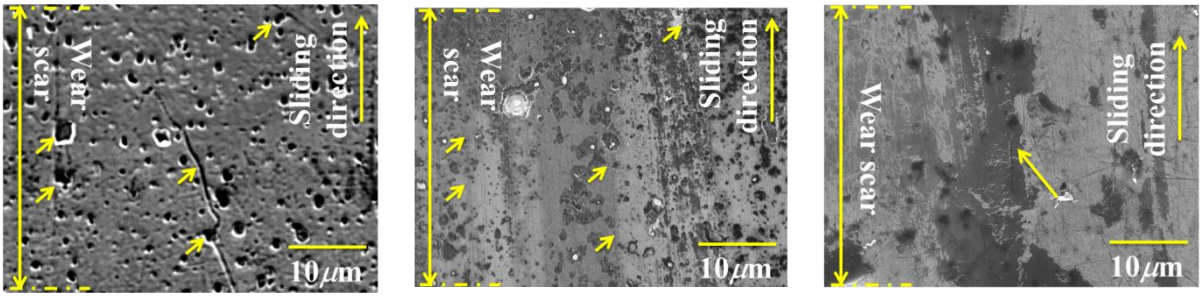

(a) (b) (c)

Figure 25 FE-SEM images of the wear track for (a) ta-C, (b) Pillar ta-C, and (c) Mesh ta-C coated cylindrical pin for an applied normal load of 10 N

illustrated in Figure 24(b) and Figure 24(d). The profile of the wear track on the SUJ-2 disk had less deep scratch marks owing to hard abrasive particles generated during friction test. Thus, friction reduction in Mesh ta-C was largely contributed by the surface smoothening which increases the lambda value from 0.24 to 0.75 after the friction test. This would favor the friction reduction by allowing the formation of a thicker oil film. Surface enhancement by solid nanoparticles has been reported to play an important effect that would reduce the friction and provide high wear resistance through interaction on the sliding surface [69]. But for the case of additive-free lubricant, the surface enhancement could be achieved by controlling the amount and size of abrasive particle produce during the friction test. Thus, the wear mechanism of the Mesh ta-C could be described through the inhibition of the micro-crack of the coating that prevents the generation of high hardness abrasive particles.

2.3.4 Crack resistance of the Pillar and Mesh ta-C

The Pillar ta-C and Mesh ta-C that is made up of sp^2-rich mesh structure offer excellent wear resistance despite the fact that the hardness of the Pillar and Mesh ta-C coating is nearly seven and three times lesser than the hardness of ta-C coatings, respectively. The

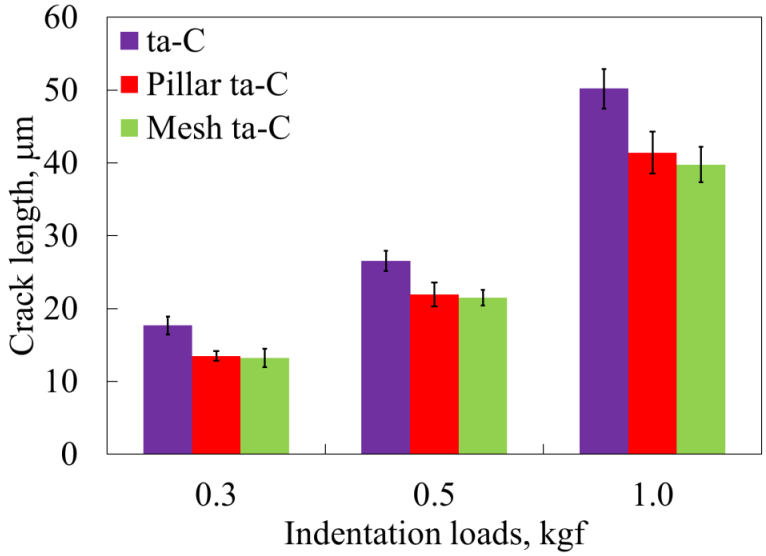

Figure 26 Radial crack length measured after indentation test under 0.3, 0.5, and 1.0 kgf loads

advantages of the Pillar and Mesh ta-C can be explained by the hardness, which has increased along with the coating depth from the topmost surface to the substrate. This leads to the prevention of the coating failures due to brittle micro-crack that results in coating spalling out and delamination. C. Charitidis et al. demonstrated that layered structure (sequence of soft/hard carbon layers) causing thick, stable and sp^3 rich films demonstrates improved adhesion strength in contrast to those that are rich in sp^2 content. This could sustain coating cracking without debonding. Layered structure coatings display nearly full elastic response, while on films rich in sp^2 content demonstrates massive brittle fragmentation [70].

As illustrated in Figure 21 and Figure 25, the Pillar ta-C and Mesh ta-C coating lack any brittle cracking and micro-fracture as compared to the conventional ta-C. Lesser micro-crack and spallation of the coating is observed on the wear track of Pillar ta-C. Furthermore, only a tiny crack without any evidence of spalling and delamination can be observed for Mesh ta-C coating. Moreover, the coating can be considered for transforming elastically in order to absorb the friction force during the test. Nonetheless, it is clear that crack is formed on the ta-C cylindrical pin even at a lower load, Figure 25(a). The brittle type cracking

observed on the cylindrical pin caused micro spalling and delamination, which formed high hardness fragments that abrasively accelerate the wear.

To further clarify the high crack resistance of Pillar ta-C and Mesh ta-C as compared to the ta-C coating, a micro-indentation test was conducted on both types of coating deposited on the Si-substrate. The radial crack length was measured from the center of the indentation mark to the crack tip. The result of the radial crack length was simplified in Figure 26 by averaging the crack length of 6 indentations test.

Mesh ta-C demonstrates the shorter radial crack length for all indentation loads applied, followed by the Pillar ta-C. The conventional ta-C shows the longest crack length, revealing poor fracture resistance of ta-C coating. By introducing the structure to the ta-C, the fracture toughness of the coating increased, and thus could prevent the crack propagation that progress into spalling and delamination of the coating. The soft structure sp^2 phase terminates the crack propagation through energy release by plastic deformation leads to film toughness enhancement [71]. This is supported by the latest finding by X. Sui et al. [72] which reported that high crack propagation resistance and elastic recovery capability through multilayer design of hard and soft film result in excellent tribological performance. Moreover, increased elastic recovery by means of reducing the plastic deformation area results in improved coating toughness [73], [74].

Figure 27(a), Figure 27(b), and Figure 27(c) show the FE-SEM images of the indentation mark on the ta-C, Pillar ta-C and Mesh ta-C coating, respectively. It is evidenced that the diagonal length of the indentation mark on ta-C, Pillar ta-C and Mesh ta-C is identical even though the ta-C is seven and three times harder than Pillar ta-C and Mesh ta-C, respectively. Furthermore, investigation of the radial crack and the indentation mark reveal

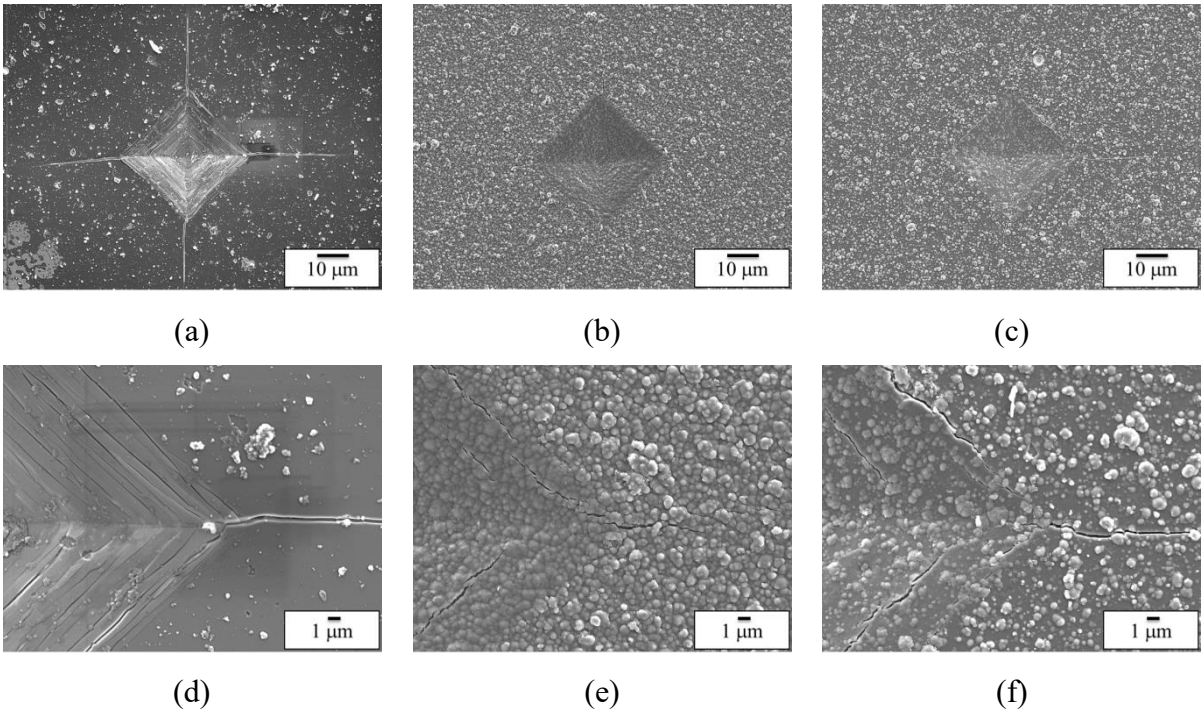

Figure 27 FE-SEM images of indentation mark and radial crack formed on (a) ta-C, (b) Pillar ta-C, and (c) Mesh ta-C coatings; and magnified indentation mark of (d) ta-C, (e) Pillar ta-C, and (f) Mesh ta-C for 1.0 kgf indentation loads

different crack type between ta-C and Pillar ta-C/Mesh ta-C. The radial crack formed on ta-C coating is finer as compared to radial crack formed on Pillar and Mesh ta-C sample. The ta-C coating also demonstrates a fine layer cracking pattern inside the indentation mark as shown in Figure 27(d), which is explained by the inability of the coating to undergo elastic/plastic deformation under loading conditions causing brittle cracking. A large number of transverse cracks in and around the indentation mark can be observed due to the high hardness and brittle characteristic of ta-C coating.

Moreover, investigation of the indentation mark of Pillar and Mesh ta-C coating shows a distinct crack type where each crack was not connected as shown in Figure 27(e) and Figure 27(f), respectively. This proves the hypothesis that both Pillar ta-C and Mesh ta-C undergoes elastic/plastic deformation to absorb the induced tensile stress upon loadings, which result in

ductile cracking. The intersection effect and soft sp^2 structure could restraint the crack propagation in Pillar and Mesh ta-C. In addition, the as-deposited Pillar and Mesh ta-C top surface form in a combination of sp^2 and sp^3 carbon phase as compared to the only sp^3 that exist in conventional ta-C. This feature has been reported to provide high toughness coating with a relatively low hardness as the sp^3 contents reduce [74]. Thus, the reasons for higher wear rates of the Pillar ta-C as compared to the Mesh ta-C coating is the lower hardness of the contact surface as well as slightly lower fracture resistance.

2.4 Conclusion

The current study examined the effect of Pillar and Mesh structure DLC coating on tribological performance, particularly with regard to friction and wear in base-oil lubrication conditions. The findings of the friction test revealed that the Mesh ta-C had a similar pattern and value of the friction coefficient to that of ta-C. Apart from that, there were no graphitized transferred-film found on the SUJ-2 disk for Pillar and Mesh ta-C. Mesh ta-C friction reduction is explained by the surface smoothening due to the polishing effect. With regard to wear, both Pillar and Mesh ta-C offers good wear resistance in contrast to the ta-C. Furthermore, specific wear rates of the Mesh ta-C at high load decreased by 93% in contrast to the ta-C at a nearly similar coefficient of friction. Raman analysis of the Pillar and Mesh ta-C and its counterpart worn area shows the reduction of wear effect due to the formation of graphite-like structure on the contact surface. Examination of the wear track of the Pillar and Mesh ta-C coated cylindrical pin demonstrates the deterrence of crack initiation and propagation, where there was a lack of evidence pertaining to cracks in contrast to the ta-C. Also, Pillar and Mesh ta-C could sustain the induced tensile stress by elastic/plastic deformations as confirmed by the indentation test. Moreover, less amount and size of high hardness abrasive particles generated also contributes to the high wear resistance of Mesh ta-

C which is verified through reduction of the as-manufactured average roughness, Ra of counterpart material. This results in increased lambda value which allows the formation of a thicker oil film. As for ta-C coating, brittle micro-fracture was observed, which progresses to partial spalling and functions as the high hardness abrasive particles to accelerate the wear. Hence, the Pillar ta-C and Mesh ta-C indicates excellent wear resistance owing to the inhibition of microfracture and cracks propagation by the structure together with the reduction of abrasive particle production.

Chapter 3
Effect of Fracture Toughness of Pillar and Mesh Structure Tetrahedral Amorphous Carbon (ta-C) Coatings on the Wear Properties under Base-oil Lubrication Condition

3.1 Introduction

Diamond-like carbon (DLC) is well-established in enhancing the tribological performance of the mechanical parts, especially in the automotive industry to decrease both friction and wear. DLC exhibits significant features including high hardness in addition to wear resistance that makes it highly promising for tribological application. The application of the DLC coatings is commonly for the high contact pressure component. Therefore, the coating crack resistance or fracture toughness often restricts the performance or service lifetime. In general, fracture toughness refers to the capability of the material to resist the pre-existing crack growth. Toughness is the measure of energy utilized to produce crack and facilitating crack to propagate causing fracture. Meanwhile, fracture toughness is known as the energy that is needed for crack propagation to failure [19]. Frequently, toughness is known as the energy absorption capacity of film material for the duration of the transition from deformation to fracture. Toughness is an essential mechanical property with regard to

the cohesive force of DLC film in which it indicates the film capacity to resist the formation of cracks near the defects in the film caused by the stress accumulation [75].

The mechanical properties are well-known to limit the performance and reliability of a thin coating like DLC. Application of DLC coating such in the automotive components by means of rubbing of two components leads to enhancing the features including the friction and wear characteristics. Therefore, there have been increased studies on enhancing the tribological characteristics of the coatings by modifying the deposition methods and doping elements. Nevertheless, there are several limitations in evaluating of the DLC coating wear performance via the fracture toughness. Evidence has shown that harder coatings like ta-C are highly brittle and can be readily fractured by high-pressure contact throughout the application. Hence, in order to examine the brittleness of the thin coating, it is crucial to quantify the fracture toughness.

Hardness is among the key factors in regulating the wear performance of the DLC coating. As such, high hardness with low crack resistance is associated with severe wear due to through-thickness crack [22]. Similarly, high sp^2 carbon atoms DLC coating that is low in hardness could lead to high wear as the results of structural alteration including graphitization of the contact surface under severe condition [23], [24]. DLC is frequently deposited with a layer of homogeneous structure excluding multilayer coating patterns. Therefore, tailoring the properties, particularly the hardness by employing the DLC structure could promote superior wear performance.

The DLC coating is associated with the deposition of the coating onto a substrate. Therefore, the technique that was employed to examine the fracture toughness for the bulk material is not feasible for evaluating the fracture toughness for the coating [25]. It should be noted that the quantification of the fracture toughness of the coating is still challenging owing

to the thickness limitation of the DLC coating [26]. The measurement of the crack length during indentation could be utilized to evaluate the fracture toughness. On that account, the current study applied Vickers indenter as it has been demonstrated to form bigger radial cracks that provide better accuracy of cracks length measurement. Thus, the radial crack formed follows the axis of diagonal of the indent and restraint the coating from secondary crack growth and chipping [27], [28]. The plastic zone that is prolonged under the loading condition deploys the tensile stress into the coating. Moreover, additional stress is generated throughout the unloading condition when the elastically strained coating initiated to resume its actual shape. Nonetheless, the aforementioned process is limited by the permanent deformation linked to the plastic zone [30]. Radial crack on the coating is generated during the unloading process, which forms the residual tensile stresses [31]. Frequently, the indentation on specimens leads to both elastic and plastic deformations. In brittle materials, plastic deformation generally exists with pointed indenter including Vickers.

Evidence has revealed that the alteration of the structure by multilayer coating deposition has shown to decrease the impact of the adhesive wear, improve the fracture resistance and load carrying capacity, as well as elastic recovery value [72], [74]. The current study evaluated wear performance and the fracture toughness of conventional tetrahedral amorphous carbon (ta-C), pillar structure ta-C (Pillar ta-C), and mesh structure ta-C (Mesh ta-C) through micro-indentation technique. The findings of this study could provide further insight into understanding how the fracture toughness affects the tribological performance of the coatings and how the structure of a coating results in higher fracture toughness in addition to wear resistance.

3.2 Experiment details

3.2.1 Specimens

Three types of ta-C coatings were differentiated by the structure variation; ta-C had the uniform structure, whereby the Pillar and Mesh ta-C were generated with pillar and mesh structure, correspondingly, as depicted in Figure 29(a), Figure 29(b), and Figure 29(c). All samples were provided by the Nippon ITF Inc. The deposition of the aforementioned coatings was performed on (100) single crystalline silicon (Si-wafer) substrates by physical vapor deposition (PVD) technique.

The thickness and surface roughness of the deposited coating was determined via the surface profilometer (S-3000, Mitsuyo, Japan). Moreover, the NANOPICS 1000 Elionix ENT-1100a Nanoindenter was used to determine the hardness and Young modulus of the coating. Residual stress induced through the deposition process was determined by Stoney equation by calculating the radius of curvature of the Si-wafer pre-deposition and post-deposition procedures. The mechanical and physical characteristics of the coating samples utilized in this study are presented in Table 4.

Table 4 Characteristics of the ta-C, Pillar ta-C, and Mesh structure ta-C coatings

Samples	**Film thickness d, μm**	**Elastic Modulus E_f, GPa**	**Hardness H, GPa**	**Compressive Residual Stress σ_c, GPa**
ta-C	1.5	310	40.1	1.75
Pillar ta-C	1.42	143	18.0	1.26
Mesh ta-C	1.25	184	20.0	2.15

3.2.2 Characteristic of Pillar and Mesh ta-C details

3.2.2.1 Concept and preparation method

A total of three types of ta-C coatings, namely conventional ta-C, Pillar ta-C, and Mesh ta-C were prepared using M720 PVD apparatus. Mesh and Pillar ta-C coating were deposited through modifying the method utilized to deposit conventional ta-C coating. In the deposition process of conventional ta-C, the cooling system was employed to maintain the temperature below 150 °C as illustrated in Figure 28.

Similarly, the heating system was applied to increase and maintain the temperature of the substrate at above 200 °C throughout the process of depositing Pillar and Mesh ta-C. The application of continuous heating resulted in a decline in the coating hardness when the coating thickness was increased as the graphitic structure formed during coating growth.

3.2.2.2 Coating structure

Cross-sectional image of the coating was generated through observation via the focused ion beam (FIB) under a transmission electron microscope (TEM H9000 UHR), Figure 29 and Figure 30.

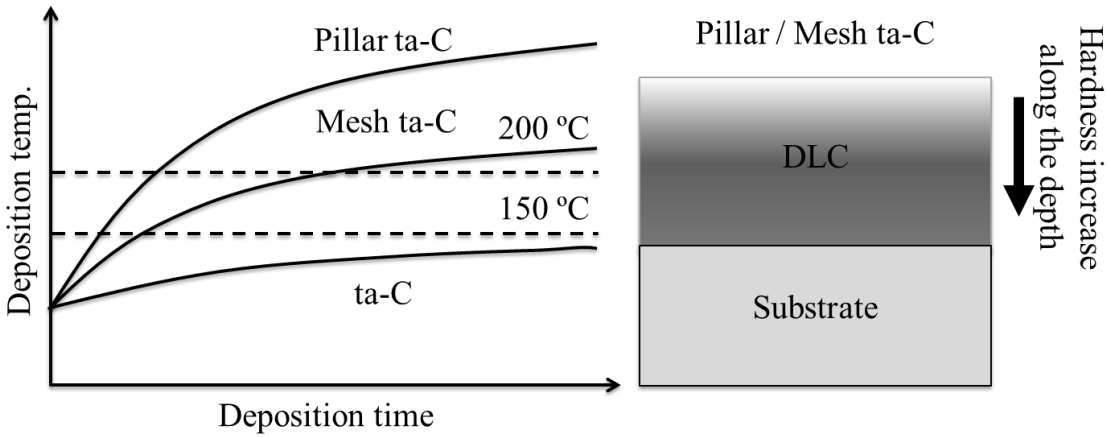

Figure 28 Analysis of conceptual deposition technique for conventional ta-C coating, Pillar and Mesh ta-C DLC coating

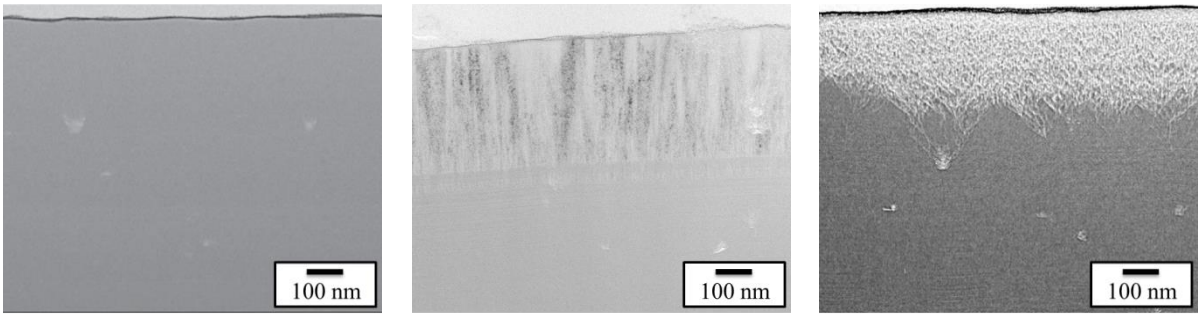

(a) (b) (c)

Figure 29 Cross sectional cut of (a) conventional ta-C, (b) Pillar ta-C, and (c) Mesh ta-C

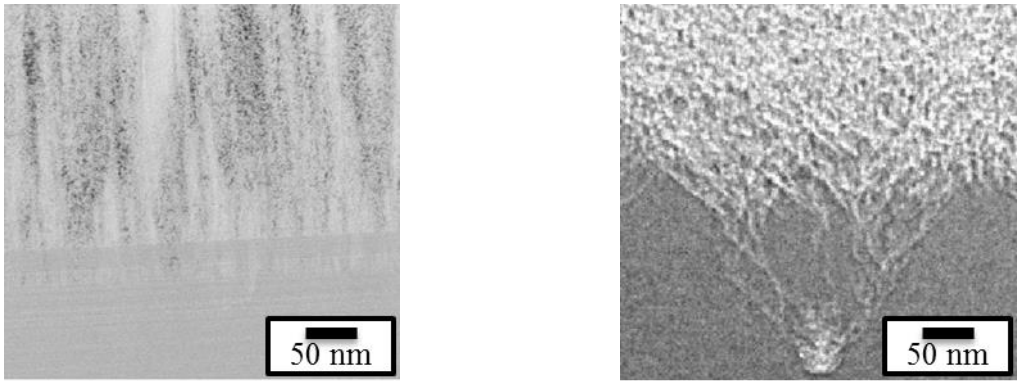

(a) (b)

Figure 30 Magnified images of reticulated structure for (a) Pillar ta-C, and (b) Mesh ta-C

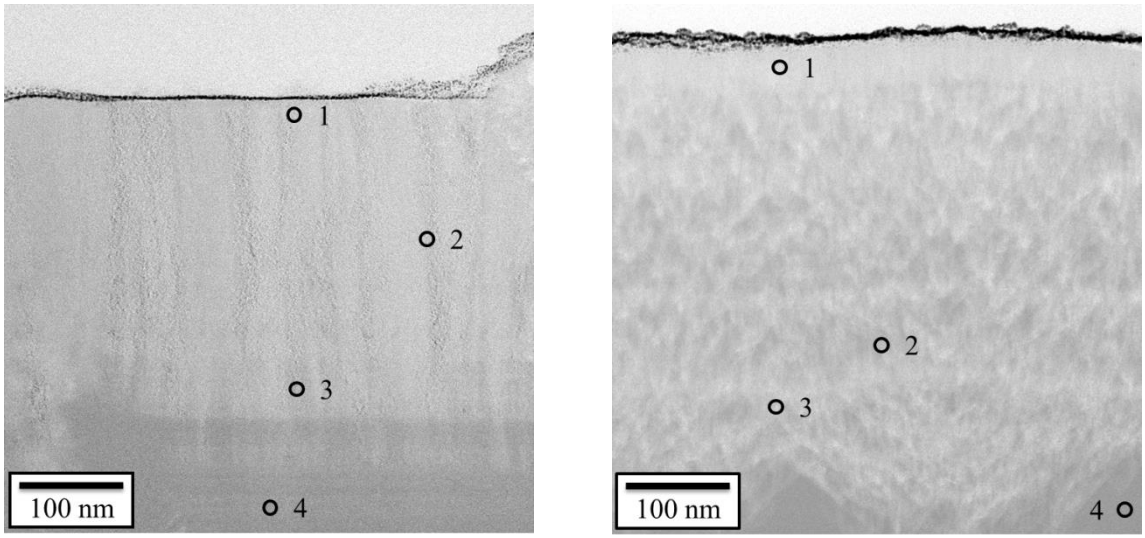

(a) (b)

Figure 31 Micro-electron diffraction acquisition position for (a) Pillar ta-C, and (b) Mesh ta-C

Concerning conventional ta-C cross-sectional images, Figure 29(a) demonstrates characteristics of a homogenous structure. Moreover, the Pillar and Mesh ta-C demonstrated a reticulated structure originated from the microparticle, produced by the arc deposition method as presented in Figure 29(b) and Figure 29(c), respectively. Micro-electron diffraction analysis was performed at many spots on the cross-sectional of the Pillar ta-C and Mesh ta-C as illustrated in Figure 31(a) and Figure 31(b), correspondingly. According to the International Center for Diffraction Data (ICDD) database, the crystalline graphite lattice spacing constant is 0.33756 nm. The results of the crystallinity experiment performed using the electron diffraction method by TEM JEM2100F are depicted in Figure 32(a) and Figure 32(b). The Pillar ta-C and Mesh ta-C were generated nearly 0.34 nm and 0.35 nm spacing, respectively. The obtained crystallinity result is almost similar to the ICDD data which indicates the presence of crystalline graphite microstructure at the quarter of the coating thickness of Pillar ta-C and Mesh ta-C.

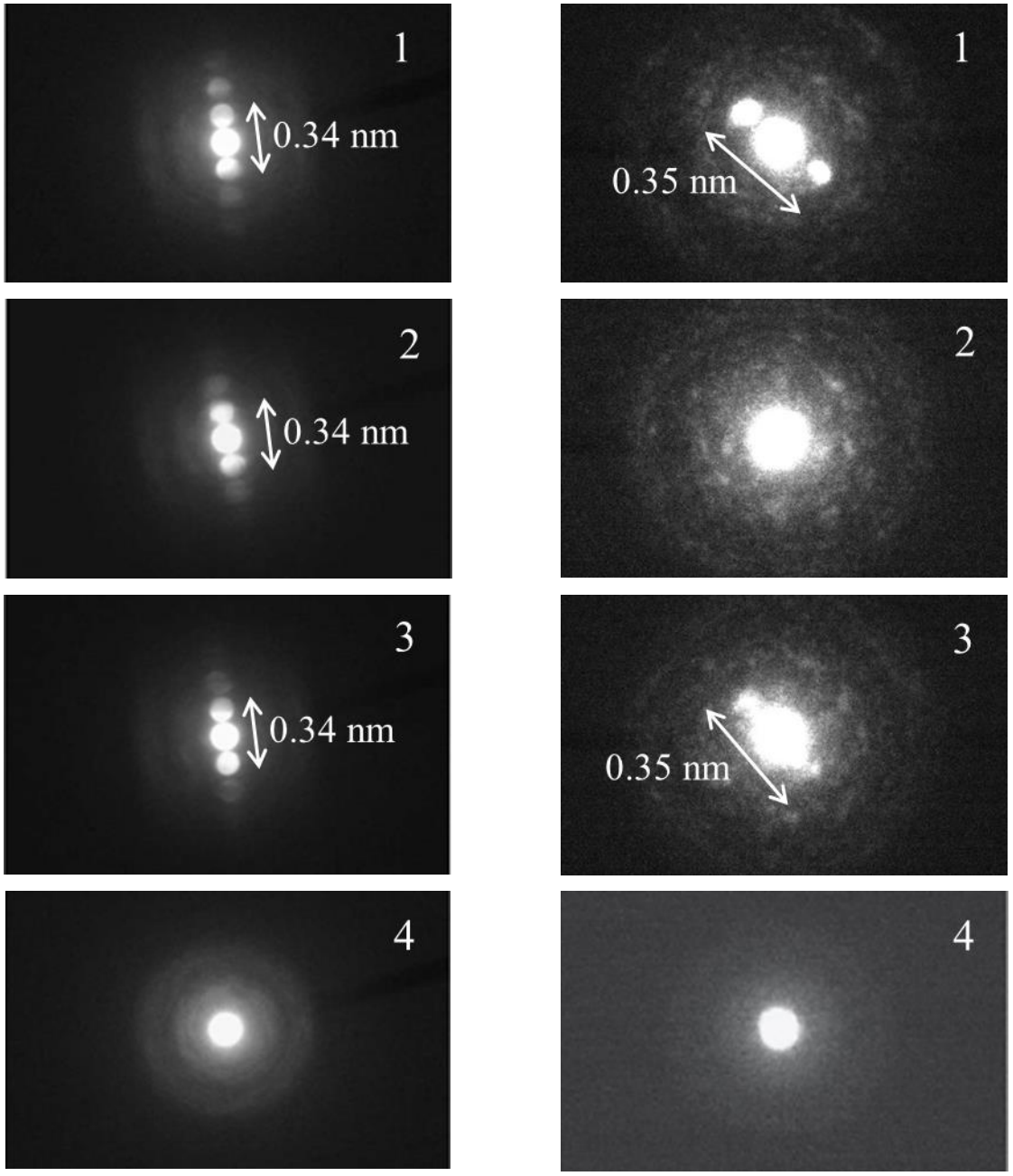

Figure 32 Crystallinity evaluation result at different position for (a) Pillar ta-C, and (b) Mesh ta-C

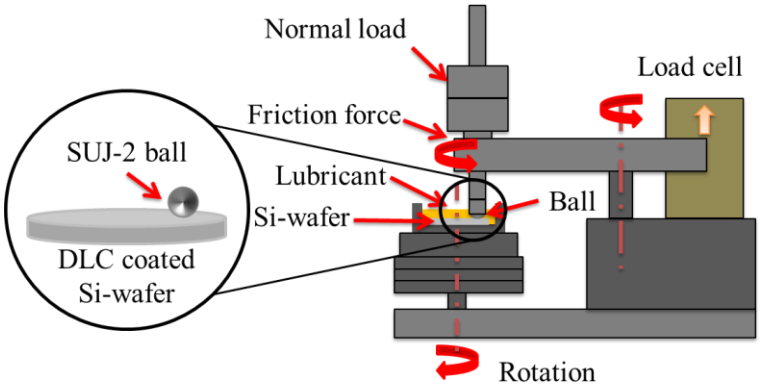

Figure 33 Tribo-tester schematic and ball-on-disk configuration

3.3 Tribological experiments

The friction tests were conducted using the ball-on-disk tribo-tester as presented in Figure 33 within the boundary lubrication regime with a constant normal load of 1 N on the SUJ-2 ball, correlated with the maximum Hertzian contact pressures of 421 MPa. The SUJ-2 ball was rubbed against coated Si-wafer placed 4.0 mm eccentrically from the center of the disk under a pure sliding condition via fixing the SUJ-2 ball to the upper jig. Moreover, the Si-wafer was fixed on the lower holder that was located on the rotary turntable. The speed and temperature of the tests were maintained at 0.042 m/s for 60 minutes that correlated with 150 m of sliding distance and 80 °C, correspondingly. Both SUJ-2 ball and counterpart Si-wafer disk were assured to submerge under the PAO4 oil level thereupon heat was applied to maintain the temperature of 80 °C throughout the friction test. The friction test was performed in triplicate to guarantee the validation and reproducibility of the results.

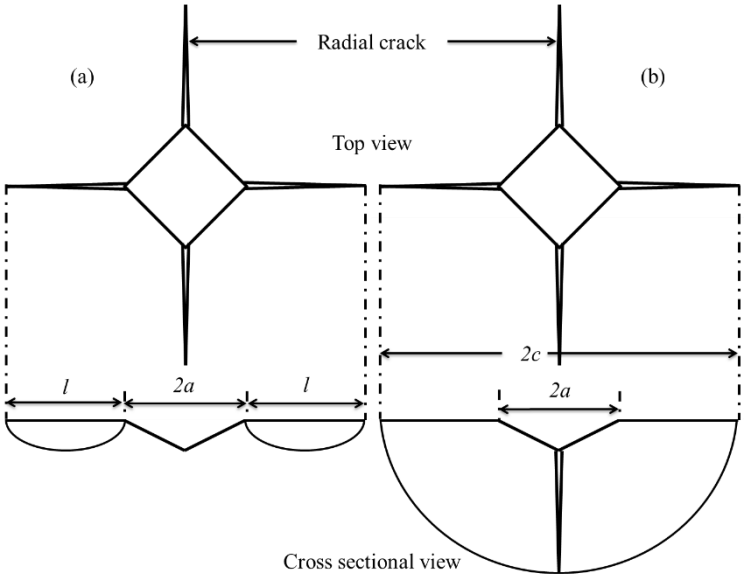

Figure 34 Top and cross-sectional views of cracks (a) lateral (Palmqvist), and (b) median (half-penny)

3.4 Fracture-toughness quantification for DLC coatings from radial-cracks on Si-substrate

The indentation of the coating or bending of the substrate could produce three forms of cracking patterns namely, circumferential cracking and spallation, channel cracking and radial cracking. The aforementioned cracking modes can be applied for a quantitative examination of the fracture-toughness of the coating [76].

Indentation tests were conducted via the micro Vickers hardness testing machine (Mitutoyo, Japan, 810-125 HM-102) with loads of 0.1, 0.2, 0.3, 0.5 and 1.0 kgf. Figure 34 illustrates that the criterion of a median crack was c > 2a, where c was the crack length quantified starting at the center of the indentation mark to the tip and 2a was the indentation mark diagonal length [29]. Field emission scanning electron microscope FE-SEM (JEOL, JSM-7000FK) was utilized to quantify the length of the crack in which an average of six indentations generated for every load was determined. K. Niihara et al. [77] demonstrated

that at a lower amount of crack-to-indent (c/a) ratio, palmqvist crack might form, whereas at a greater amount of crack-to-indent (c/a) ratio generates median (half penny) cracks.

A previous study demonstrated the method applied for fracture-toughness determination from the crack that was produced on the DLC coating/Si system [25]. The radial cracks formed on the DLC/Si system were revealed as mode I crack, which the semi-circular half-penny crack geometry with full adhesion of DLC coating over the Si substrate. Hence, the fracture-toughness is denoted as;

$$K_f = \sqrt{GE} \qquad \textbf{Eqn. 7}$$

Where K_f is the fracture-toughness, E is the modulus of elasticity of the coating, and G denotes the total work of fracture. The amount of work for elastic/brittle fracture is the amount of work to form two novel surfaces. The system fracture-toughness is measured by the combination of the total work of fracture of the system and the composite modulus of the system, which include a substrate and the coating. Applying boundary condition at the thickness of 0; effective fracture-toughness, $K_r = \sqrt{G_s/E_s}$ and $c = c_0$ yield;

$$\left[\left(\frac{c_0}{c}\right)^3 - 1\right] = \frac{2d}{\pi c}\left(\frac{G_f}{G_s} - \frac{E_f}{E_s} - 2\right) \qquad \textbf{Eqn. 8}$$

Where c and c_0 is the half radial crack length of the coated substrate and uncoated substrate, correspondingly, E_s is the elastic modulus of the substrate, and E_f is the elastic modulus of the film, G_S and G_f are the work of fracture for Si-substrate and DLC coating, respectively. The fracture of the Si-substrate is elastic and the G_s for Si-wafer is measured by surface energy, which is 3.03 J/m^2 [78], [79].

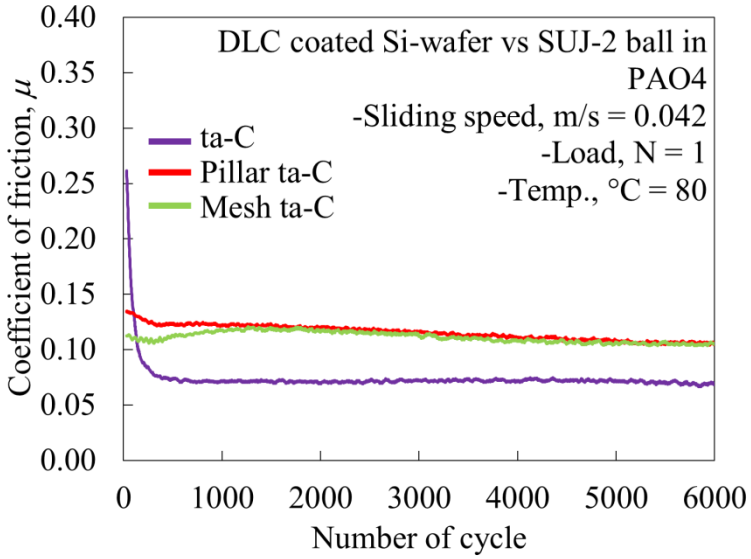

Figure 35 Coefficient of friction result for ta-C, Pillar ta-C, and Mesh ta-C as a function of number of cycle

3.5 Result and discussion

3.5.1 Friction and wear

Figure 35 and Figure 36 illustrate the coefficients that were plotted against the number of cycles for each coating and the average value, correspondingly. The average amount of friction coefficient was quantified from the coefficient of friction reading at the last 2000 cycles. The result of the coefficient of friction for each coating was ranged from 0.071 to 0.108 where conventional ta-C had the lowest value. In addition, the Pillar ta-C and Mesh ta-C demonstrated a higher value for the coefficient of friction because of the greater average surface roughness, Ra as indicated by a previous study [80]. The coefficient of friction for the Pillar and Mesh ta-C decreased as the number of cycles increased. This is caused by the reduction of the surface asperities due to the deposition process, which consequently lowered the average surface roughness.

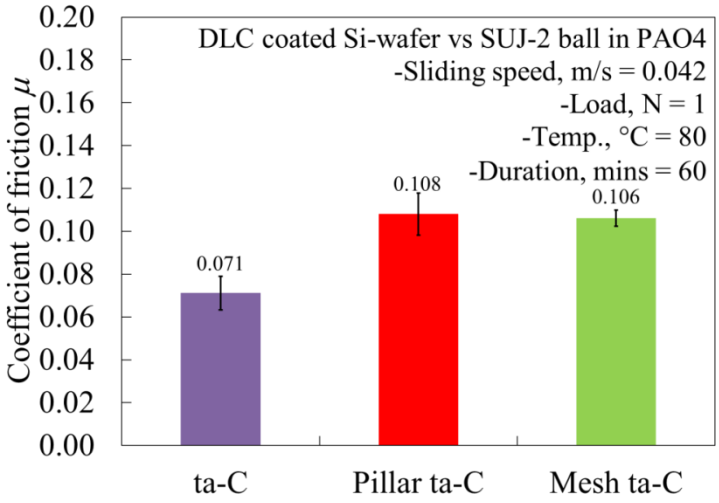

Figure 36 Average coefficient of friction result for ta-C, Pillar ta-C, and Mesh ta-C under 1 N load

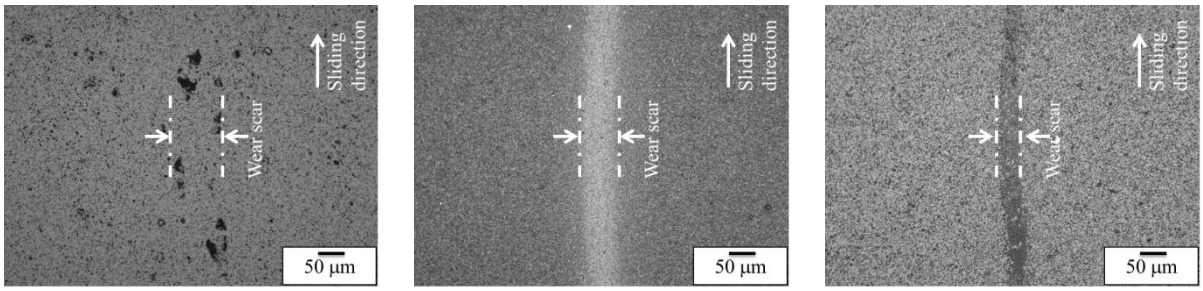

(a) (b) (c)

Figure 37 Optical microscope images of the wear track on the (a) ta-C, (b) Pillar ta-C, and (c) Mesh ta-C under 1 N loads

The DLC-coated Si-wafer was used to measure specific wear rates for each friction test. This was done to determine the impact of DLC structure on wear behavior. Figure 37 illustrates the wear track generated on each coating that was detected via the optical microscope. A number of spalling areas observed on the wear track of the conventional ta-C are illustrated in Figure 37(a). Additionally, the wear rate was determined through the 3D measuring laser microscope (Olympus, LEXT OLS5000). Figure 38 indicates the results of

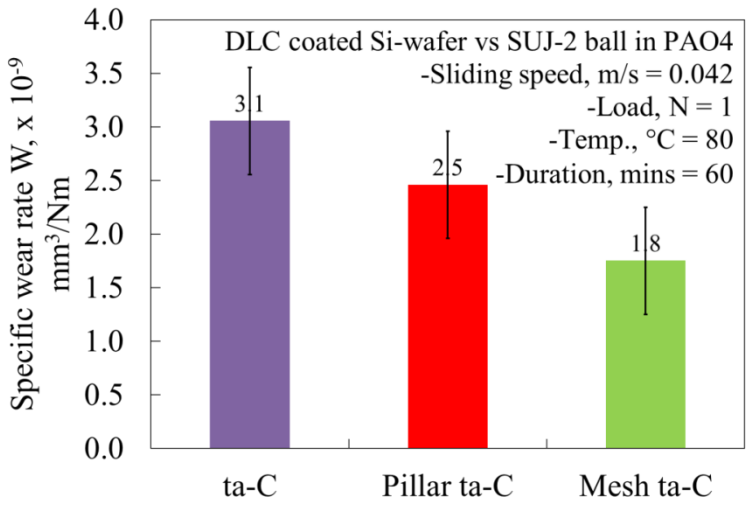

Figure 38 Specific wear rates result for ta-C, Pillar ta-C, and Mesh ta-C coated specimen

specific wear rates for all three types of DLC coatings under the similar applied normal loads. The application of Pillar and Mesh to the ta-C coating enhanced the wear resistance of the DLC coating. Mesh ta-C revealed a superior wear resistance with specific wear rates approximately 50% in comparison with conventional ta-C. The findings were in accordance with preceding research that utilized the DLC-coated cylindrical-pin-on-disk friction test under PAO4 boundary lubrication condition [80].

A detailed analysis was conducted on the wear track of each DLC coating via the FE-SEM instrument. The wear track of the conventional ta-C, Pillar ta-C, and Mesh ta-C are demonstrated in Figure 39(a), Figure 39(b), and Figure 39(c), correspondingly. For the case of ta-C, the brittle form of cohesive micro-crack can be detected on the wear scar, which caused the destruction of the coating by spalling and also delamination, Figure 39(a). Similarly, the crack was formed as the result of the deformation of the coating despite the Pillar ta-C demonstrated a few crack formations on the wear track of the coating. Evidence revealed that the crack formations were not generating any spallation of the coating. The

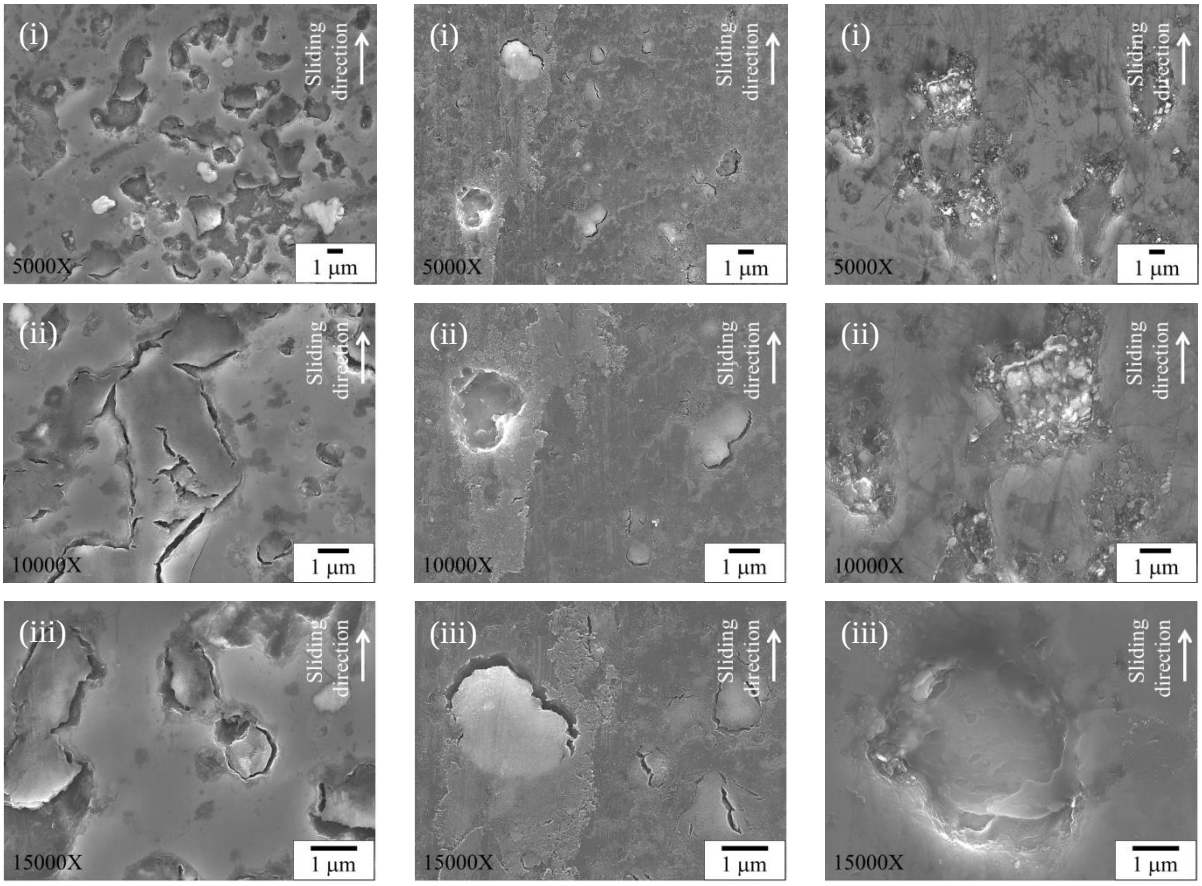

(a) (b) (c)

Figure 39 FE-SEM images of the wear track on the (a) ta-C, (b) Pillar ta-C, and Mesh ta-C specimens under 1 N loads

deformation area observed at the high sp^2 fraction, which consequently resulted in the deformed coating to adhere to the local area, Figure 39(b). Moreover, only a tiny crack can be detected on the wear track of Mesh ta-C as illustrated in Figure 39(C). Additionally, the elimination of nano-size coating from the contact area that occurred in the area of sp^2 rich structure was also observed.

There was a reduction in the number and size of the crack generated on the wear track of Pillar ta-C and Mesh ta-C coating in contrast to the conventional ta-C following the introduction of the Pillar and Mesh structure to the ta-C. Subsequently, the dependence of the wear to the fracture toughness of the coating was determined.

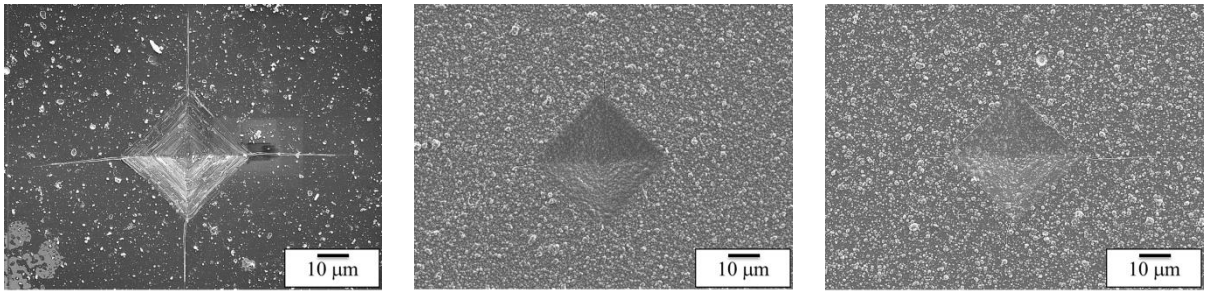

(a) (b) (c)

Figure 40 Indentation spot on the (a) ta-C, (b) Pillar ta-C, and (c) Mesh ta-C under 10 N loads

3.5.2 Fracture-toughness of the coatings

Figure 40 demonstrates the radial crack length, c that was quantified on the indentation spot for every coating corresponding to the load. As the substrate work of fracture G_s is fixed, therefore the film work of fracture G_f can be calculated using the slope of the trend line by plotting the terms $[(c_0/c)^3 - 1]$ against $1/c$ of Eqn. 8 as depicted in Figure 41.

Table 5 depicts the findings of the fracture-toughness analysis. Mesh ta-C demonstrated the highest fracture-toughness with 16.7 MPa·m$^{1/2}$, followed by the Pillar ta-C with 13.4 MPa·m$^{1/2}$, and ta-C with 11.3 MPa·m$^{1/2}$. The introduction of structure within the ta-C increased the coatings fracture-toughness, which was linked with the greater resistance to crack. In this study, FE-SEM was utilized to detect the indentation spot and the crack on conventional ta-C, Pillar and Mesh structure ta-C as shown in Figure 42 and Figure 43. This was done to further elucidate the involvement of the structure in improving the fracture-toughness.

The comparison of the fracture mechanism was performed by evaluating the characteristics of the crack formed on each of the coatings. Primarily, there were two forms of crack generated on DLC coating following the indentation procedure. On that account, the

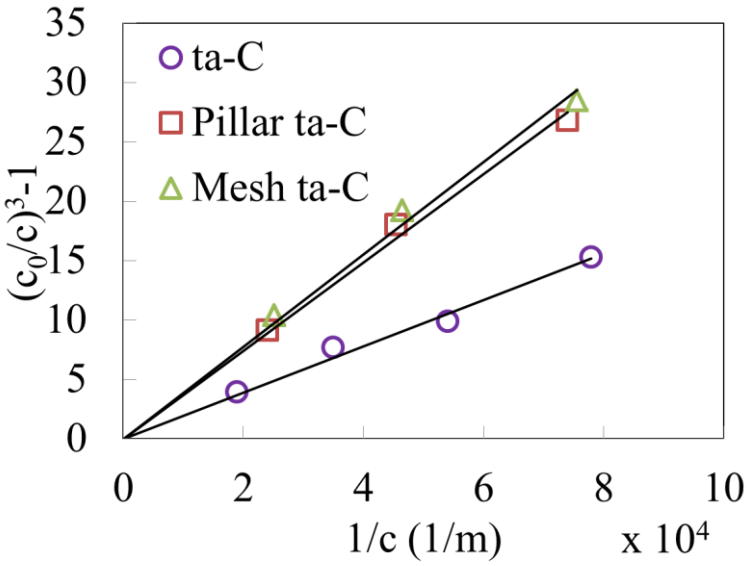

Figure 41 Crack length data for the ta-C, Pillar and Mesh structure ta-C samples plotted following the format of Eqn. 8

ring crack was generated by tensile stress produced near the contact area of indenter under the loading process and the spiral crack was developed during the unloading process [81]. The formation of ring crack in a thin film is governed by the substrate plastic zone under the indenter [76]. This effect becomes ineffective for the thick film due to the ratio of the film thickness and the critical depth. Furthermore, during the withdrawal of the indenter, a small defect grows to spiral crack, which then extended by the arising of equi-biaxial stress field due to film bending curvature effect [81], [82].

The investigation within the indentation mark for Pillar and Mesh ta-C coating demonstrated that every crack produced was detached and revealed a zigzag path pattern, which was corresponded to a mixture of Modes I and II cracks [83], that consequently resulted in ductile cracking as illustrated in Figure 42(b), and Figure 42(c), correspondingly. This zigzag or crinkled crack pattern provided stress relief by permitting a greater rate of crack energy dissipation in comparison with ta-C coating. In addition, the ta-C also

demonstrated a smooth step/layer crack shape and transverse crack in the indentation mark as depicted in Figure 42(a). This step/layer crack pattern was elucidated by the brittleness of the ta-C that restrained the coating from deformation when the load was induced. Additionally, Figure 42 illustrates that spallation can only be detected in conventional ta-C. It should be noted that both Pillar and Mesh ta-C coating revealed larger cohesive cracks spacing in comparison with the conventional ta-C. The crack spacing could decline under good adhesion conditions as the results of the transfer of the misfit stress amongst the film and the substrate to the film deprived of interface failures [84]–[86]. As such, this revealed that the adhesion strength was elevated by the introduction of the Pillar and Mesh structure to the ta-C.

Notably, the ta-C indentation mark diagonal length (2a) was comparable to that of Pillar and Mesh type ta-C although ta-C DLC coating hardness is approximately two times higher than that of structured ta-C as depicted in Figure 40. As such, this is the impact of greater elastic recovery value, W_e of the Pillar and Mesh ta-C in comparison with homogeneous ta-C DLC coating as demonstrated in Figure 44. As such, this could result in a greater degree of coating toughness [74], [87]. W_e can be obtained from the typical load-displacement curves as summarized in Eqn. 9.

$$W_e = [(d_{max} - d_{res})/d_{max}] \times 100\% \qquad \textbf{Eqn. 9}$$

Where;

- d_{max} = maximum indentation depth during loading
- d_{res}= residual indentation depth after unloading

Figure 43 demonstrates the radial channel-type cohesive cracking on every form of DLC coating. The cohesive crack has a vital function as a flaw starting the interface delamination [88]. Following subsequent straining, further buckling delamination happened

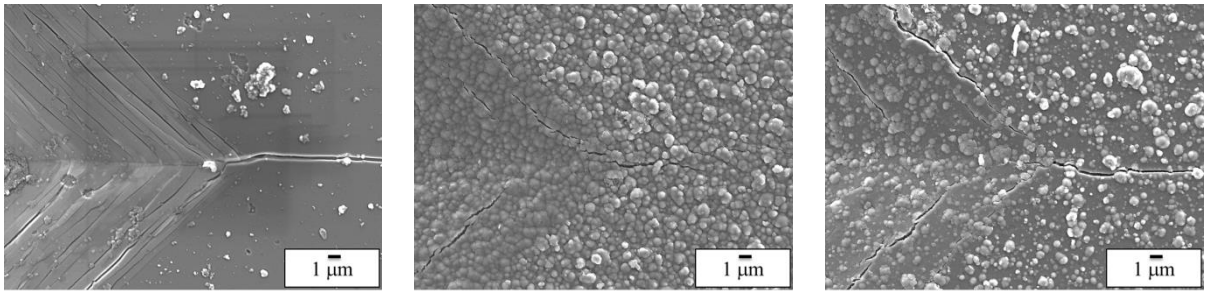

(a) (b) (c)

Figure 42 Magnified indentation spot on the (a) ta-C, (b) Pillar ta-C, and (c) Mesh ta-C under 10 N loads

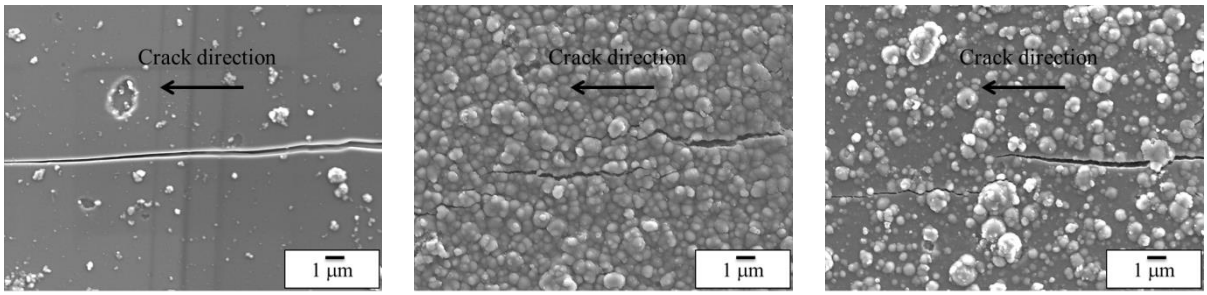

(a) (b) (c)

Figure 43 Magnified FE-SEM images of the radial cracks on the (a) ta-C, (b) Pillar ta-C, and (c) Mesh ta-C under 10 N loads

at the free edge of the cohesive crack of ta-C coating because of the increased energy release rate and compressive strain that was generated by Poisson's contraction normal to the tensile direction as illustrated in Figure 42(a) and Figure 43(a) [89]. Finer radial crack can be detected on the ta-C coating, which is in comparison with the radial crack of Pillar and Mesh ta-C as depicted in Figure 43(a), Figure 43(b), and Figure 43(c), correspondingly. Inferior fracture-toughness of the Pillar ta-C to that of Mesh ta-C was caused by its lower hardness features and elastic recovery value (Figure 44). Figure 43(b) depicts the features of the pillar

Table 5 Result of the fracture-toughness of the coatings

Samples	Film thickness d, μm	Elastic Modulus E_f, GPa	Compressive Residual Stress σ_c, GPa	Film work of fracture G_f, kJ/m^2	Fracture-toughness K_f, MPa · m$^{1/2}$
ta-C	1.5	310	1.75	0.45	11.3
Pillar ta-C	1.42	143	1.26	1.25	13.4
Mesh ta-C	1.25	184	2.15	1.14	16.7

structure that facilitated the formation of longer parallel crack. Mesh ta-C and Pillar ta-C demonstrated a shorter crack length in comparison with that of ta-C coating, indicating conventional ta-C had lower fracture-toughness. On the other hand, higher coating fracture-toughness restrained the crack propagation, consequently inhibited coating from spalling and delamination. The combined impact of soft sp^2 structure and intersection restricted the crack from propagating in Pillar ta-C and Mesh ta-C. A higher rate of energy dissipation via plastic deformation of the sp^2 phase soft structure resulted in an improvement in film toughness, which subsequently caused the termination of the crack propagation [71].

3.6 Fracture-toughness in relations to wear rates

The wear rates for non-structured and structured ta-C were plotted against fracture-toughness of the coating to examine the link between the crack resistance to the wear rates of the coating (Figure 45). The characterization of the coating by virtue of its mechanical properties is crucial to provide detailed information on the tribological procedure in the boundary lubrication regime as the direct contact of surface asperities exists. There was an inverse relationship between the wear rates and the fracture-toughness, at which the wear

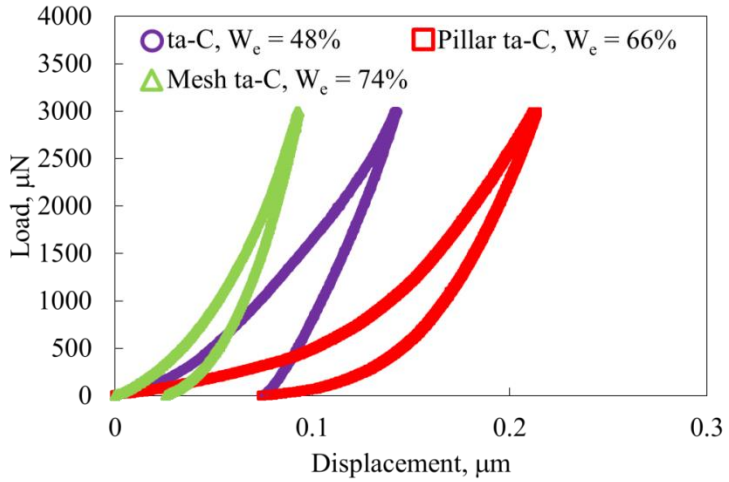

Figure 44 Elastic recovery value, W_e for DLC coatings from loading–unloading curves during indentation test

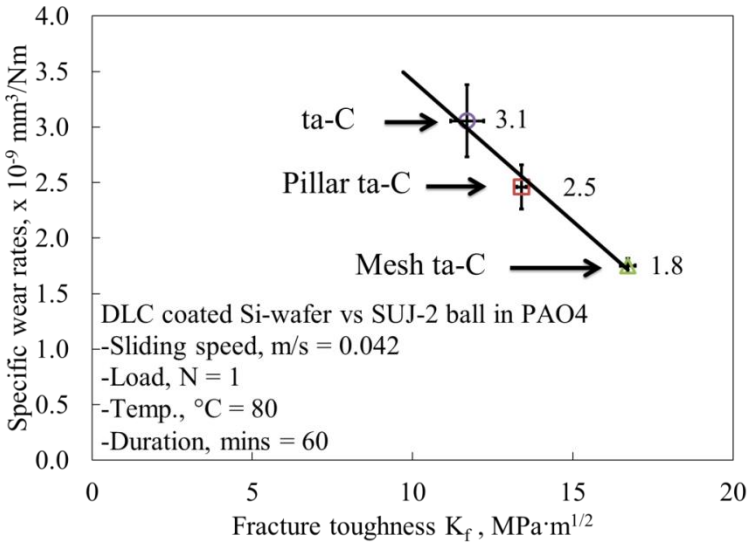

Figure 45 Specific wear rates plotted against fracture-toughness of the coating for DLC-coated Si-disk vs. SUJ-2 ball

rates were declined following the improvement in the fracture-toughness. The findings revealed that the corresponding wear resistance was increased following the improvement in the fracture toughness of the coating. As such, higher Pillar and Mesh ta-C coating resistance to wear was observed as the results of an elevated fracture-toughness. This consequently

declined the coating destruction as an effect of fracture-induced wear in conventional ta-C that further evolved to spalling and delamination of the coating. The small fragments spall ta-C coating could then act as an abrasive particle to promote the wear acceleration.

3.7 Conclusion

In order to discuss the effect of the structure of Pillar and Mesh to the ta-C wear properties, fracture-toughness evaluation via micro indentation for these various ta-C was evaluated. In addition, the effect of fracture-toughness of the DLC on wear properties in oil lubrication was clarified. Superior fracture-toughness was observed following the introduction of pillar and mesh structure to the ta-C coating in which the fracture-toughness of the Pillar and Mesh ta-C DLC-coatings were comparatively higher than the conventional ta-C. Furthermore, the elevation of fracture-toughness led to the higher wear resistance of the ta-C coating due to the fracture-induced wear suppression through the improvement of the crack propagation inhibition. In addition, the introduction of Pillar and Mesh structure to the ta-C DLC coating prevented the brittle characteristics of the ta-C by decreasing channel-type cohesive cracking. Moreover, Pillar and Mesh structure ta-C provided a greater degree of stress relief by permitting the higher rate of crack energy dissipation in contrast to conventional ta-C coating. Also, the increased crack spacing in Pillar and Mesh ta-C was facilitated by an improved adhesion strength, which prevented the interface failures. The friction coefficient for Pillar ta-C and Mesh ta-C are comparatively higher to that of ta-C due to higher contact surface roughness.

Chapter 4

Effect of Pillar and Mesh Structure of Tetrahedral Amorphous Carbon (ta-C) Coatings on Friction and Wear Properties under Base- oil with MoDTC and ZnDTP Additives Lubrication Condition

4.1 Introduction

Friction and wear of material have become one of the important issues relating to the energy conservation and efficiency. The interaction between two materials has led to the loss of both material and energy. The energy dissipated to overcome the friction force has taken one-third of the total world energy resource in mechanical applications [3], [4]. It is further reported in details that tribological contacts have consumed a total of 23% (119 EJ) of the world's total energy, in which 20% to overcome the friction and 3% was used for reproducing and replacement of the part due to wear and wear-related failures [5].

Diamond-like carbon (DLC) coatings are one of the solid lubricants which formed in combination of sp^2 and sp^3 carbon structure that offer excellent mechanical and tribological properties. Numerous studies have been conducted to elucidate the effect of lubrication types

and conditions on the DLC coating. DLC could provide excellent tribological performance in terms of friction and wear with the use of appropriate base oil and lubricant additives [49].

The friction modifier Molybdenum Dithiocarbamates (MoDTC), and anti-oxidant and anti-wear Zinc dialkyldithioposphate (ZnDTP) is among the most common additives used in lubrication due to their excellent properties. It is reported that with the presence of MoDTC and ZnDTP additives, the friction and wear performance of DLC coating under boundary lubrication conditions is improved [90], [91].

Wear protective tribo-films could be generated due to the tribo-chemical reaction between the ferrous surface and the ZnDTP additives [92]. However, several studies have reported that the ZnDTP anti-wear tribo-film could not be generated on the DLC contact surface [47], [93], [94]. These claims were then counter by the reports that show the evidence of weak tribo-film formation on the DLC surface [95]–[97]. Moreover, the concentration of hydrogen in the DLC coating could affect the tribo-film formation [98]. Likewise, ultra-low friction under boundary lubrication conditions is achievable with ester-containing lubricants [99]–[101].

The fraction of carbon sp^2 structure in ta-C is one of the factors that controlled the formation of tribo-film on the friction surface. The previous study conducted by using the ta-C coating has shown that a low friction coefficient is recorded at the initial phase, but it begins to raise afterward which is explained by the low-friction surface being restricted by the ZnDTP molecules [96]. Also, recent studies reported that ‘tetrahedral’ Si-contain hydrogenated DLC shows excellent tribological performance under MoDTC and ZnDTP additive containing oil [102]. Furthermore, the ta-C contact surface structure was retained and not affected by the MoDTC additives in oil which result in high wear resistance of the

coating, but in the case of a-C:H coating that are richer in sp^2 structure, the contact surface change and causing higher average roughness as compared to before friction test [103].

A recent development in coating deposition methods has enables the introduction of structure to the DLC coating as well as controlling hardness of the coating over a wide range which attributed by the sp^2/sp^3 carbon bonding ratio. This could enhance the adsorption of an oiliness agent. The current study introduced and investigated the novel Pillar ta-C and Mesh ta-C with as deposited pillar and mesh structure, together with conventional ta-C for comparison under base-oil containing additives boundary lubrication conditions. This research works aimed to clarify the effect and influence of oil additives to the tribological performance of newly developed coating with as-deposited structure.

4.2 Experimental details

4.2.1 Material characterization and lubricants

Nippon ITF Incorporated has prepared three types of ta-C coatings which are deposited on the pin substrate made of high carbon chrome steel (SUJ-2). The three type's ta-C coating was prepared by the physical vapor deposition (PVD). These ta-C coatings were characterized by the structure named as conventional ta-C, Pillar ta-C develop with pillar structure, and Mesh ta-C develop with mesh structure as illustrated in Figure 46. In order to prepare the conventional ta-C, the deposition temperature controlled below 150 °C using the integrated cooling system. Likewise, continuous heating was applied during the deposition process of Pillar and Mesh ta-C coating to sustain the temperature of the substrate above 200 °C. As a result, a quarter of the Pillar and Mesh ta-C coating thickness present a white layer

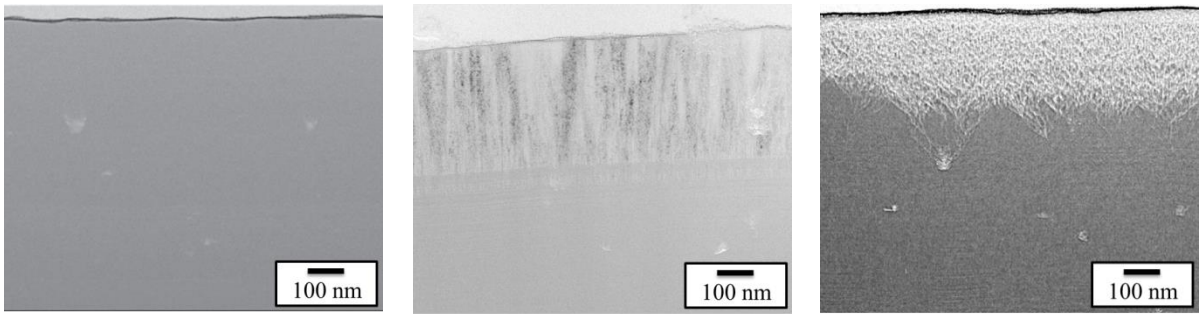

(a) (b) (c)

Figure 46 Cross-sectional cut of (a) conventional ta-C, (b) Pillar ta-C, and (C) Mesh ta-C

that originates and grows from the microparticle as a result of the deposition's arc technique as shown in Figure 46(c) and Figure 46(d). The above-mentioned coatings underwent the fluid polishing process to remove the droplets result from deposition. There are four types of lubricants used in this study which are PAO4, Mineral oil with MoDTC, ZnDTP and five common additives (CA – Calcium, Phosphorus, Sulfur, Boron and Nitrogen), PAO4 with MODTC, and. PAO4 with ZnDTP, which from this point onwards referred as PAO4, Mineral oil + MoDTC + ZnDTP, PAO4 + MoDTC, and PAO4 + ZnDTP, respectively.

4.2.2 Tribological experiments

The friction test conducted using the Pin-on-Disk tribo-tester as shown in Figure 47 with an applied normal load of 20 N that corresponds to maximum initial contact pressures of 311 MPa. The speed and temperature of the tests were fixed at 0.068 m/s (100 rpm) for 60 minutes that corresponds to 250 m of sliding distance and 80 °C, respectively (Table 6). Both the cylinder and disk were immersed in an oil bath in which the temperature was maintained at 80 °C during the friction test. The dimensions of the pin were 5 mm diameter and 5 mm length, whereas disk of 22.5 mm diameter and 4 mm thick were applied in all experiments. In

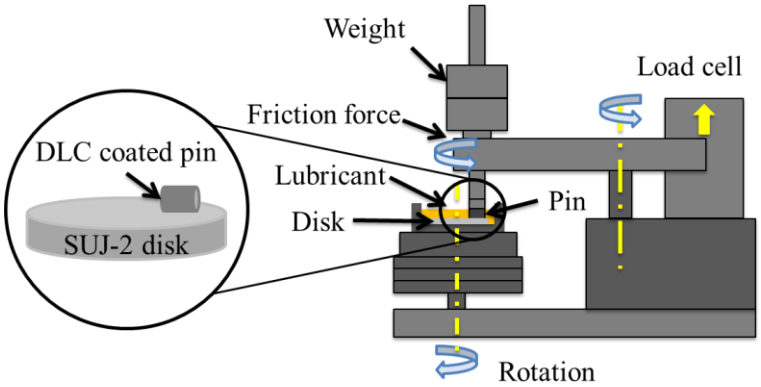

Figure 47 Tribo-tester schematic and Pin-on-Disk configuration

order to ensure verification and reproducibility of the findings, each friction tests were repeated three times. DLC-coated pin and disk were cleaned with benzene and acetone in an ultrasonic bath to eliminate any impurities and oil.

Wear volume loss and wear rates of the DLC-coated pin were quantified via Archard wear equations by calculating the width of the wear scar by assuming that the shape of the wear scar is rectangular-shape observed under the optical microscope as below:

$$k = \frac{V}{Fs} \qquad \textbf{Eqn. 10}$$

$$V = 2l \int_{\sqrt{r^2-\left(\frac{d}{2}\right)^2}}^{r} \sqrt{r^2 - x^2}\, dx \qquad \textbf{Eqn. 11}$$

Where k denotes dimensional wear rate (m^3/Nm), F characterizes the applied normal load (N), s indicates the sliding distance (m), V symbolizes wear volume loss (m^3), l denotes the length of the cylinder (m), r indicates the radius of the cylinder (m), and d denotes the width of the wear scar (m). The minimum film thickness (h_{min}) for rectangular conjunctions and dimensionless lambda ratio (Λ) were calculated using Eqn. 12 and Eqn. 13, respectively.

$$h_{min} = 1.806(w_z')^{-0.128}(\eta_0 \tilde{u})^{0.694}\zeta^{0.568}{R_x}^{0.434} \qquad \textbf{Eqn. 12}$$

$$\Lambda = \frac{h_{min}}{\sqrt{R_{q.a}^2 + R_{q.b}^2}} \qquad \textbf{Eqn. 13}$$

Here, w_z' is the normal load per unit width, η_0 is the absolute viscosity of the lubricants at the pressure of 0 Pa, $\tilde{u}$ is the mean surface velocity in the sliding direction, ζ is the pressure-viscosity coefficient, R_x is the effective radius of the cylinder, $R_{q.a}$ is the curved surface roughness of the cylinder, and $R_{q.b}$ is the surface roughness of the disk. The calculated lambda ratio under the initial contact condition was less than unity, indicating that the operating lubrication regime is boundary lubrication.

4.2.3 Surface analysis

Nanoindenter (NANOPICS 1000 Elionix ENT-1100a) was utilized to quantify hardness and Young's modulus of the DLC coatings. The surface roughness was quantified via atomic force microscopy (AFM, SPM-9700HT), and the structure of the DLC was elucidated by the Raman spectroscopy (NRS-1000 Laser, Jasco Inc., Japan), where 532 nm Ne laser radiation was applied. The worn surface of the pin and disk were examined by optical microscope and field emission scanning electron microscope (FE-SEM, JEOL, JSM-7000FK). The X-ray photoelectron spectroscopy (XPS; PHI Quantera II, ULVAC-PHI, Japan.) operated with Al Kα X-ray source (25 W, 15 kV) was used to quantify the tribo-film formation on DLC-coated pin and SUJ-2 disk. Table 7 demonstrates the detailed properties of the DLC-coated pin and disk.

Table 6 Friction test condition

Experimental setup	
Specimens	ta-C
(Cylindrical pin)	Pillar ta-C
	Mesh ta-C
Specimens (Disk)	SUJ-2
	Hardness: 9.9 GPa
	Ra: 0.01μm
Rotation speed (m/s)	0.068
Fix normal load (N)	20
Temperature (°C)	80
Lubricants	PAO4
	Mineral oil + MoDTC + ZnDTP
	PAO4 + MoDTC
	PAO4 +ZnDTP
Duration (minutes)	60

Table 7 Mechanical properties of the a-C:H, ta-C, Pillar and Mesh ta-C coatings

Properties	**Disk**	**Cylindrical pin**		
		ta-C	**Pillar ta-C**	**Mesh ta-C**
Dimension (mm)	22.5 x 4	5 x 5	5 x 5	5 x 5
Substrate material	SUJ-2	SUJ-2	SUJ-2	SUJ-2
Coating method	-	PVD	PVD	PVD
Thickness (μm)	-	0.8	1.65	1.17
Elastic modulus, E_f (GPa)	275.5	661	110	232
Hardness, H (GPa)	9.9	78.3	11.0	27.5
Roughness, Ra (μm)	0.010	0.021	0.055	0.026

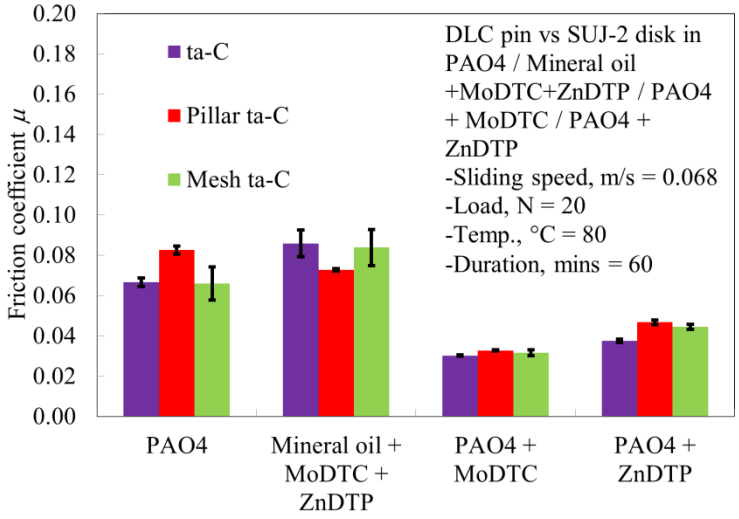

Figure 48 Steady state friction coefficient result for ta-C, Pillar ta-C and Mesh ta-C coated specimen lubricated under PAO4, Mineral oil + MoDTC + ZnDTP, PAO4 + MoDTC, and PAO4 + ZnDTP

4.3 Result and discussions

4.3.1 Tribological performance for various DLC under base oil with additives boundary lubrication condition

Figure 48 illustrates the average coefficient of friction for each DLC specimens tested in PAO4, Mineral oil + MoDTC + ZnDTP, PAO4 + MoDTC, and PAO4 + ZnDTP oil. The coefficient of friction was ranging from 0.04 to 0.09 with lubrication in PAO4 is showing lower value compared to the lubrication in Mineral oil + MoDTC + ZnDTP. In addition, only Pillar ta-C coating shows the reduction in friction coefficient when lubricated in Mineral oil + MoDTC + ZnDTP. Furthermore, the friction coefficient of ta-C, Pillar ta-C and Mesh ta-C are lower under single additive oil lubrication. Ultra-low friction is achieved by using the PAO4 + MoDTC oil lubrication for all types of ta-C.

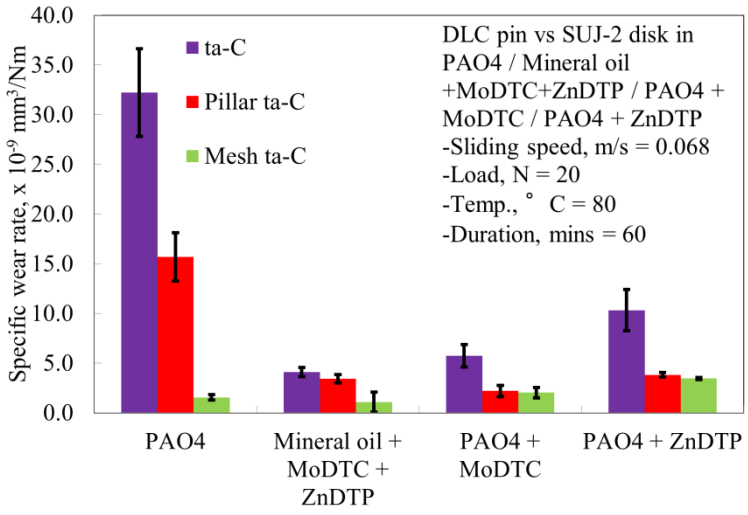

Figure 49 Wear rates result for ta-C, Pillar ta-C and Mesh ta-C coated specimen lubricated under PAO4, Mineral oil + MoDTC + ZnDTP, PAO4 + MoDTC, and PAO4 + ZnDTP

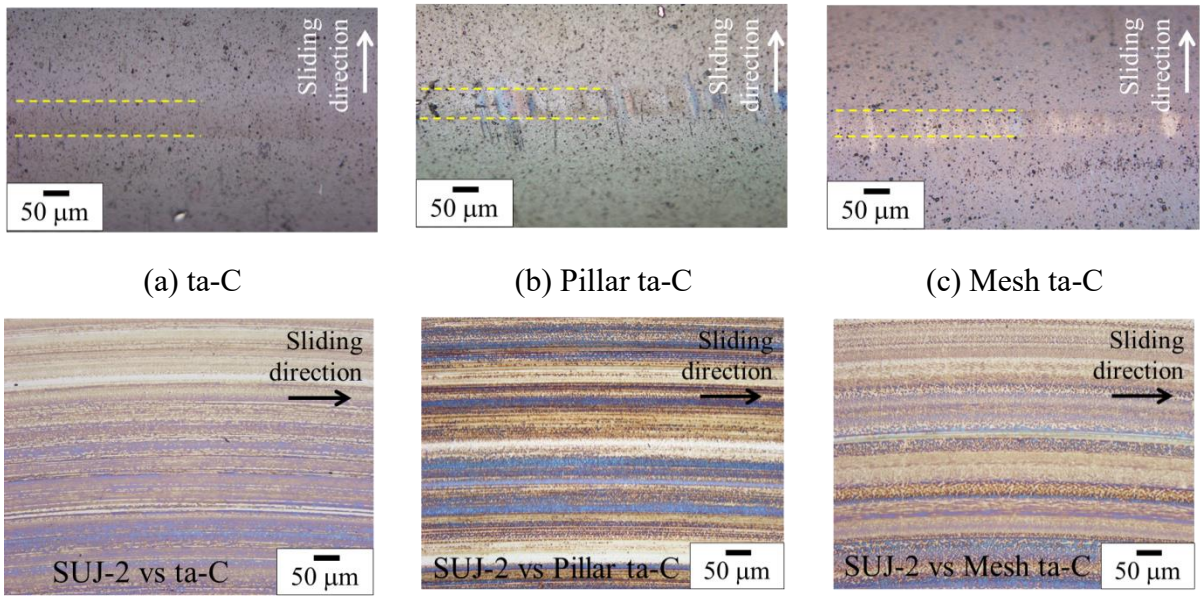

(a) ta-C (b) Pillar ta-C (c) Mesh ta-C

(d) SUJ-2 vs. ta-C (e) SUJ-2 vs. Pillar ta-C (f) SUJ-2 vs. Mesh ta-C

Figure 50 Optical microscope images of the wear scar on the DLC coated cylindrical-pin and counterpart SUJ-2 disk under Mineral oil + MoDTC + ZnDTP lubrication

The wear rates for every friction test were determined from the DLC-coated pins for characterizing the influence of the DLC structure as well as lubricants to the wear behavior of

the DLC. Figure 49 shows the findings of wear rates of every DLC lubricated in PAO4, Mineral oil + MoDTC + ZnDTP, PAO4 + MoDTC, and PAO4 + ZnDTP at 20 N load. The wear rates for every DLC-coated pins shows reduction under Mineral oil + MoDTC + ZnDTP, PAO4 + MoDTC, and PAO4 + ZnDTP lubrication as compared to in PAO4 lubrications. The ta-C coating shows great improvement where the wear rates in Mineral oil + MoDTC + ZnDTP is 8 times lower than that in PAO4. Moreover, Pillar ta-C also shows greater protection against wear in additive oil lubrication as compared to only in PAO4 lubrication conditions. Furthermore, Pillar ta-C and Mesh ta-C show lower wear rates as compared to the ta-C in PAO4 + MoDTC and PAO4 + ZnDTP lubrication conditions.

From the optical microscope image of the wear scar formed on the DLC coated cylindrical pin Figure 50(b), Pillar ta-C shows the existence of the tribo layer formed during the friction test under Mineral oil + MoDTC + ZnDTP lubrication condition. While the other type of the DLC coating does not show any colorful layer on the wear scar. Furthermore, Figure 50(d), Figure 50(e), and Figure 50(f) show the wear scar on the SUJ-2 disk counterpart of ta-C, Pillar ta-C, and Mesh ta-C, respectively as observed under the optical microscope. The SUJ-2 disk counterpart of ta-C, Pillar ta-C and Mesh ta-C are showing a similar colorful layer that could originate from the formation of tribo-film.

Figure 51 shows the optical microscope image of the wear track on the DLC coated pin and SUJ-2 counterpart disk under PAO4 + MoDTC lubrication condition. It is evident that there is the possibility of tribo-film derived from MoDTC formed on the wear track of Pillar and Mesh ta-C with the presence of the coloured layer at the center and edge of wear track as shown in Figure 51(b) and Figure 51(c). Further observation on the wear formed on the SUJ-2 counterpart disk of Pillar ta-C, and Mesh ta-C as shown in Figure 51(e) and Figure 51(f)

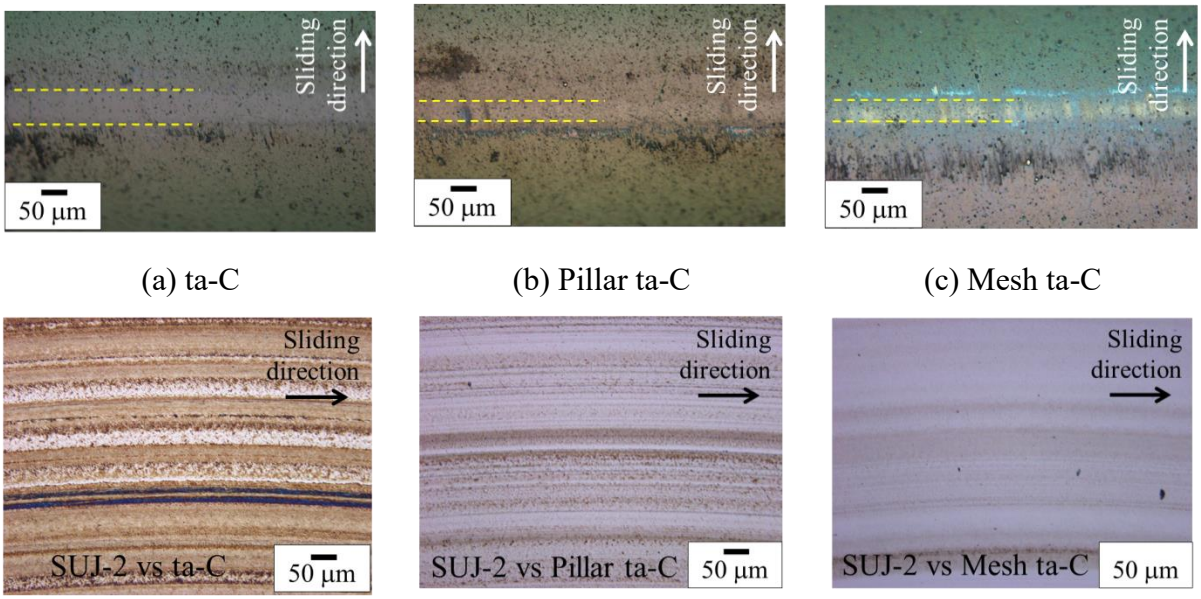

(a) ta-C (b) Pillar ta-C (c) Mesh ta-C

(d) SUJ-2 vs. ta-C (e) SUJ-2 vs. Pillar ta-C (f) SUJ-2 vs. Mesh ta-C

Figure 51 Optical microscope images of the wear scar on the DLC coated cylindrical-pin and counterpart SUJ-2 disk under PAO4 + MoDTC lubrication

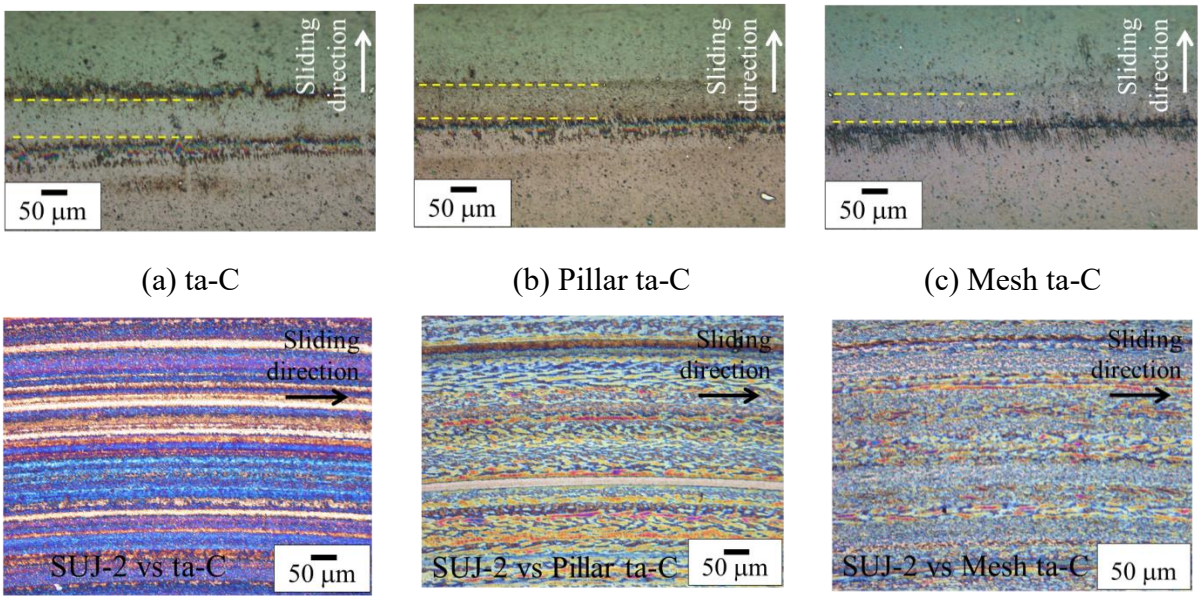

(a) ta-C (b) Pillar ta-C (c) Mesh ta-C

(d) SUJ-2 vs. ta-C (e) SUJ-2 vs. Pillar ta-C (f) SUJ-2 vs. Mesh ta-C

Figure 52 Optical microscope images of the wear scar on the DLC coated cylindrical-pin and counterpart SUJ-2 disk under PAO4 + ZnDTP lubrication

shows no evidence of tribo-film can be observed. Likewise, observation on the wear track of the SUJ-2 disk counterpart ta-C Figure 51(d) shows the possibility of the existence of either transfer material or tribo-film.

In the case of lubrication under PAO4 + ZnDTP, there is the possibility of tribo-film derived from Zn formed on the wear track of ta-C and Pillar ta-C with the present of the coloured layer as shown in Figure 52(a) and Figure 52(b), respectively. Different from the lubrication in PAO4 + MoDTC, the SUJ-2 disk counterpart for ta-C, Pillar ta-C and Mesh ta-C does show the existence of tribo-film under PAO4 + ZnDTP lubrications as shown in Figure 52(d), Figure 52(e), and Figure 52(f), respectively. Furthermore, the tribo-film form on the SUJ-2 disk counterpart of Pillar ta-C and Mesh ta-C is completely different from the tribo-film on the SUJ-2 disk counterpart of ta-C. Despite the tribo-film formation, the friction coefficient for ta-C, Pillar ta-C and Mesh ta-C lubricated with PAO4 + ZnDTP is slightly higher than that of PAO4 + MoDTC lubrication. Thus, further examination of tribo-film species and type is required to elucidate these phenomena.

4.3.2 Analysis of tribo-film on the wear track

4.3.2.1 FE-SEM images of the wear track

Detail observation made on ta-C coated cylindrical pin lubricated under Mineral oil + MoDTC + ZnDTP reveals the formation of white patch-like tribo-film together with the accumulation of approximately 10 nm size of wear particle in the spalling area as shown in Figure 53(a). Interestingly, the micro-cracks formed on the wear track after the friction test under PAO4 lubrication was not visible when lubricated Mineral oil + MoDTC + ZnDTP. The possible explanation for this phenomenon is the tribo-film derived from the ZnDTP has

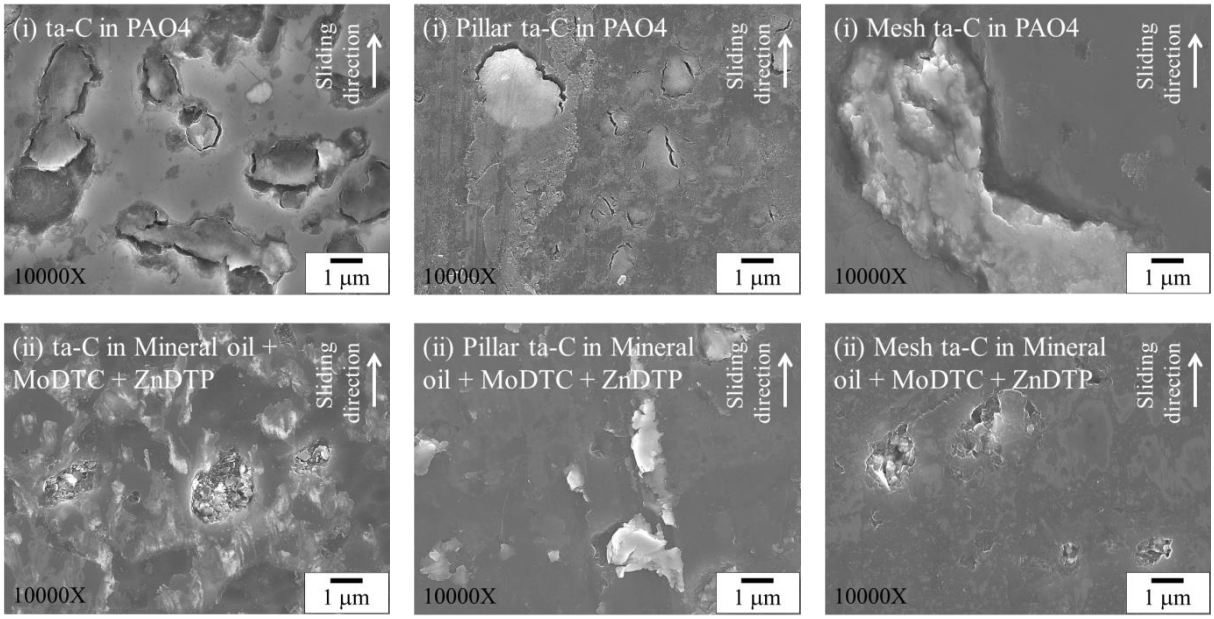

(a) ta-C (b) Pillar ta-C (c) Mesh ta-C

Figure 53 FE-SEM images of the wear scar on the DLC coated cylindrical-pin under PAO4, and Mineral oil + MoDTC + ZnDTP lubrication

generate a protective layer that suppressing the stress-induced on the contact surface and thus preventing the fracture.

Pillar ta-C as shown in Figure 53(b) reveals the removal of the soft sp^2 layer that adhered back to the local area in the direction of sliding. Moreover, the asperities formed during the deposition process of Mesh ta-C act to trap the abrasive particle produce during the friction test, as well as smoothening of the surface as shown in Figure 53(c). Both of the Pillar and Mesh ta-C coatings do not show any visible tribo-film on the wear track.

Figure 54 shows the detail observation of the wear track on the SUJ-2 counterpart disk by using FE-SEM lubricated under Mineral oil + MoDTC + ZnDTP. The SUJ-2 counterpart of ta-C reveals the formation of tribo-film without deep scratch mark as shown in Figure 54(a). Furthermore, observation on the SUJ-2 disk counterpart of Pillar ta-C and Mesh ta-C

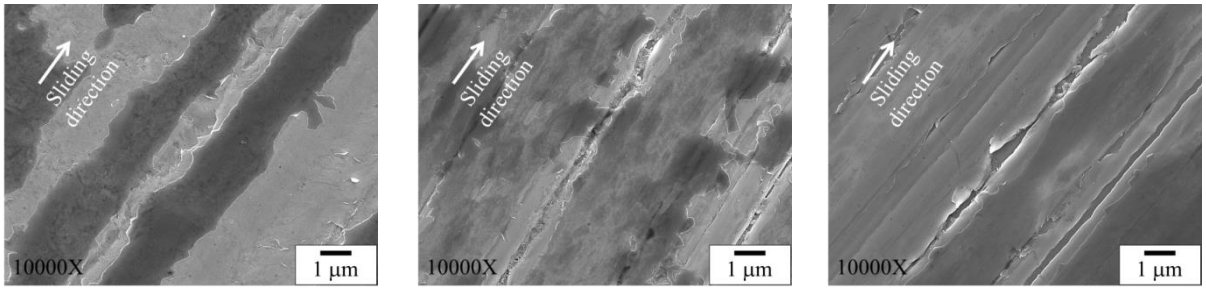

(a) SUJ-2 disk counterpart of ta-C

(b) SUJ-2 disk counterpart of Pillar ta-C

(c) SUJ-2 disk counterpart of Mesh ta-C

Figure 54 FE-SEM images of the wear scar on the SUJ-2 disk counterpart material under Mineral oil + MoDTC + ZnDTP lubrication condition

shows the formation of tribo-film on the wear track, as well as wear particle located in the scratch mark as shown in Figure 54(b) and Figure 54(c), respectively. But the scratch mark on the SUJ-2 disk counterpart of Mesh ta-C show less accumulated wear particles as compared to the SUJ-2 disk counterpart of Pillar ta-C.

4.3.2.2 Characterization of tribo-film by XPS analysis

XPS analysis was conducted to further elucidates the chemical composition of the tribo-film on the wear track of DLC coated cylindrical-pin and SUJ-2 disk counterpart. Table 8 and Table 9 show the atomic concentration of the elements measured on DLC coated cylindrical-pin and SUJ-2 disk counterpart material, respectively under Mineral oil + MoDTC + ZnDTP, PAO4 + MoDTC, and PAO4 + ZnDTP lubrication. Furthermore, Table 10 shows the sp^2/sp^3 ratio measured on as-deposited ta-C, Pillar ta-C, and Mesh ta-C as well as on the wear track after friction test in Mineral oil + MoDTC + ZnDTP, PAO4 + MoDTC, and PAO4 + ZnDTP oil.

Table 8 Atomic concentration measured on ta-C, Pillar and Mesh ta-C coatings lubricated under Mineral oil + MoDTC + ZnDTP, PAO4 + MoDTC, and PAO4 + ZnDTP

Lubricants	DLC	Atomic ratio, %						
		C	O	P	S	Fe	Zn	Mo
Mineral oil + MoDTC + ZnDTP	ta-C	86.6	9.4	0.4	0.8	0.5	1.0	0.0
	Pillar ta-C	90.8	8.2	0.0	0.2	0.1	0.2	0.0
	Mesh ta-C	87.3	11.0	0.5	0.4	0.0	0.0	0.0
PAO4 + MoDTC	ta-C	85.9	4.4	-	2.5	1.9	-	3.6
	Pillar ta-C	86.2	5.4	-	2.6	2.3	-	2.5
	Mesh ta-C	86.9	6.5	-	1.3	2.7	-	1.4
PAO4 + ZnDTP	ta-C	57.2	21.1	7.5	-	8.5	4.5	-
	Pillar ta-C	77.3	10.4	6.5	-	0.4	4.2	-
	Mesh ta-C	57.8	18.0	10.8	-	0.5	11.5	-

Table 9 Atomic concentration measured on SUJ-2 disk counterpart material lubricated under Mineral oil + MoDTC + ZnDTP, PAO4 + MoDTC, and PAO4 + ZnDTP

Lubricants	Counter DLC	Atomic ratio, %						
		C	O	P	S	Fe	Zn	Mo
Mineral oil + MoDTC + ZnDTP	ta-C	9.1	71.9	7.8	1.4	6.7	1.2	1.9
	Pillar ta-C	10.6	66.5	3.9	3.1	8.7	1.2	5.9
	Mesh ta-C	10.2	71.1	5.4	4.3	0.8	1.1	7.2
PAO4 + MoDTC	ta-C	2.9	49.0	-	5.1	26.8	-	16.2
	Pillar ta-C	3.1	47.0	-	5.4	31.6	-	12.9
	Mesh ta-C	4.4	48.8	-	2.3	35.1	-	9.5
PAO4 + ZnDTP	ta-C	2.0	48.4	14.7	-	15.3	18.7	-
	Pillar ta-C	3.7	46.6	20.7	-	3.3	24.8	-
	Mesh ta-C	2.6	43.3	10.7	-	25.5	16.8	-

Table 10 as-deposited and after friction test sp^2/sp^3 ratio measured on the DLC coated cylindrical-pin

sp^2/sp^3 ratio	as-deposited	Mineral oil + MoDTC + ZnDTP	PAO4 + MoDTC	PAO4 + ZnDTP
ta-C	0.77	0.83	1.07	3.23
Pillar ta-C	3.62	1.63	1.08	1.08
Mesh ta-C	0.98	2.40	1.19	1.99

Table 11 as-deposited sp^3 carbon atoms measured on the DLC coated cylindrical-pin and the coefficient of friction result lubricated under PAO4, Mineral oil + MoDTC + ZnDTP, PAO4 + MoDTC, and PAO4 + ZnDTP

		COF			
	sp^3 %	PAO4	Mineral oil + MoDTC + ZnDTP	PAO4 + MoDTC	PAO4 + ZnDTP
ta-C	45.1	0.067	0.086	0.031	0.037
Pillar ta-C	14.2	0.083	0.073	0.033	0.048
Mesh ta-C	40.8	0.066	0.084	0.030	0.043

Pillar ta-C consists of high sp^2 carbon atoms, followed by the Mesh ta-C as compared to the conventional ta-C. Consequently, the sp^2/sp^3 ratio on the ta-C, Pillar ta-C, and Mesh ta-C changes following friction test in each lubricant. The change of the sp^2/sp^3 ratio could be related to the reaction of the carbon atoms with the presence of additives in each lubricant in which affecting the friction and wear behavior of the ta-C, Pillar ta-C and Mesh ta-C. Figure 55 shows the friction coefficient result plotted against the sp^3 ratio % for each

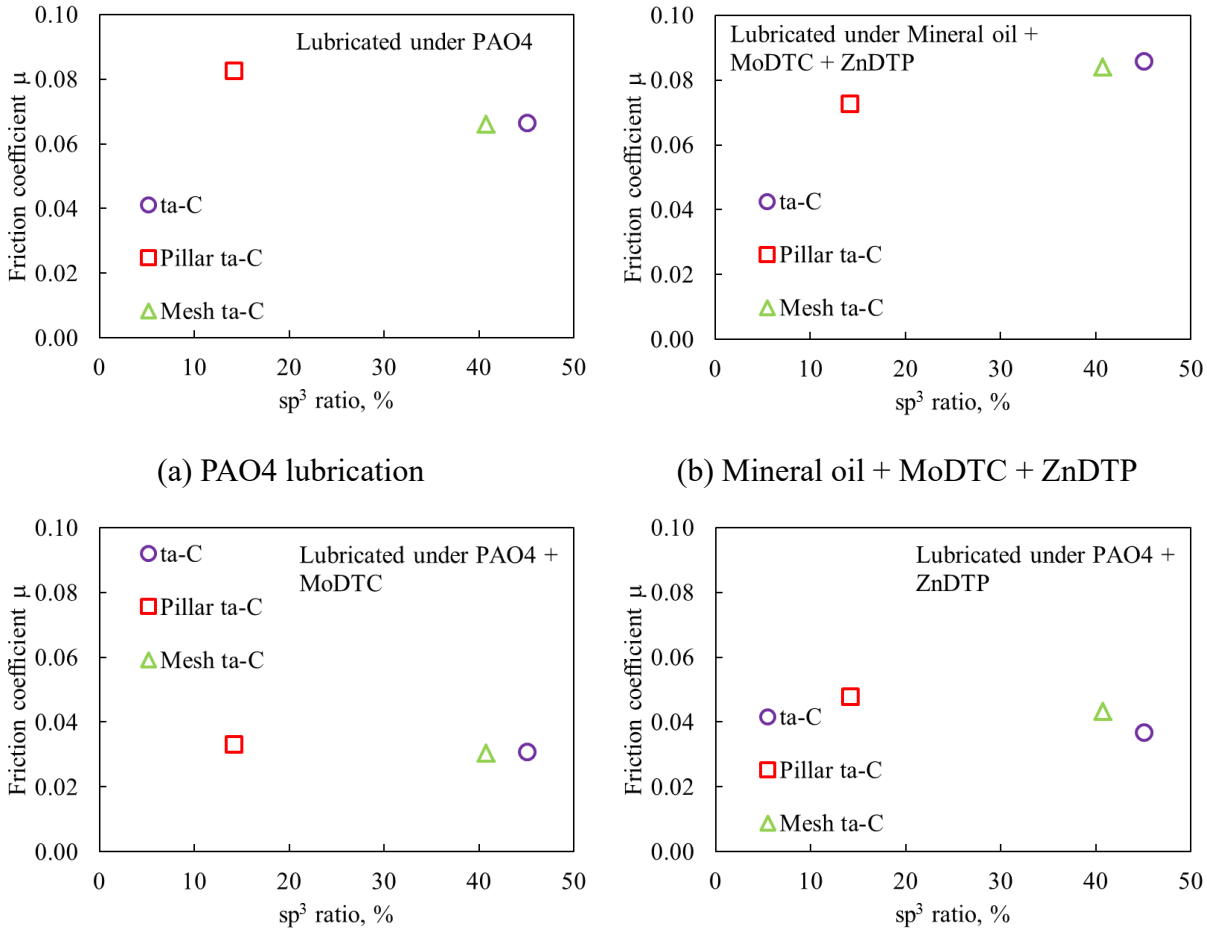

(a) PAO4 lubrication

(b) Mineral oil + MoDTC + ZnDTP

(c) PAO4 + MoDTC

(d) PAO4 + ZnDTP

Figure 55 Coefficient of friction plotted against sp^3 ratio for lubrication under (a) PAO4 lubrication, (b) Mineral oil + MoDTC + ZnDTP, (c) PAO4 + MoDTC, and (d) PAO4 + ZnDTP

lubricants used in this study. For lubrication under PAO4, PAO4 + MoDTC and PAO4 + ZnDTP, the tendency of lower friction coefficient with the increase of sp^3 carbon structure can be observed as shown in Figure 55(a), Figure 55(c), and Figure 55(d), respectively. A study conducted by the previous researcher has shown similar result where the hydrogen-free DLC coatings show the higher coefficient of friction with a lower sp^3 bonds due to the decreased number of dangling bonds which act as the oiliness agent adsorption sites on the DLC surface [34]. Likewise, the friction coefficient tended to increase with the increasing of

sp^3 ratio under Mineral oil + MoDTC + ZnDTP lubrication as shown in Figure 55(b). This reverse tendency could be explained by the additive competitive adsorption that occurs which will be further clarified in the following section.

4.3.2.2.1 Mineral oil + MoDTC + ZnDTP lubrication

The analysis performed on the wear track of DLC coated cylindrical-pin and SUJ-2 disk counterpart material reveals the presence of carbon, oxygen, phosphorus, sulfur, iron, zinc, and molybdenum as shown in Table 8 and Table 9. It has been observed that molybdenum related peaks were not detected on the wear track of DLC coated cylindrical-pin under Mineral oil + MoDTC + ZnDTP lubrication condition. From the percentage of atomic ratio measured on the DLC coated cylindrical-pin, there was evidence that the tribo-film derived from zinc, phosphorus, and sulfur may form on the ta-C, Pillar ta-C and Mesh ta-C as shown in Table 8. Furthermore, the measurement of the atomic ratio on the wear track of counterpart disk reveals a high percentage of molybdenum and sulfur on SUJ-2 of Pillar ta-C and Mesh ta-C as compared to the conventional ta-C.

Figure 56 shows the Mo3d XPS spectrum measured on the SUJ-2 disk counterpart for ta-C, Pillar ta-C, and Mesh ta-C. In addition, Figure 57 and Figure 58 shows the Zn2p3 spectrum measured on the DLC coated cylindrical-pin and SUJ-2 counterpart disk, respectively. It should be noted that Mo3d peaks were not detected on ta-C, Pillar ta-C and Mesh ta-C coated pins. Also, the Zn2p3 peak was not detected on the Pillar ta-C and Mesh ta-C coated pins.

XPS analysis result of Mo3d peak as shown in Figure 56(b) and Figure 56(c) reveals a high signal of molybdenum carbide (Mo_2C) on the SUJ-2 disk counterpart material for Pillar

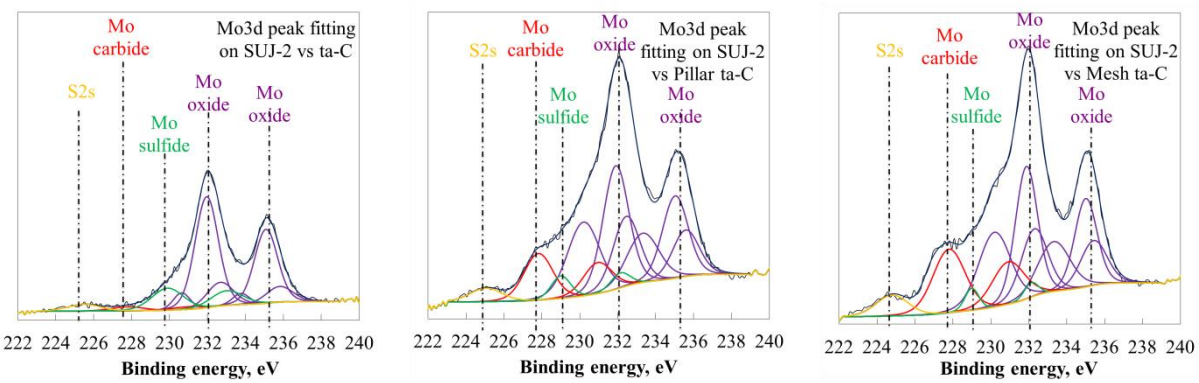

(a) (b) (c)

Figure 56 Mo3d peak deconvolution result on the SUJ-2 disk counterpart for (a) ta-C, (b) Pillar ta-C, and (c) Mesh ta-C lubricated with Mineral oil + MoDTC + ZnDTP

ta-C and Mesh ta-C which explain the reason for severe scratch on the SUJ-2 disk wear track as observed by FE-SEM, Figure 54(b), and Figure 54(c). Previous research has reported that DLCs is not easily worn by the formation of the Mo_2C because of the hardness which is lesser than that of DLC [104]. This factor has contributed to the high friction coefficient as a result of abrasive wear.

Furthermore, Figure 57 and Figure 58 show the XPS analysis result of Zn2p3 peak on both DLC coated cylindrical-pin and SUJ-2 disk counterpart material, respectively. It is reported that the formation of pad-like ZnDTP derived tribo-film on both DLC pin and SUJ-2 disk result in a higher friction coefficient due to high shear strength [105]. The deconvolution result reveals the formation of zinc derived tribo-film formed on the wear scar of ta-C which characterized the white solid tribo-film as observed under FE-SEM, Figure 53(a).

Thermal decomposition and degradation of ZnDTP are evidenced with the presence of iron produce ZnO and zinc sulfate $ZnSO_4$ on the ta-C pin, as well as on the ta-C, Pillar and Mesh ta-C counterpart disk. The phenomena of the degradation of ZnDTP only give little

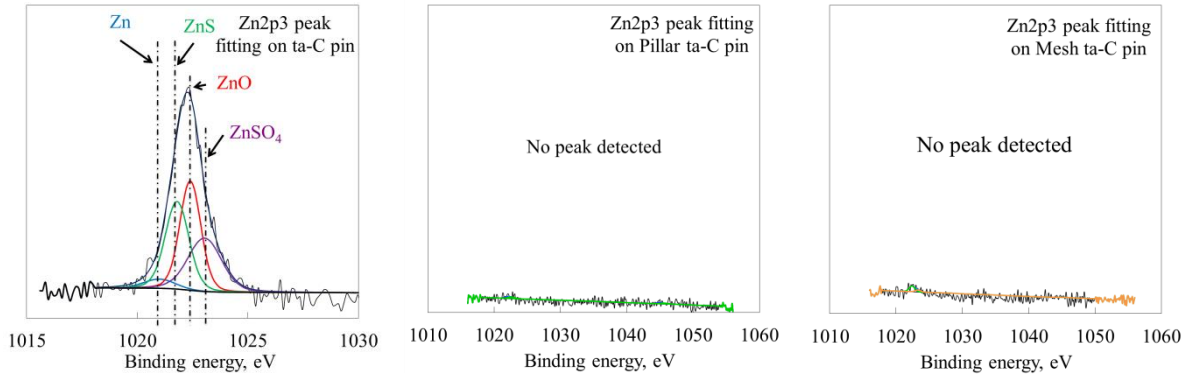

(a) (b) (c)

Figure 57 Zn2p3 peak deconvolution result on the (a) ta-C, (b) Pillar ta-C, and (c) Mesh ta-C lubricated with Mineral oil + MoDTC + ZnDTP

effect to the ZnDTP anti-wear performance [106]. The formation of Zn-derived stable pad-like tribo-film on the wear track of ta-C coated pin, and the counterpart SUJ-2 disk for ta-C, Pillar ta-C and Mesh ta-C as shown in Figure 53 and Figure 54, respectively has led to the excellent wear protection, but with slightly increased of friction coefficient as compared to only in PAO4 lubrication.

Interestingly, both Pillar and Mesh ta-C show high wear-resistant when lubricated under Mineral oil + MoDTC + ZnDTP even though there were no tribo-film derived from Mo or Zn can be observed on the wear track of the coating. This could be explained by the weak Zn-derived tribo-film formed on the wear track of Pillar ta-C and Mesh ta-C that is easily removed during the cleaning process with benzene and acetone after the friction [49]. It is reported that the presence of iron could result in a weak Zn-derived tribo-film [95].

Furthermore, the transfer of ferrous molecules from steel disk to the coating is the reason for the formation of Zn-derived tribo-film on the ta-C despite the chemical reaction of the ZnDTP molecules with ta-C coating [49], [53]. Thus, in the case of Pillar ta-C and Mesh

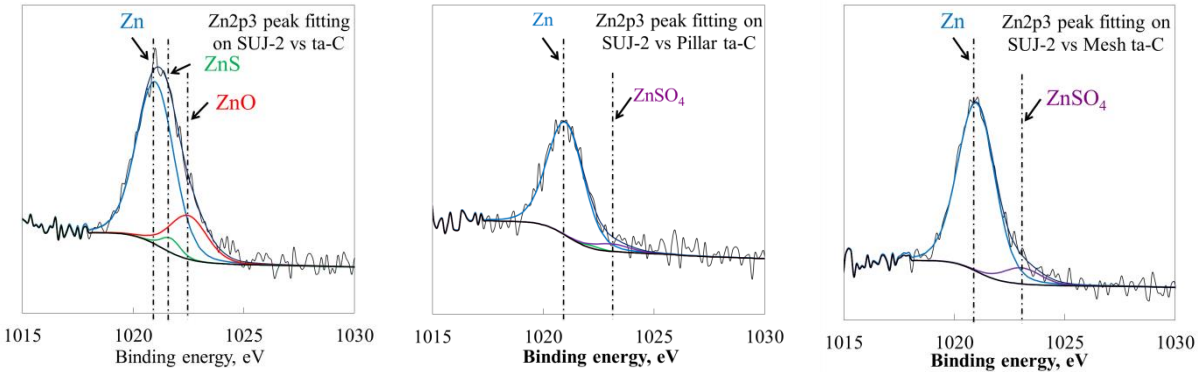

(a) (b) (c)

Figure 58 Zn2p3 peak deconvolution result on the SUJ-2 disk counterpart for (a) ta-C, (b) Pillar ta-C, and (c) Mesh ta-C lubricated with Mineral oil + MoDTC + ZnDTP

ta-C, lack of ferrous transfer molecules to the coating due to formation of Mo-derived and Zn-derived tribo-film on SUJ-2 disk result in a weak Zn-derived tribo-film on the wear track of the coated pin. In addition, the formation of Zn-derive tribo-film on the counterpart SUJ-2 disk prevents the carbon diffusion from DLC to the SUJ-2 steel surface that results in high wear resistance of ta-C, Pillar ta-C, and Mesh ta-C. Furthermore, higher crack resistance of the Pillar ta-C and Mesh ta-C coatings extend the protection against high wear of the coatings [80]. The formation of the weak Zn-derived tribo-film on the wear track of Pillar ta-C and Mesh ta-C permits the reaction of oxidize-Mo (MoO_3) with the carbon from coating to produce Mo_2C.

4.3.2.2.2 PAO4 + MoDTC lubrication

The measured atomic percentage (at.%) has shown that the Mo-derived tribo-film may form on the DLC coated cylindrical-pin under PAO4 + MoDTC (Table 8), which not detected under Mineral oil + MoDTC + ZnDTP lubrication condition. Furthermore, XPS analysis on the wear track of DLC coated cylindrical-pin and SUJ-2 disk counterpart material

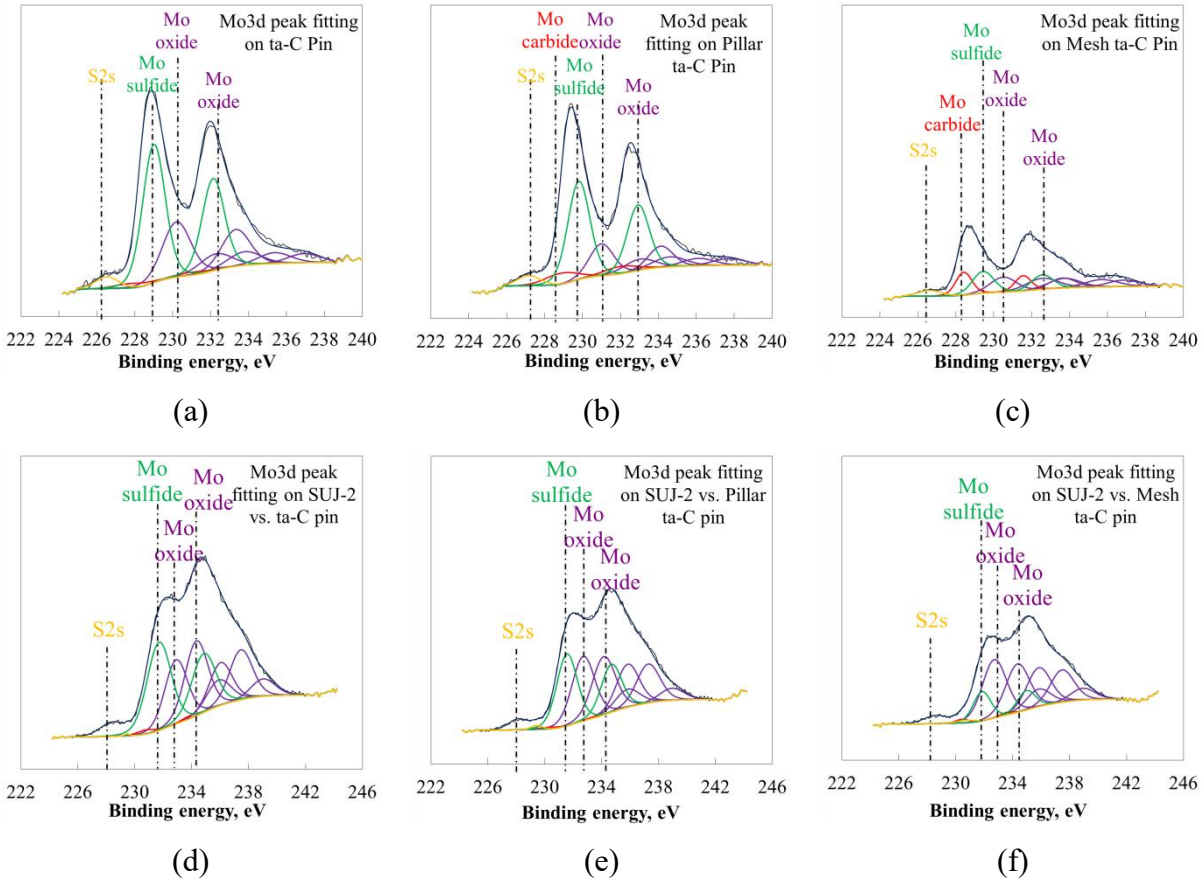

Figure 59 Mo3d peak deconvolution result on (a) ta-C pin, (b) Pillar ta-C pin, (c) Mesh ta-C pin and on the SUJ-2 disk counterpart for (d) ta-C, (e) Pillar ta-C, and (f) Mesh ta-C lubricated under PAO4 + MoDTC

lubricated with PAO4 + MoDTC characterized that Mo at% is higher in the case of conventional ta-C as compared to the Pillar and Mesh ta-C as depicted in Table 8 and Table 9.

Mo3d peak deconvolution on both DLC coated cylindrical-pin and SUJ-2 counterpart disk are shown in Figure 59. It can be observed that molybdenum carbide, Mo_2C is detected on the wear track of Pillar ta-C and Mesh ta-C as shown in Figure 59(b) and Figure 59(c). The formation of the Mo_2C on both of Pillar ta-C and Mesh ta-C could be explained by the existence of high sp^2 carbon atoms on the contact surface which facilitate the carbon atoms

release from the coating. This is further clarified by the low intensity of the Mo-oxide detected on the Pillar ta-C and Mesh ta-C coating due to the reaction with carbon atoms producing the Mo_2C peak as shown in Figure 59(b) and Figure 59(c). The gasification to CO and CO_2 from the MoO_3 oxidation, which is regarded as the main factor controlling the wear of ta-C under MoDTC lubrication also have led to the smoother contact surface of ta-C and Mesh ta-C [103]. This is supported by the increase of sp^2 carbon atoms at the contact surface of the ta-C and Mesh ta-C as compared to the as-deposited sp^2/sp^3 ratio depicted in Table 10.Nonetheless, the gasification from the oxidize Mo does not affect the wear rates of ta-C and Mesh ta-C due to its high hardness.

Furthermore, the formation of MoS_2 tribo-film can be observed on the DLC coated cylindrical-pin and SUJ-2 counterpart disk. The formation of MoS_2 tribo-film on the wear track of DLC coated cylindrical-pin and counterpart SUJ-2 disk results in lower friction coefficient and high wear resistance for ta-C, Pillar ta-C, and Mesh ta-C in PAO4 + MoDTC lubrication as compared to lubrication under PAO4 and Mineral oil + MoDTC + ZnDTP lubrication condition. In addition, the Mesh ta-C high wear resistance remains as recorded under PAO4 lubrication even with low intensity of MoS_2 tribo-film on the wear track of the coating.

4.3.2.2.3 PAO4 + ZnDTP lubrication

Table 8 and Table 9 reveals that the use of the single additive has led to an increase of Zn at. % on both wear track of DLC coated cylindrical-pin and SUJ-2 counterpart disk as compared to Zn at. % measured in the case of lubrication under Mineral oil + MoDTC + ZnDTP lubrication. Figure 60 shows the Zn2p3 peak deconvolution result on both DLC coated cylindrical-pin and counterpart SUJ-2 disk.

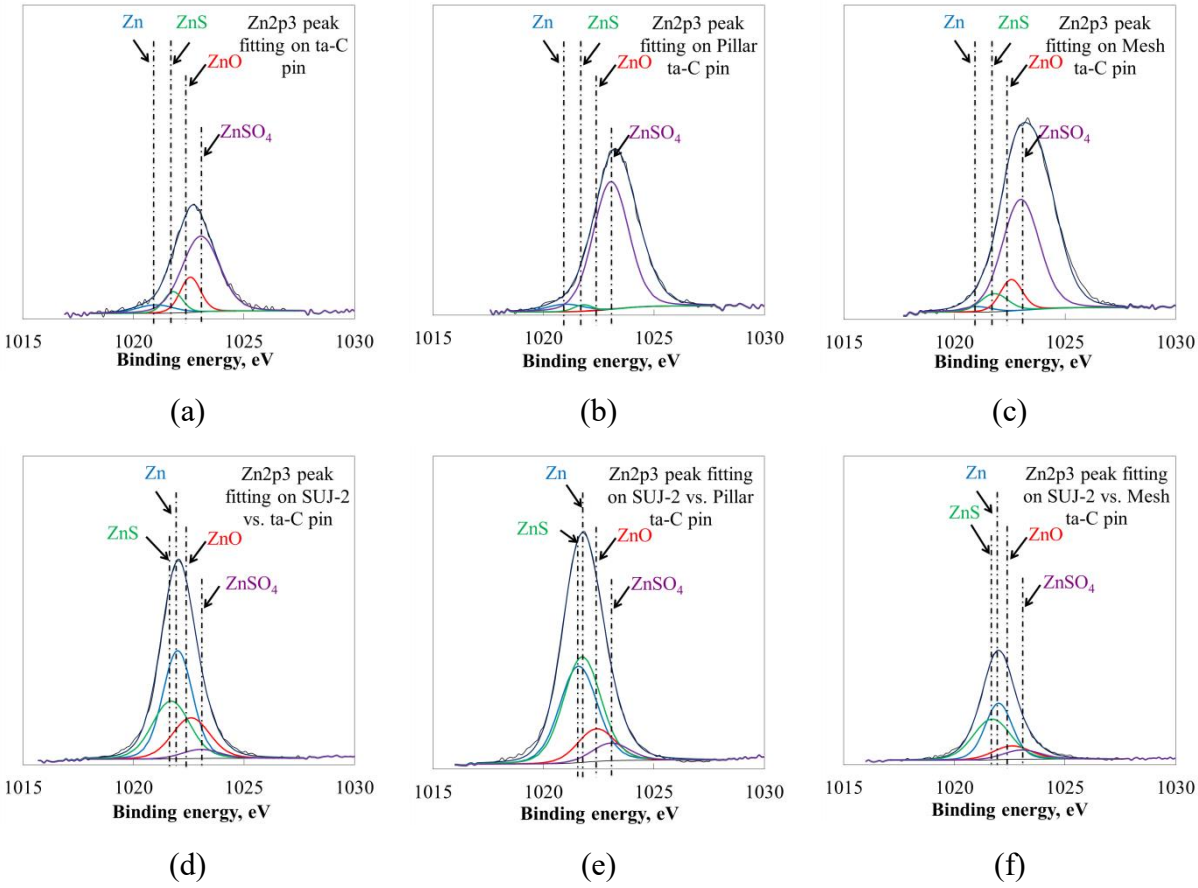

Figure 60 Zn2p3 peak deconvolution result on (a) ta-C pin, (b) Pillar ta-C pin, (c) Mesh ta-C pin and on the SUJ-2 disk counterpart for (d) ta-C, (e) Pillar ta-C, and (f) Mesh ta-C lubricated under PAO4 + ZnDTP

In the view of friction coefficient, the result shows that the ta-C, Pillar ta-C and Mesh ta-C in PAO4 + ZnDTP are comparatively higher to the friction coefficient result in PAO4 + MoDTC lubrication condition. This result confirms that the formation of Zn-derived tribo-film has contributed to a higher friction coefficient due to the high shear strength. Nonetheless, the coefficient of friction results under PAO4 + ZnDTP lubrication lower as compared to the lubrication under PAO4 and Mineral oil + MoDTC + ZnDTP.

Furthermore, the sp^2/sp^3 ratio (Table 10) measured on the ta-C and Mesh ta-C under PAO4 + ZnDTP is higher as compared to the Pillar ta-C. Also, the formation of ZnS on the

wear track of ta-C and Mesh ta-C coating result in a lower friction coefficient as compared Pillar ta-C. This contributes to the lower friction coefficient of ta-C and Mesh ta-C as compared to Pillar ta-C. It is evidence that Zn derived tribo-film mainly consists of $ZnSO_4$ existed the ta-C, Pillar ta-C and Mesh ta-C coated pin under PAO4 + ZnDTP. The formation of the $ZnSO_4$ under PAO4 + ZnDTP lubrication results in excellent protection against high wear as compared to the lubrication with the only PAO4.

4.4 Conclusions

The current study examined the effect of Pillar ta-C and Mesh ta-C coating on the tribological performance, particularly with regard to friction and wear in the presence of MoDTC and ZnDTP additives lubrication conditions. The findings of friction test for several types of lubrication oil with an additive as compared to only base-oil PAO4 can be summarized as follow;

- In the case of Mineral oil + MoDTC + ZnDTP lubrication condition, the overall friction coefficient for ta-C and Mesh ta-C increased as a result of Zn-derived pad-like tribo-film formed on the DLC coated-pin and SUJ-2 disk counterpart that protect the coating from severe wear and microfracture. Passivation of ferrous transfer from SUJ-2 disk results in a weak Zn-derived tribo-film formed on the Pillar ta-C and Mesh ta-C. As for Pillar ta-C, the weak Zn-derived tribo-film formed on the DLC coating contributes to the high wear resistance and the coefficient of friction reduction mainly contributed by the high sp^2 carbon structure on the contact surface.

- Furthermore, lower friction coefficient and high wear resistance recorded under PAO4 + MoDTC lubrication condition which contributed by the formation of MoS_2 tribo-film formation.

- Moreover, lubrication in PAO4 + ZnDTP provides high wear resistance for ta-C, Pillar ta-C and Mesh ta-C coating with the presence of $ZnSO_4$ tribo-film on the wear track. In addition, the formation of ZnS on the wear track of the coating and counterpart SUJ-2 disk results in a lower friction coefficient.

The characteristics of Pillar ta-C and Mesh ta-C which is low in sp^3 carbon bond does not affect the tribo-film formation on the coating in single additive lubrication with MoDTC and ZnDTP.

Chapter 5
Conclusion and Future Outlook

This thesis introduced and synthesized the mechanical, friction and wear properties of the novel structure-controlled Pillar ta-C and Mesh ta-C coatings to further the understanding towards ta-C coating with as-deposited structure. The development of the novel Pillar and Mesh ta-C is based on the conventional ta-C which is one of available DLC coating that could provide low friction coefficient and high wear resistance due to its high hardness. Nonetheless, the excellent performance of high hardness ta-C is reported to be limited by the brittle characteristic and high load condition. Thus, taking advantage of the ta-C excellent mechanical and tribological properties by introducing the structure and controlling the hardness can result in a superior mechanical and tribological performance. At first, the Pillar ta-C and Mesh ta-C coating tribological performance under PAO4 base-oil boundary lubrication condition were comprehensively investigated together with conventional ta-C for comparison presented in Chapter 2. To further understand the wear mechanism that took place under base-oil boundary lubricated condition, Chapter 3 presents the outcomes of the effect of the DLC fracture toughness to the wear properties of ta-C, Pillar ta-C and Mesh ta-C. Finally, the performance of the Pillar ta-C and Mesh ta-C together with ta-C coating were investigated under the additive oil boundary lubrication condition which presented in Chapter 4. Main findings of this work resulting from our experimental investigations can be summarized as follows:

(1) Under PAO4 base oil boundary lubrication condition, Pillar ta-C and Mesh ta-C indicate excellent wear resistance owing to the inhibition of micro-fracture and cracks propagation by the structure together with the reduction of abrasive particle production. Likewise, brittle micro-fracture was observed on the ta-C coating, which progresses to partial spalling and functions as the high hardness abrasive particles to accelerate the wear. Mesh ta-C friction reduction is explained by the surface smoothening due to the polishing effect.

(2) Superior fracture-toughness was observed following the introduction of pillar and mesh structure to the ta-C coating in which the fracture-toughness of the Pillar and Mesh ta-C DLC-coatings were comparatively higher than the conventional ta-C. Furthermore, the elevation of fracture-toughness led to the higher wear resistance of the Pillar and Mesh ta-C coating due to the fracture-induced wear suppression through the improvement of the crack propagation inhibition. In addition, the introduction of Pillar and Mesh structure to the ta-C DLC coating prevented the brittle characteristics of the ta-C by decreasing channel-type cohesive cracking. Moreover, Pillar and Mesh structure ta-C provided a greater degree of stress relief by permitting the higher rate of crack energy dissipation in contrast to conventional ta-C coating. Also, the increased crack spacing in Pillar and Mesh ta-C was facilitated by an improved adhesion strength, which prevented the interface failures.

(3) In the case of Mineral oil + MoDTC + ZnDTP lubrication condition, the overall friction coefficient for ta-C, Pillar ta-C and Mesh ta-C comparatively higher as compare to lubrication under PAO4 as a result of Zn-derived pad-like tribo-film formed on the DLC coated-pin and SUJ-2 disk counterpart as well as molybdenum carbide formation on Pillar and Mesh ta-C. Nonetheless, the Zn-derived tribo-film protects the coating from severe wear and microfracture. Furthermore, lower friction

coefficient and high wear resistance recorded under PAO4 + MoDTC lubrication condition which contributed by the formation of MoS_2 tribo-film formation. Moreover, lubrication in PAO4 + ZnDTP provides low friction and wear rates for ta-C, Pillar ta-C and Mesh ta-C coating with the presence of $ZnSO_4$ and ZnS tribo-film on the wear track of coated cylindrical-pin and counterpart SUJ-2 disk.

The findings of this research indicate that introducing the structure to the ta-C coating result in the excellent mechanical and tribological performance of the Pillar ta-C and Mesh ta-C coating. Under the base oil boundary lubrication condition, fracture toughness of the coating plays a key role in the wear of DLC coating especially for ta-C, Pillar ta-C and Mesh ta-C coating. The presence of sp^2 carbon structure in the Pillar and Mesh ta-C coating leads to superior protection against micro-crack. The performance of Pillar ta-C and Mesh ta-C, as well as conventional ta-C in additive oil lubrication is enhanced with the formation of tribo-film that protects against micro-crack and high wear of the coating. Therefore, the future direction for this work would be to synthesize the Pillar ta-C and Mesh ta-C coating under the dry condition as well as the investigation on the mating material for the counterpart of Pillar and Mesh ta-C coatings for industrial application.

Bibliography

[1] I. Tzanakis, M. Hadfield, B. Thomas, S. M. Noya, I. Henshaw, and S. Austen, "Future perspectives on sustainable tribology," *Renew. Sustain. Energy Rev.*, vol. 16, no. 6, pp. 4126–4140, 2012.

[2] G. W. Stachowiak, "Wear: Materials, Mechanisms and Practice," *John Wiley & Sons*, 2006. [Online]. Available: https://www.wiley.com/en-jp/Wear:+Materials,+Mechanisms+and+Practice-p-9780470016282. [Accessed: 31-Oct-2019].

[3] K. Kato, "Industrial Tribology in the Past and Future," *Tribol. Online*, vol. 6, no. 1, pp. 1–9, 2011.

[4] K. Holmberg, P. Andersson, and A. Erdemir, "Global energy consumption due to friction in passenger cars," *Tribol. Int.*, vol. 47, pp. 221–234, 2012.

[5] K. Holmberg and A. Erdemir, "Influence of tribology on global energy consumption, costs and emissions," *Friction*, vol. 5, no. 3, pp. 263–284, 2017.

[6] H. Singh, K. C. Mutyala, H. Mohseni, T. W. Scharf, R. D. Evans, and G. L. Doll, "Tribological Performance and Coating Characteristics of Sputter-Deposited Ti-Doped MoS2 in Rolling and Sliding Contact," *Tribol. Trans.*, vol. 58, no. 5, pp. 767–777, 2015.

[7] J. Vetter, "60years of DLC coatings: Historical highlights and technical review of cathodic arc processes to synthesize various DLC types, and their evolution for industrial applications," *Surf. Coatings Technol.*, vol. 257, pp. 213–240, 2014.

[8] L. Dobrenizki *et al.*, "Efficiency improvement in automobile bucket tappet/camshaft contacts by DLC coatings – Influence of engine oil, temperature and camshaft speed," *Surf. Coatings Technol.*, 2016.

[9] Y. Mabuchi, T. Higuchi, Y. Inagaki, H. Kousaka, and N. Umehara, "Wear analysis of hydrogen-free diamond-like carbon coatings under a lubricated condition," *Wear*, vol. 298–299, no. 1, pp. 48–56, 2013.

[10] K. Bewilogua and D. Hofmann, "History of diamond-like carbon films - From first experiments to worldwide applications," *Surf. Coatings Technol.*, vol. 242, pp. 214–225, 2014.

[11] Y. Mabuchi, T. Hamada, H. Izumi, Y. Yasuda, and M. Kano, "The development of hydrogen-free DLC-coated valve-lifter," *SAE Tech. Pap.*, vol. 01–1752, no. April, 2007.

[12] T. Higuchi, Y. Mabuchi, H. Ichihara, T. Murata, and M. Moronuki, "Development of hydrogen-free diamond-like carbon coating for piston rings," *Tribol. Online*, vol. 12, no. 3, pp. 117–122, 2017.

[13] X. Deng, H. Kousaka, T. Tokoroyama, and N. Umehara, “Tribology International Tribological behavior of tetrahedral amorphous carbon (ta-C) coatings at elevated temperatures,” *Tribiology Int.*, vol. 75, pp. 98–103, 2014.

[14] B. Vengudusamy, R. A. Mufti, G. D. Lamb, J. H. Green, and H. A. Spikes, “Friction properties of DLC/DLC contacts in base oil,” *Tribol. Int.*, vol. 44, no. 7–8, pp. 922–932, 2011.

[15] H. Ronkainen, S. Varjus, J. Koskinen, and K. Holmberg, “Differentiating the tribological performance of hydrogenated and hydrogen-free DLC coatings,” *Wear*, vol. 249, no. 3–4, pp. 260–266, 2001.

[16] A. Leyland and A. Matthews, “On the significance of the H/E ratio in wear control: A nanocomposite coating approach to optimised tribological behaviour,” *Wear*, vol. 246, no. 1–2, pp. 1–11, 2000.

[17] A. Gilewicz, B. Warcholinski, W. Szymanski, and W. Grimm, “CrCN/CrNta-C multilayer coating for applications in wood processing,” *Tribol. Int.*, vol. 57, pp. 1–7, 2013.

[18] H. Moriguchi, A. Shibata, and J. Watanabe, “Tribological Properties of New Type DLC Film ‘Geniuscoat HAM,’” *Nissin Electr. Rev.*, vol. 62, no. 2, 2017.

[19] S. M. Rasel, Y. Q. Wang, H. K. Ku, J. M. Byeon, T. K. Kim, and J. I. Song, “Determination of Fracture Toughness of Amorphous Carbon Coatings Using Indentation Method,” in *International Conference on Composite Materials*, 2011, pp. 5–8.

[20] Y. Wang and X. Yu, “Exploring Film Failure Mechanism and Scratch Toughness Characterization of Diamond-Like Carbon Film,” pp. 306–309, 2015.

[21] M. Nastasi, P. Kodali, K. C. Walter, and J. D. Embury, “Fracture toughness of diamond-like carbon films,” *Mod. Phys. Letts B*, vol. 15, pp. 157–162, 2001.

[22] S. J. Bull, “Tribology of carbon coatings: DLC, diamond and beyond,” *Diam. Relat. Mater.*, vol. 4, no. 5–6, pp. 827–836, 1995.

[23] X. Li, X. Deng, H. Kousaka, and N. Umehara, “Comparative study on effects of load and sliding distance on amorphous hydrogenated carbon (a-C:H) coating and tetrahedral amorphous carbon (ta-C) coating under base-oil lubrication condition,” *Wear*, vol. 392–393, no. February, pp. 84–92, 2017.

[24] T. Van der Donck, M. Muchlado, W. Zein Eddine, S. Achanta, N. J. M. Carvalho, and J. P. Celis, “Effect of hydrogen content in a-C:H coatings on their tribological behaviour at room temperature up to 150 °C,” *Surf. Coatings Technol.*, vol. 203, no. 22, pp. 3472–3479, 2009.

[25] M. Nastasi, P. Kodali, K. C. Walter, and J. D. Embury, “Fracture toughness of diamond-like carbon films,” *J. Mater. Res.*, vol. 15, pp. 157–162, 2001.

[26] D. K. Leung, M. Y. He, and A. G. Evans, “The cracking resistance of nanoscale layers and films,” *J. Mater. Res.*, vol. 10, no. 7, pp. 1693–1699, 1995.

[27] Y. Feng, T. Zhang, and R. Yang, “A work approach to determine vickers indentation

fracture toughness," *J. Am. Ceram. Soc.*, vol. 94, no. 2, pp. 332–335, 2011.

[28] D. Chicot, A. Pertuz, F. Roudet, M. H. Staia, and J. Lesage, "New developments for fracture toughness determination by Vickers indentation," *Mater. Sci. Technol.*, vol. 20, no. 7, pp. 877–884, Jul. 2004.

[29] G. R. Antis, P. Chantikul, B. R. Lawn, and D. B. Marshall, "A Critical Evaluation of Indenation Techniques for Measuring Fracture Toughness: I, Direct Crack Measurements," *J. Am. Ceram. Soc.*, vol. 46, no. September, pp. 533–538, 1981.

[30] S. Kalpakjian, *Manufacturing engineering and technology*. Pearson/Prentice Hall, 2005.

[31] J. J. Kruzic and R. O. Ritchie, "Determining the toughness of ceramics from vickers indentations using the crack-opening displacements: An experimental study," *J. Am. Ceram. Soc.*, vol. 86, no. 8, pp. 1433–1436, 2003.

[32] K. A. H. Al Mahmud, M. Varman, M. A. Kalam, H. H. Masjuki, H. M. Mobarak, and N. W. M. Zulkifli, "Tribological characteristics of amorphous hydrogenated (a-C: H) and tetrahedral (ta-C) diamond-like carbon coating at different test temperatures in the presence of commercial lubricating oil," *Surf. Coatings Technol.*, vol. 245, pp. 133–147, 2014.

[33] H. A. Tasdemir, T. Tokoroyama, H. Kousaka, N. Umehara, and Y. Mabuchi, "Friction and wear performance of boundary-lubricated DLC/DLC contacts in synthetic base oil," *Procedia Eng.*, vol. 68, pp. 518–524, 2013.

[34] Y. Mabuchi, T. Higuchi, and V. Weihnacht, "Effect of sp2/sp3 bonding ratio and nitrogen content on friction properties of hydrogen-free DLC coatings," *Tribol. Int.*, vol. 62, pp. 130–140, 2013.

[35] N. A. Bin Masripan *et al.*, "Hardness effect of DLC on tribological properties for sliding bearing under boundary lubrication condition in additive-free mineral base oil," *Tribol. Int.*, vol. 65, pp. 265–269, 2013.

[36] M. Kalin, J. Vižintin, J. Barriga, K. Vercammen, K. van Acker, and A. Arnšek, "The effect of doping elements and oil additives on the tribological performance of boundary-lubricated DLC/DLC contacts," *Tribol. Lett.*, vol. 17, no. 4, pp. 679–688, 2004.

[37] X. Liu, R. Yamaguchi, N. Umehara, X. Deng, H. Kousaka, and M. Murashima, "Clarification of high wear resistance mechanism of ta-CNx coating under poly alpha-olefin (PAO) lubrication," *Tribiology Int.*, vol. 105, no. July 2016, pp. 193–200, 2017.

[38] J. Sotres and T. Arnebrant, "Experimental investigations of biological lubrication at the nanoscale: The cases of synovial joints and the oral cavity," *Lubricants*, vol. 1, no. 4, pp. 102–131, 2013.

[39] C. Bovington, S. Korcek, and J. Sorab, "The importance of the Stribeck curve in the minimisation of engine friction," *Tribol. Ser.*, vol. 36, pp. 205–214, 1999.

[40] K. Kato, "Wear in relation to friction - A review," *Wear*, vol. 241, no. 2, pp. 151–157, 2000.

[41] J. Halling, “The tribology of surface films,” *Thin Solid Films*, vol. 108, no. 2, pp. 103–115, 1983.

[42] S. R. Polaki *et al.*, “Tribological behavior of hydrogenated DLC film: Chemical and physical transformations at nano-scale,” *Wear*, vol. 338–339, pp. 105–113, 2015.

[43] M. Masuko, T. Ono, S. Aoki, A. Suzuki, and H. Ito, “Friction and wear characteristics of DLC coatings with different hydrogen content lubricated with several Mo-containing compounds and their related compounds,” *Tribol. Int.*, vol. 82, no. PB, pp. 350–357, 2015.

[44] a. P. Semenov and M. M. Khrushchov, “Influence of environment and temperature on tribological behavior of diamond and diamond-like coatings,” *J. Frict. Wear*, vol. 31, no. 2, pp. 142–158, 2010.

[45] H. Abdullah Tasdemir *et al.*, “The effect of oil temperature and additive concentration on the wear of non-hydrogenated DLC coating,” *Tribol. Int.*, vol. 77, pp. 65–71, 2014.

[46] B. Vengudusamy, R. A. Mufti, G. D. Lamb, J. H. Green, and H. A. Spikes, “Friction properties of DLC/DLC contacts in base oil,” *Tribol. Int.*, vol. 44, no. 7–8, pp. 922–932, 2011.

[47] B. Podgornik, S. Jacobson, and S. Hogmark, “DLC coating of boundary lubricated components - Advantages of coating one of the contact surfaces rather than both or none,” *Tribol. Int.*, vol. 36, no. 11, pp. 843–849, 2003.

[48] K. Topolovec-Miklozic, F. Lockwood, and H. Spikes, “Behaviour of boundary lubricating additives on DLC coatings,” *Wear*, vol. 265, no. 11–12, pp. 1893–1901, 2008.

[49] H. Abdullah Tasdemir *et al.*, “Ultra-low friction of tetrahedral amorphous diamond-like carbon (ta-C DLC) under boundary lubrication in poly alpha-olefin (PAO) with additives,” *Tribol. Int.*, vol. 65, pp. 286–294, 2013.

[50] J. M. Herdan, “Lubricating oil additives and the environment - An overview,” *Lubr. Sci.*, vol. 9, no. 2, pp. 161–172, 1997.

[51] M. A. Moore and F. S. King, “Abrasive wear of brittle solids,” *Wear*, vol. 60, no. 1, pp. 123–140, 1980.

[52] P. L. Wong, F. He, and X. Zhou, “Interpretation of the hardness of worn DLC particles using micro-Raman spectroscopy,” *Tribol. Int.*, vol. 43, no. 10, pp. 1806–1810, 2010.

[53] H. A. Tasdemir *et al.*, “Wear behaviour of tetrahedral amorphous diamond-like carbon (ta-C DLC) in additive containing lubricants,” *Wear*, vol. 307, no. 1–2, pp. 1–9, 2013.

[54] B. J. Hamrock, S. R. Schmid, and B. O. Jacobson, *Fundamentals of fluid film lubrication*. CRC Press, 2004.

[55] H. Harima, “UV-Raman observation of Si surface layer with very shallow ion-implantation,” *Kenbikyo*, vol. 43, no. 2, pp. 133–136, 2008.

[56] A. C. Ferrari and J. Robertson, “Interpretation of Raman spectra of disordered and amorphous carbon,” vol. 61, no. 20, pp. 95–107, 2000.

[57] M. Kalin and J. Vižintin, “Real contact temperatures as the criteria for the reactivity of diamond-like-carbon coatings with oil additives,” *Thin Solid Films*, vol. 518, no. 8, pp. 2029–2036, 2010.

[58] F. Bremond, P. Fournier, and F. Platon, “Test temperature effect on the tribological behavior of DLC-coated 100C6-steel couples in dry friction,” *Wear*, vol. 254, no. 7–8, pp. 774–783, 2003.

[59] D. R. Tallant, J. E. Parmeter, M. P. Siegal, and R. L. Simpson, “The thermal stability of diamond-like carbon,” *Diam. Relat. Mater.*, vol. 4, no. 3, pp. 191–199, 1995.

[60] A. A. Ogwu, R. W. Lamberton, S. Morley, P. Maguire, and J. McLaughlin, “Characterization of thermally annealed diamond like carbon (DLC) and silicon modified DLC films by Raman spectroscopy,” *Phys. B Condens. Matter*, vol. 269, no. 3–4, pp. 335–344, 1999.

[61] A. Erdemir and C. Donnet, “Tribology of diamond-like carbon films: Recent progress and future prospects,” *J. Phys. D. Appl. Phys.*, vol. 39, no. 18, 2006.

[62] W. Zhuang *et al.*, “Comparing space adaptability of diamond-like carbon and molybdenum disulfide films toward synergistic lubrication,” *Carbon N. Y.*, vol. 134, pp. 163–173, 2018.

[63] W. Li, X. Fan, H. Li, M. Zhu, and L. Wang, “Probing carbon-based composite coatings toward high vacuum lubrication application,” *Tribol. Int.*, vol. 128, no. May, pp. 386–396, 2018.

[64] X. Deng, H. Kousaka, T. Tokoroyama, and N. Umehara, “Tribological behavior of tetrahedral amorphous carbon (ta-C) coatings at elevated temperatures,” *Tribol. Int.*, vol. 75, pp. 98–103, 2014.

[65] K. Komori and N. Umehara, “Effect of surface morphology of diamond-like carbon coating on friction, wear behavior and tribo-chemical reactions under engine-oil lubricated condition,” *Tribol. Int.*, vol. 84, pp. 100–109, 2015.

[66] S. J. Park, K. R. Lee, and D. H. Ko, “Tribological behavior of nano-undulated surface of diamond-like carbon films,” *Diam. Relat. Mater.*, vol. 14, no. 8, pp. 1291–1296, 2005.

[67] M. F. Bin Abdollah, Y. Yamaguchi, T. Akao, N. Inayoshi, N. Umehara, and T. Tokoroyama, “Phase transformation studies on the a-C coating under repetitive impacts,” *Surf. Coatings Technol.*, vol. 205, no. 2, pp. 625–631, 2010.

[68] M. A. Moore and F. S. King, “Abrasive wear of brittle solids*,” vol. 60, no. April 1979, pp. 123–140, 1980.

[69] X. Fan, L. Wang, W. Li, and S. Wan, “Improving Tribological Properties of Multialkylated Cyclopentanes under Simulated Space Environment: Two Feasible Approaches,” *ACS Appl. Mater. Interfaces*, vol. 7, no. 26, pp. 14359–14368, 2015.

[70] C. Charitidis, S. Logothetidis, and M. Gioti, “A comparative study of the nanoscratching behavior of amorphous carbon films grown under various deposition conditions,” vol. 125, pp. 201–206, 2000.

[71] C. Subramanian and K. N. Strafford, “Review of multicomponent and multilayer coatings for tribological applications,” *Wear*, vol. 165, no. 1, pp. 85–95, 1993.

[72] X. Sui, J. Liu, S. Zhang, J. Yang, and J. Hao, “Microstructure, mechanical and tribological characterization of CrN/DLC/Cr-DLC multilayer coating with improved adhesive wear resistance,” *Appl. Surf. Sci.*, vol. 439, pp. 24–32, 2018.

[73] J. Y. Zhang, G. Liu, X. Zhang, G. J. Zhang, J. Sun, and E. Ma, “A maximum in ductility and fracture toughness in nanostructured Cu/Cr multilayer films,” *Scr. Mater.*, vol. 62, no. 6, pp. 333–336, 2010.

[74] C. Q. Guo, Z. L. Pei, D. Fan, J. Gong, and C. Sun, “Microstructure and tribomechanical properties of (Cr, N)-DLC/DLC multilayer films deposited by a combination of filtered and direct cathodic vacuum arcs,” *Diam. Relat. Mater.*, vol. 60, pp. 66–74, 2015.

[75] Y. Wang and X. Yu, “Exploring Film Failure Mechanism and Scratch Toughness Characterization of Diamond-Like Carbon Film,” in *International Conference on Chemical, Material and Food Engineering*, 2015, pp. 306–309.

[76] S. Zhang and X. Zhang, “Toughness evaluation of hard coatings and thin films,” *Thin Solid Films*, vol. 520, no. 7, pp. 2375–2389, 2012.

[77] K. Niihara, R. Morena, and D. P. . Hasselman, “Evaluation of Klc of Brittle Solids By the Indentation Method With Low Crack To Indent Ratios,” *J. Mater. Sci. Lett.*, vol. 1, pp. 13–16, 1982.

[78] R. J. Jaccodine, “Surface Energy of Germanium and Silicon,” *J. Electrochem. Soc.*, vol. 110, no. 6, p. 524, 1963.

[79] J. J. Gilman, “Direct measurements of the surface energies of crystals,” *J. Appl. Phys.*, vol. 31, no. 12, pp. 2208–2218, 1960.

[80] M. M. Bin Mustafa *et al.*, “Effect of mesh structure of tetrahedral amorphous carbon (ta-C) coating on friction and wear properties under base-oil lubrication condition,” *Tribol. Int.*, no. January, 2019.

[81] A. Yonezu, T. Nakayama, and T. Ogawa, “Fracture Mechanism of Diamond Like Carbon (DLC) Film Subjected to Contact Loading,” *J. Soc. Mater. Sci. Japan*, vol. 57, no. 5, pp. 474–480, 2008.

[82] K. Fu, L. Chang, L. Ye, and Y. Yin, “Indentation stress-based models to predict fracture properties of brittle thin film on a ductile substrate,” *Surf. Coatings Technol.*, vol. 296, pp. 46–57, 2016.

[83] M. Li, T. Deng, B. Zheng, Y. Zhang, Y. Liao, and H. Zhou, “Effect of Defects on the Mechanical and Thermal Properties of Graphene,” *Nanomaterials*, vol. 9, no. 3, p. 347, 2019.

[84] B. A. Latella, G. Triani, and P. J. Evans, “Toughness and Adhesion of Atomic Layer Deposited Alumina Films on Polycarbonate Substrates,” *Scr. Mater.*, vol. 56, no. 6, pp. 493–496, 2007.

[85] J.-H. Jeong and D. Kwon, “Evaluation of the Adhesion Strength in DLC Film-Coated

Systems Using the Film-Cracking Technique," *J. Adhes. Sci. Technol.*, vol. 12, no. 1, pp. 29–46, Jan. 1998.

[86] H. J. Kim, M. W. Moon, D. I. Kim, K. R. Lee, and K. H. Oh, "Observation of the Failure Mechanism for Diamond-like Carbon Film on Stainless Steel Under Tensile Loading," *Scr. Mater.*, vol. 57, no. 11, pp. 1016–1019, 2007.

[87] P. K. P. Rupa, P. C. Chakraborti, and S. K. Mishra, "Structure and indentation behavior of nanocomposite Ti-B-N films," *Thin Solid Films*, vol. 564, pp. 160–169, 2014.

[88] M. W. Moon, J. W. Chung, K. R. Lee, K. H. Oh, R. Wang, and A. G. Evans, "An experimental study of the influence of imperfections on the buckling of compressed thin films," *Acta Mater.*, vol. 50, no. 5, pp. 1219–1227, 2002.

[89] J. W. Hutchinson and Z. Suo, "Mixed mode cracking in layered material," *Adv. Appl. Mech.*, vol. 29, pp. 63–191, 2002.

[90] S. Kosarieh, A. Morina, E. Lainé, J. Flemming, and A. Neville, "Tribological performance and tribochemical processes in a DLC/steel system when lubricated in a fully formulated oil and base oil," *Surf. Coatings Technol.*, vol. 217, pp. 1–12, 2013.

[91] T. Haque, A. Morina, A. Neville, R. Kapadia, and S. Arrowsmith, "Effect of oil additives on the durability of hydrogenated DLC coating under boundary lubrication conditions," *Wear*, vol. 266, no. 1–2, pp. 147–157, 2009.

[92] H. Spikes, "The history and mechanisms of ZDDP," *Tribol. Lett.*, vol. 17, no. 3, pp. 469–489, 2004.

[93] T. Haque, A. Morina, A. Neville, R. Kapadia, and S. Arrowsmith, "Non-ferrous coating/lubricant interactions in tribological contacts: Assessment of tribofilms," *Tribol. Int.*, vol. 40, no. 10-12 SPEC. ISS., pp. 1603–1612, 2007.

[94] M. Kalin and J. Vižintin, "Differences in the tribological mechanisms when using non-doped, metal-doped (Ti, WC), and non-metal-doped (Si) diamond-like carbon against steel under boundary lubrication, with and without oil additives," *Thin Solid Films*, vol. 515, no. 4, pp. 2734–2747, 2006.

[95] S. Equey, S. Roos, U. Mueller, R. Hauert, N. D. Spencer, and R. Crockett, "Tribofilm formation from ZnDTP on diamond-like carbon," *Wear*, vol. 264, no. 3–4, pp. 316–321, 2008.

[96] B. Vengudusamy, J. H. Green, G. D. Lamb, and H. A. Spikes, "Tribological properties of tribofilms formed from ZDDP in DLC/DLC and DLC/steel contacts," *Tribol. Int.*, vol. 44, no. 2, pp. 165–174, 2011.

[97] T. Haque, A. Morina, and A. Neville, "Effect of friction modifiers and antiwear additives on the tribological performance of a hydrogenated DLC coating," *Surf. Coatings Technol.*, vol. 204, no. 24, pp. 4001–4011, 2010.

[98] B. Vengudusamy, J. H. Green, G. D. Lamb, and H. A. Spikes, "Influence of hydrogen and tungsten concentration on the tribological properties of DLC/DLC contacts with ZDDP," *Wear*, vol. 298–299, no. 1, pp. 109–119, 2013.

[99] M. Kano *et al.*, “Ultralow friction of DLC in presence of glycerol mono-oleate (GMO),” *Tribol. Lett.*, vol. 18, no. 2, pp. 245–251, 2005.

[100] M. Kano, “Super low friction of DLC applied to engine cam follower lubricated with ester-containing oil,” *Tribol. Int.*, vol. 39, no. 12, pp. 1682–1685, 2006.

[101] L. Joly-Pottuz, C. Matta, M. I. De Barros Bouchet, B. Vacher, J. M. Martin, and T. Sagawa, “Superlow friction of ta-C lubricated by glycerol: An electron energy loss spectroscopy study,” *J. Appl. Phys.*, vol. 102, no. 6, 2007.

[102] K. Komori and N. Umehara, “Friction and wear properties of tetrahedral si-containing hydrogenated diamond-like carbon coating under lubricated condition with engine-oil containing zndtp and modtc,” *Tribol. Online*, vol. 12, no. 3, pp. 123–134, 2017.

[103] K. Ohara *et al.*, “Analysis of wear track on DLC coatings after sliding with MoDTC-containing lubricants,” *Tribol. Online*, vol. 12, no. 3, pp. 110–116, 2017.

[104] M. De Feo *et al.*, “MoDTC lubrication of DLC-involving contacts. Impact of MoDTC degradation,” *Wear*, vol. 348–349, pp. 116–125, 2016.

[105] S. Kosarieh, A. Morina, J. Flemming, E. Lainé, and A. Neville, “Wear Mechanisms of Hydrogenated DLC in Oils Containing MoDTC,” *Tribol. Lett.*, vol. 64, no. 1, 2016.

[106] M. Masuko, T. Ohkido, A. Suzuki, and T. Ueno, “Fundamental study of changes in friction and wear characteristics due to ZnDTP deterioration in simulating engine oil degradation during use,” in *Tribology Series*, 2003, vol. 43, pp. 359–366.

Publication List

[1] Mohd Muhyiddin Bin Mustafa, Noritsugu Umehara, Takayuki Tokoroyama, Motoyuki Murashima, Akinori Shibata, Yoshiharu Utsumi, Hideki Moriguchi
Effect of mesh structure of tetrahedral amorphous carbon (ta-C) coating on friction and wear properties under base-oil lubrication condition,
Tribology International, 2019, DOI: 10.1016/j.triboint.2019.01.016.

[2] Mohd Muhyiddin Bin Mustafa, Noritsugu Umehara, Takayuki Tokoroyama, Motoyuki Murashima, Akinori Shibata, Yoshiharu Utsumi, Hideki Moriguchi
Effect of pillar and mesh structure of tetrahedral amorphous carbon (ta-C) coatings on the wear properties and fracture toughness of the coating,
Tribology Online, vol. 14, no. 5, pp. 388-397, 2019.

International Conference

[1] Proceeding of the 6th Asia International Conference on Tribology (ASIATRIB), September 17th-20th, 2018, pp. 173-175, Sarawak, Malaysia.
Mohd Muhyiddin Bin Mustafa, Noritsugu Umehara, Takayuki Tokoroyama, Motoyuki Murashima, Akinori Shibata, Yoshiharu Utsumi, Hideki Moriguchi

Effect of structure of tetrahedral amorphous carbon (ta-C) coating on friction and wear properties under base-oil lubrication condition

[2] 8th International Conference on Manufacturing, Machine Design and Tribology (ICMDT), April 24th – 27th, 2019, Kagoshima, Japan.
Mohd Muhyiddin Bin Mustafa, Noritsugu Umehara, Takayuki Tokoroyama, Motoyuki Murashima, Akinori Shibata, Yoshiharu Utsumi, Hideki Moriguchi

Effect of mesh structure of tetrahedral amorphous carbon (ta-C) coating on friction and wear properties under base-oil lubrication condition with regard to fracture behavior

[3] 8th International Conference on Mechanics and Materials in Design (M2D), September 4th – 6th, 2019, Bologna, Italy.
Mohd Muhyiddin Bin Mustafa, Noritsugu Umehara, Takayuki Tokoroyama, Motoyuki Murashima, Akinori Shibata, Yoshiharu Utsumi, Hideki Moriguchi

Effect of fracture toughness on the wear behavior of tetrahedral amorphous carbon (ta-C) coating

[4] International Tribology Conference (ITC), September 17th – 21st, 2019, Sendai, Japan.
Mohd Muhyiddin Bin Mustafa, Noritsugu Umehara, Takayuki Tokoroyama, Motoyuki Murashima, Akinori Shibata, Yoshiharu Utsumi, Hideki Moriguchi

Effect of Mesh and Pillar structure of tetrahedral amorphous carbon (ta-C) on the coatings' fracture toughness